POLITECNICO

MILANO 1863

School of Industrial and Information Engineering

Master of Science in
Mechanical Engineering

Characterization and compensation of the thermal expansion of Al5754 during the laser cutting process

Supervisor: Dr. Leonardo Caprio

Co-supervisor: Matteo Busatto

Master of Science Thesis by

Andrea Daloiso

Student ID 918319

Academic Year 2021-2022

"Success is the ability to go from
one failure to another
with no loss of enthusiasm"

- Winston Churchill

Abstract

Laser cutting, not only of sheet metal, but also of tubes, has become a key production technology for the industrial sector today due to its numerous advantages such as reliability, efficiency and high productivity.

Since the development and improvement of fibre laser cutting, it has also been possible to cut highly reflective materials such as aluminium, which has become an extremely widespread material over the years due to its mechanical and physical characteristics.

Despite the many advances that have been made, however, such operations are by no means free of problems that affect the quality of the cut.

While optimal cutting parameters have been sought for the boundary conditions that can be controlled, there are numerous factors that cannot be controlled by the user that often led to a drop in quality. One of these is the increase in the temperature of the workpiece after repeated cuts, which is inevitable and not well controllable.

To understand the effects of the increase in temperature on the quality of aluminium laser cutting, a thermal expansion model was analysed, which was well supported for the experiments by the realisation of a special architecture, designed and constructed to ensure correct and homogeneous heating of the workpiece before cutting the sample.

During the experimental campaign, the behaviour of the material at various increasing temperatures was measured, and the quality of the cut was assessed on the basis of the analysis of the roughness of the cut surface, the formation of burrs on the lower surface of the piece and finally the dimensional correctness of the final sample.

From this thesis work it emerged that for aluminium Al5754, the quality parameters of roughness and burr formation are not significantly affected as the temperature increases, while a dimensional correction is essential due to the material's high thermal expansion coefficient, which leads to non-negligible geometric inaccuracies.

In fact, the size of the samples analysed increased by approximately 0.16 mm for every 75°C increase in temperature, which on a sample with a total length of 100 mm corresponds to a 0.16% increase for the aforementioned temperature increase.

After these analyses, we then went on to correct any problems that may have arisen, by correcting the parameters and developing a compensation model to solve the dimensional problem.

Keywords: Laser cutting, Aluminium, Cutting quality, Thermal expansion

Sommario

Il taglio laser, non soltanto di lamiere, ma anche di tubi, è diventato una tecnologia di produzione di fondamentale importanza al giorno d'oggi per il settore industriale, grazie ai numerosi vantaggi che da esso derivano, come affidabilità, efficienza e elevata produttività.

Dopo lo sviluppo e il miglioramento del taglio laser tramite fibra, inoltre, è stato anche possibile effettuare tagli su materiali alto-riflettenti come l'alluminio che è diventato un materiale estremamente utilizzato in vari ambiti.

Nonostante i numerosi progressi fatti però, tali operazioni non sono assolutamente esenti da problemi che vanno ad inficiare la qualità del taglio.

Se da una parte si sono ricercati i parametri di taglio ottimali per le condizioni al contorno controllabili, vi sono numerosi fattori non controllabili dall'utente che spesso portano ad un abbassamento della qualità, uno di questi è l'aumento della temperatura del pezzo dopo tagli ripetuti, che risulta inevitabile e non ben controllabile.

Per comprendere gli effetti dell'aumento della temperatura sulla qualità del taglio laser dell'alluminio, è stato preso in analisi un modello di espansione termica, il quale è stato ben supportato per le sperimentazioni dalla realizzazione di una apposita architettura, studiata e realizzata in modo da garantire un corretto ed omogeneo riscaldamento del pezzo in esame, prima del taglio del campione.

Nella campagna sperimentale si è dunque osservato il comportamento del materiale a varie temperature sempre crescenti, e la qualità del taglio è stata valutata sulla base dell'analisi della rugosità della superficie tagliata, della formazione di bava sulla superfice inferiore del pezzo ed infine sulla correttezza dimensionale del campione finale.

Da questo lavoro di tesi è emerso come per l'alluminio Al5754, i parametri di qualità di rugosità e formazione di bava non vengano significativamente influenzati all'aumentare della temperatura, mentre una correzione dimensionale risulta fondamentale per via dell'alto coefficiente di espansione termica del materiale, che porta ad inaccuratezze geometriche non trascurabili. La dimensione dei campioni analizzati infatti, aumentava di circa 0.16 mm ogni 75°C di incremento di temperatura, che su un campione di 100 mm di lunghezza totale, corrispondono dunque allo 0.16% di incremento per il suddetto incremento di temperatura.

Dopo tali analisi si è dunque passato alla correzione di questi eventuali problemi venutisi a creare, tramite la correzione dei parametri e l'elaborazione di un modello di compensazione per risolvere il problema dimensionale.

Parole chiave: Taglio laser, Alluminio, Qualità di taglio, Espansione termica

IV

Contents

1. Introduction

Laser cutting has attracted a lot of attention as a new generation cutting method, widely used in many different industries, including aerospace, nuclear, medical and automotive.

As one of the fastest and most precise cutting processes available today, laser cutting has several advantages over conventional cutting technologies, but also over unconventional ones such as abrasive water jet cutting (AWJ), including the absence of cutting forces, a minimal cutting width, a high cutting speed as well as environmental protection.

Thanks to these advantages, laser cutting has become extremely popular for its use in machining numerous types of materials.

During the laser cutting process, the laser beam is focused on the sample through the cutting head and through concentrated energy, the material is melted after absorbing the high-density laser energy, and the resulting melted material is subsequently blown away by an auxiliary gas co-axial or lateral to the laser beam. The cutting head controlled by a computer numerical control (CNC) system moves along the processing path set by the user to complete the processing.

The two most common types of laser cutting processes are both based on the fusion process of the material to be cut, and are divided into 'inert gas fusion cutting' and 'reactive gas fusion cutting', where, as the name implies, for the first type, an inert gas (argon or nitrogen) is used as an auxiliary gas responsible for expelling the fused material, while in the second case, a reactive gas such as oxygen is used, which also actively participates in increasing the total energy of the cut through the exothermic reaction of oxidation.

With the continuous advances in fibre laser technology, the cutting capability of the high-power fibre laser has been greatly improved, firstly, leading to the possibility of cutting thicker materials with greater efficiency, and secondly, thanks to this new cutting technology, it has been possible to reduce the spot diameter, thus reducing errors such as cutting taper and geometric errors.

Above all, however, the advent of fibre laser cutting technology, thanks to its specific wavelength, has led to the possibility of cutting a highly reflective material such as aluminium, which until then was impossible to cut by laser cutting because almost all the incident energy was reflected and there was no possibility of melting the material for cutting. This has become an increasingly important and used material in various sectors, also due to its special characteristics such as light weight, corrosion resistance, formability, high resistance to breakage and fatigue, and also high recyclability.

Although this technology has evolved a lot over the years, there are still no numerical or analytical models that can explain the physical phenomena behind the laser cutting

process, which is why experiments and therefore empirical methodology are often used to optimise the parameters of the cutting process.

The optimal cutting parameters obtained are usually obtained under standard and perfectly controlled working conditions.

For this reason, it often happens that these parameters need to be 'revisited' due to the numerous uncontrollable and continuously changing factors that usually involve the cutting process in the working environment, thus modifying the boundary conditions; parameters such as a different material condition, a more or less oxidised, or more or less opaque surface condition, variations in ambient and processing temperature, dirty lenses or damage to machine parts.

Over the past twenty years, therefore, researchers have continuously investigated the effects of various cutting processes and parameters on cutting quality, in order to achieve the best possible quality even under different external conditions and to increase work efficiency.

Process parameters such as the laser source (which includes wavelength, laser beam size and beam quality), cutting speed, auxiliary gas pressure, power used, nozzle-to-blade distance and many other parameters, are indeed crucial in achieving optimum cutting quality, and these parameters vary greatly depending on the material to be cut, its thickness and also its surface conditions.

Cutting quality that includes roughness of the cutting surface, formation or non-formation of striations, burr formation, taper of the cutting gap, heat-affected zones and other parameters are analysed more in detail in the following chapters.

Despite the fact that in the past there has often been a search for the best parameters for making cuts, there are not many of articles in the literature analysing the variation of these optimal parameters and the response of the material as the temperature of the part increases.

Since laser cutting is a thermal process, heating of the workpiece is unavoidable, and over the years solutions have been sought to overcome this problem, for example by using different cutting paths, avoiding paths that are too close together to avoid overheating the workpiece or to give it a chance to cool down, or the use of a coolant to guarantee continuous control of the temperature of the sheet metal.

The aim of this thesis work, was to specifically analyse the behaviour of aluminium Al5754 at varying temperatures, analysing the cutting quality at high temperatures and the possibility of optimising the cutting parameters even at these temperatures.

In addition, we wanted to analyse an extremely important problem in the industrial field when we speak of increasing temperature, namely the problem of the dimensional correctness of the parts after cutting, due to the strong expansion of the sheets at high temperatures.

The objective of this thesis was to analyse the response of this specific material to high temperatures, studying the shear quality trend for different thicknesses, and identifying a possible temperature range in which the shear quality was acceptable.

We also wanted to analyse the expansion trend of the plates subjected to heating, studying the process through the linear expansion model and observing experimentally whether this behaviour was respected.

For this reason, it was necessary to devise and develop a heating system that was suitable for the purpose, whereby first the laser cutter itself was used to carry out the heating, using specific geometries, and then a heating system was developed and implemented using cartridge heaters, which turned out to be much more stable and reliable.

The present thesis work consists of 10 chapters. After a brief introduction, Chapter 2 is presented, where we look at the material studied, namely aluminium and its importance in the modern industry, the typical characteristics of laser cutting, as well as the typical laser cutting parameters for aluminium at different thicknesses.

The main defects studied at an industrial level, such as streak formation, burr formation or the dimensional problem, are then shown, where an initial explanation of the thermal expansion model and its industrial relevance is given.

The methods by which temperatures are conventionally measured in the literature are then presented, which are divided into contact and non-contact methods, and finally the importance of the emissivity value and its detection is explained.

The next two chapters (Chapter 3 and Chapter 4) present the aims of the work and the thermal expansion model used for the subsequent experiments to investigate the thermal expansion problem and the resulting dimensional inaccuracies.

Chapter 5 shows the experimental set-up as well as all the necessary instrumentation used during this thesis work.

Chapter 6, on the other hand, provides an overview of the possible heating methods to be used in order to obtain sufficient and as homogeneous heating of the sheet metal as possible.

In Chapter 7 we have the experimental campaign carried out using laser cutting itself as the heating method by means of specific geometries, where the material's response to cutting after this heating method is analysed.

Chapter 8 presents instead, the experimental campaign carried out through heating using a special electric resistance allocation base itself heated by means of cartridge heating elements, again showing the various problems encountered in the material at the various temperatures, and also analysing the problem of geometric inaccuracies, as this method proved to be extremely more effective and controlled, guaranteeing homogeneous heating of the sheet.

A final campaign for the correction of the geometric error at the various temperatures and thicknesses is therefore carried out in Chapter 9, using the linear thermal expansion model

obtained through the experimental campaign, in which a compensation method is used for the variation of the dimensions of the part due to its heating based on a system already present within the laser machine itself.

Finally, in the concluding chapter (Chapter 10), closing considerations are drawn and possible future developments and investigations are presented.

2. State of the art

2.1 Aluminium (Al) and its alloy

Aluminium (Al), occurs in great abundance, being the second most plentiful element in the earth's crust (1), its compounds in fact form 8 percent of the latter.

Because of its reactive nature it does not normally exist in the metallic state but rather in combination with oxygen, silicon, fluorine, and other elements (2) in the mineral form of Bauxite.

It is a fundamental metal of the era of technological development with immense possibilities for its use in industry, construction, aerospace, electronics and packaging.

Table 1: Physical and mechanical properties of aluminium (3)

Property of Aluminium					
Density [Kg*m^3]	Elastic Modulus [MPa]	Poisson's ratio	Tensile strength [MPa]	Ultimate strength [MPa]	Maximum allowable stress [MPa]
5754	0.40	0.40	0.10	0.50	93.75

Aluminium metal is supplied by two distinct aluminium-production sectors: primary aluminium producers and secondary aluminium smelters (3). The primary aluminium industry produces aluminium mostly from mined ore (bauxite), while the secondary aluminium is derived from the recycling of the aluminium scraps.

The continuing growth in aluminium recycling has increased the value of aluminium itself, yielded energy savings, and resulted in ecological benefits. (4)

A concise list of the peculiarities of aluminium may well explain why this metal production and usage is increasing so much over the years. (5)

- LIGHTWEIGHT: At the same volume, aluminium weighs about 1/3 of copper and steel. (6) Also, for this reason, a large proportion of modern transportation vehicles of modern design are built using high percentages of aluminium: the new legal requirements concerning fuel consumption and environment protection have, in fact, intensified the weight-reduction attempts by automakers (6).

- RESISTANCE TO CORROSION: Aluminium oxidises immediately in contact with air, creating a surface protection film of Aluminium oxide that makes it resistant to water and some chemicals. This characteristic makes it the most widely used metal in the industries of transportation, building and construction industries.

- DUCTILITY AND MALLEABILITY: Aluminium is easily machined and suitable for undergoing processes at both high and low temperatures. Given the countless processes to which aluminium can be subjected, there is the possibility of obtaining endless profiles with different shapes that can be used for different fields of application.

- PRODUCTION COST: Producing aluminium from scratch, has an energy cost of 13 kWh/kg. Producing recycled aluminium cuts this cost by 95%. Worldwide, 80 million tons of aluminium are produced annually, of which nearly 30 million tons come from recycling.

- RECYCLABILITY: Aluminium can be recycled 100 percent and countless times without losing its original characteristics that remain unchanged indefinitely, even following numerous recycling stages, that is, when from being primary aluminium the metal acquires the definition of "recycling aluminium" or "secondary aluminium".
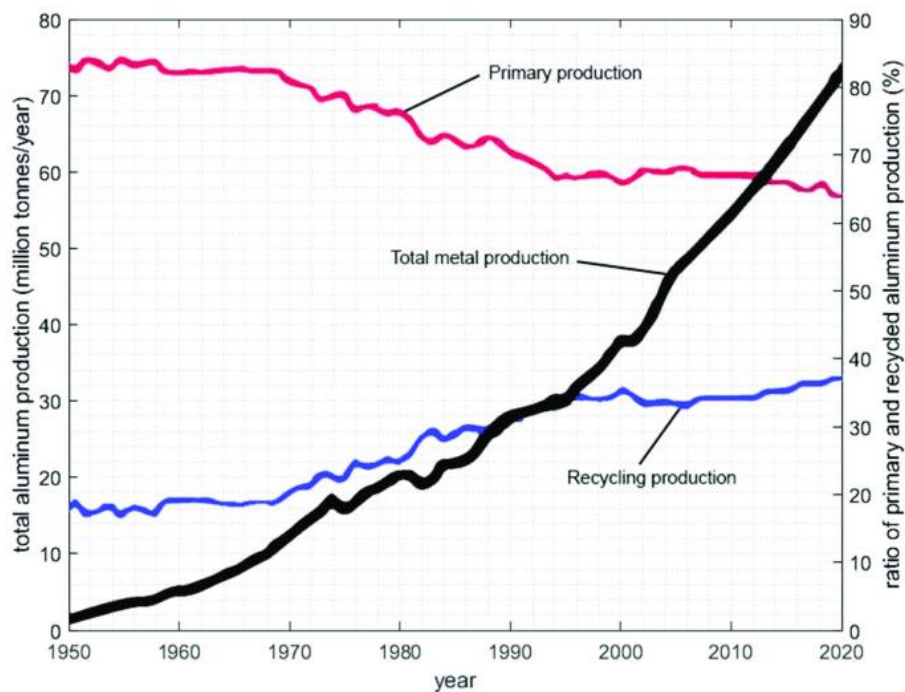

Figure 1: Aluminium yearly production & the percentage of recycling component in aluminium production
(7)

- HIGH ELECTRIC and THERMAL CONDUCTIVITY: used for the majority of high-voltage conductors, heat conditioning equipment and cooking containers for food.

- REFLECTIVE CAPACITY: It diffuses and reflects light, reducing the dispersion of the brightness from the light source and thus promoting energy conservation.

- AMAGNETICITY: This characteristic allows its use in the construction of devices such as radios, radars, and stereos.

The importance of aluminium and its alloys as engineering materials is reflected by the fact that out of over 1600 engineering materials available in the market today more than 300 wrought aluminium alloys with 50 in common use. (7)

Wrought alloys are subdivided into different categories and identified with different codes/digits basing on their compositions (see Table 2):

Table 2: Wrought alloys designation system (8)

Alloy Series	Principal Alloying Element
1xxx	99.00% Minimum Aluminium
2xxx	Copper
3xxx	Manganese
4xxx	Silicon
5xxx	Magnesium
6xxx	Magnesium and Silicon
7xxx	Zinc
8xxx	Other Elements

For the 2XXX to 8XXX groups, the last two digits identify different aluminium alloys in the group. The second digit indicates alloy modifications. A second digit of zero indicates the original alloy and integers 1 to 9 indicate consecutive alloy modifications. (9)

2.2 Laser cutting of Aluminium and its alloys

"LASER" is an acronym for Light Amplification by Stimulated Emission of Radiation.

Lasers are devices that amplify light by producing monochromatic and coherent light beams, with frequencies from infrared to ultraviolet, and recently also in the X-ray range. Laser light is characterized by high power and strong directionality and has proven to be a valuable tool in the industry, scientific research, and communication techniques. They also find important applications in medicine, military technology and even the arts, despite the fact that it was first defined as "a solution to a concrete problem" when, in 1960, Theodore Maiman created the first synthetic ruby laser producing a perfectly straight red laser beam (10).

A typical working station for laser is constituted by:

- an active medium, which is a material (gas, crystal, liquid) with a suitable set of energy levels to support population inversion;
- a pumping system, which supplies energy to the active medium to obtain population inversion;
- an optical cavity, or optical resonator, to produce optical feedback and sustain population inversion;
- laser beam transport system;
- laser beam focusing system;
- laser beam handling system.

2.2.1 Laser characteristics

A laser beam is characterized by:

- Monochromaticity: all photons are emitted with the same energy, and since it is known that the energy of a photon determines its wavelength, all the emitted photons have also the same wavelength (and frequency).
- Coherence: electromagnetic waves are moving precisely with the same phase (space coherence and time coherence).
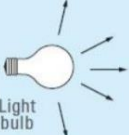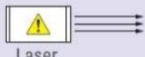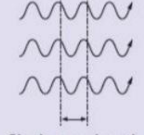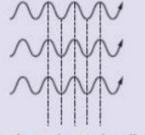
Figure 2: Monochromaticity and Coherence of lasers (21)

- Collimation/Directionality: Laser beam follows parallel rays with a very low divergence angle ϑ.

$$Divergence\ angle \quad \vartheta = \frac{1}{\pi} \times \frac{\lambda}{d_0} \tag{2.1}$$

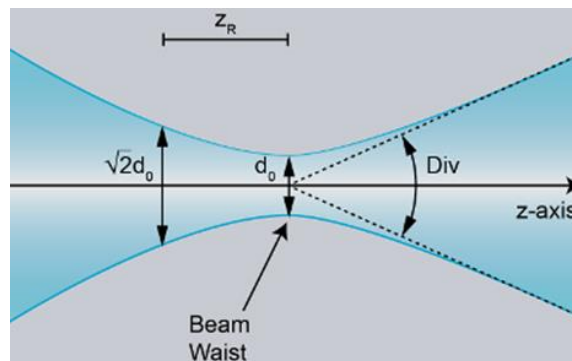Where d_0 represents the minimum diameter inside the source.

Figure 3: Laser beam divergence angle (22)

- Irradiance I or power density $[W/m^2]$ of the beam: that represents the amount of energy per unit of surface.

The power density is not constant across the cross-section of the laser beam but has a spatial distribution due to the size and geometry of the resonant cavity.

The most important distribution is certainly the Gaussian one in which most of the power density is concentrated right on the axis of the beam.

In this way we can also identify a non-dimensional parameter called Beam quality factor, expressed with the symbol M^2, which is defined as the ratio between the divergence angle of our beam and the divergence angle of the Gaussian beam.

$$\textit{Beam quality factor} \qquad\qquad M^2 = \frac{\vartheta}{\vartheta_G} \qquad\qquad\qquad (2.2)$$

Where ϑ_G is the divergence angle of a Gaussian and allows us to compare our beam with the Gaussian one in terms of quality.

The Beam quality factor of a Gaussian is equal to 1 and we can express, joining the two equations, the divergence of our beam as

$$\textit{Divergence angle} \qquad\qquad \vartheta = M^2 \times \vartheta_G = M^2 \times \frac{1}{\pi} \times \frac{\lambda}{d_0} \qquad\qquad (2.3)$$

So, we want M^2 and λ as smaller as possible to decrease the divergence and decrease the spot size of the laser and increase the radiance.

Once generated, the beam must be transported from the source to the area where processing takes place, ensuring the necessary degrees of freedom for relative movement between the beam and workpiece.

There are generally two transport systems that can be used:

- Optical chain:

The beam is transported by mirrors, which are sometimes movable. In general they are made of copper or silicon and can be coated with highly reflective materials with strong antioxidant properties.

- Optical fiber:

Consisting of a circular-section core of material transparent to the laser beam contained in an outer sheath that reflects the radiation. The operation of this technology is based on the phenomenon of total internal reflection of light based on the principle of the Snell's law that assesses that overcoming a certain critical angle (θ_c) of incidence of the light, there will be no more transmission but only reflection. This happens when light attempts to move from a medium having a given refractive index to a medium having a *lower* refractive index. (8) The main issues to be taken into account are the different behaviour of the optical fibers as the wavelength changes. For example, the excessive absorption makes this transport system ineffective for wavelengths of 10.6 μm.
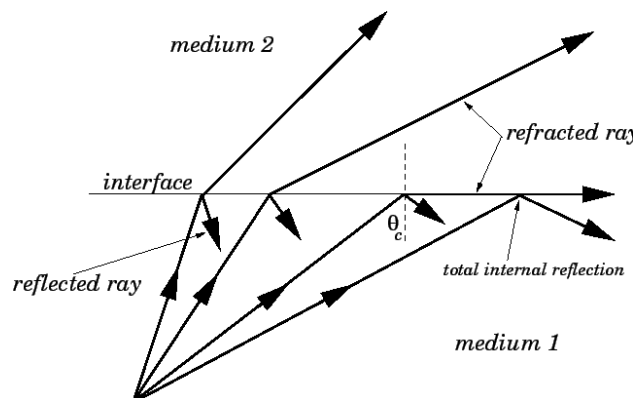

Figure 4: total internal reflection (23)

Once transported to the working zone, the laser beam must be focused on the desired spot, both to increase the power density and to have the precision of processing required.

The first solution is typical of lasers that exploit as active material Nd:YAG (solid-state) or CO_2 (gaseous state) of relatively low power (indicatively up to 4 kW). For higher powers, the lens undergoes excessive temperature rise which leads to damage to the lens itself. In contrast, the mirror solution is mandatory for CO_2 laser sources since these do not pass through the glass.

The focusing of a beam carried by optical fiber is done through two different lenses. At the output of the optical fiber, in fact, the beam diverges and must be collimated through a collimation lens and then focused with a focusing lens, as depicted in Figure 5.
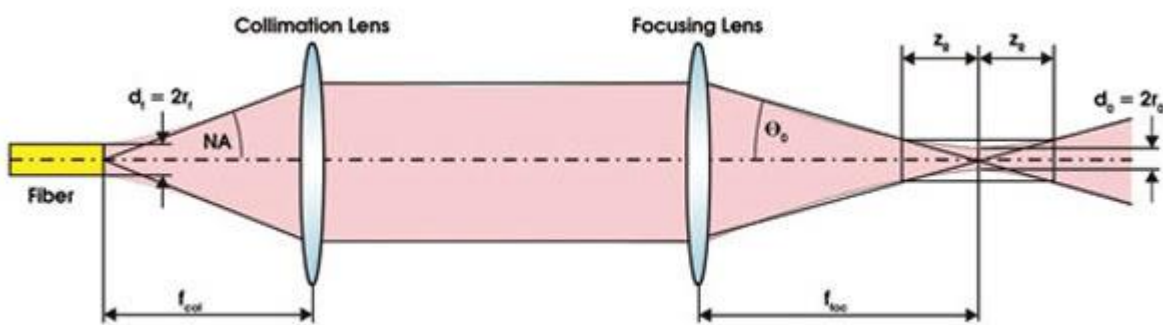
Figure 5: Collimation and focalization of a fiber laser beam (24)

From the focusing distance f_{foc} and the collimation distance f_{col} (as well as the wavelength λ) will depend on the minimum focal spot size, which can be obtained according to the following relationship:

Waist diameter
$$d_0 = d_{f0} \times \frac{f_{foc}}{f_{col}}$$
(2. 4)

With d_{f0} the core diameter of the transmission fiber.

2.2.2 Laser cutting

In the past, laser sources have been widely used in metal processing such as cutting, welding, and heat treatment. Laser cutting is now widely used industrially in the processing of both flat elements (with thicknesses ranging from a few micrometers up to 30 mm approximately), as well as components with extremely complex 3-D geometry, thanks to the high degree of automation achievable with this technology.

During the process, the material directly invested by the laser beam will be melted and/or vaporized (depending on the type of material being processed and depending on the energy delivered) while a gas jet coaxial to the beam will remove the material from the

affected area. A vertical channel called "keyhole" will be generated that runs along the entire thickness and will ensure the separation of the parts.

The energy provided by the laser beam will partly allow the phase transition of the material, partly will be dissipated by conduction within the bulk and partly will be absorbed and/or reflected by the plasma that is formed within the keyhole itself, following the vaporization of the material itself.

One of the main aspects to consider is the interaction between the laser and the material being processed.

If, in fact, our laser beam possesses a certain power, not all of that power will be useful in achieving our goal for the purpose of cutting or other technological processes. This happens because part of this energy is transmitted and/or reflected and only the remaining part is absorbed, and it should be noted that the reflected energy especially for highly reflective materials such as aluminium or copper, turns out to be almost the entirety of the incident power.
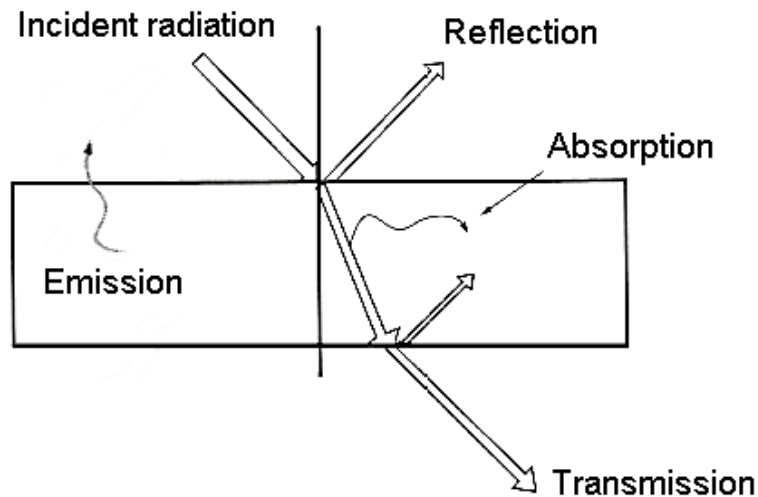
Figure 6: Laser-Material interaction (25)

We can call the ratio between the absorbed power (P_a) and the incident one (P_i) as A, Absorption coefficient:

$$\text{Coefficient of Absorption} \qquad A = \frac{P_a}{P_i} \qquad\qquad (2.5)$$

The ratio between the reflected power P_r and the incident power called Reflection coefficient R:

$$\text{Coefficient of reflection} \qquad R = \frac{P_r}{P_i} \qquad\qquad (2.6)$$

And then the ratio between the transmitted power P_t and the incident one called Transmission coefficient T:

$$\text{Coefficient of transmission} \qquad T = \frac{P_t}{P_i} \qquad\qquad (2.7)$$

We obtain that the sum of these three coefficients is equal to 1, because we consider that all the incident power is subdivided into the described three terms:

Incident power
$$P_i = P_a + P_r + P_t \tag{2.8}$$

$$A + R + T = 1 \tag{2.9}$$

The absorption coefficient depends on different factors:

- Laser source
- Material
- Surface roughness – higher the surface roughness higher the absorptivity
- Temperature –
  If the temperature of the material increase, also the absorptivity coefficient increase. What is also clear from the graph in Figure 7 is that with the phase change, the liquid or vaporized material can see a very rapid increase in the absorptivity, with that, if during the process we have the creation of a layer of liquid metal on the top of the surface the process can proceed easily.
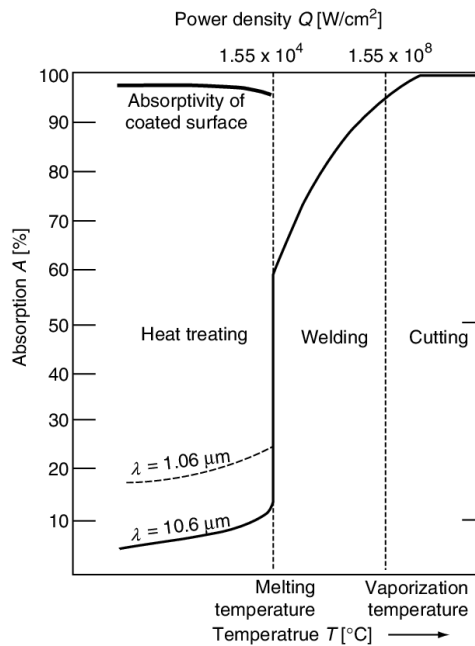
Figure 7: The effect of the temperature on the laser light absorptivity (26)

- Wavelength –
  Absorption coefficient depends also on the wavelength of the laser source and on the working material; higher wavelengths are most useful with iron and steel, or for non-metals, while lower wavelengths are preferable with highly reflective metals like aluminium or copper.
  From the graph below it is also possible to see a peak of absorption for the aluminium for a wavelength around 1 μm and for this reason cutting aluminium with fiber laser is one of the best choices.
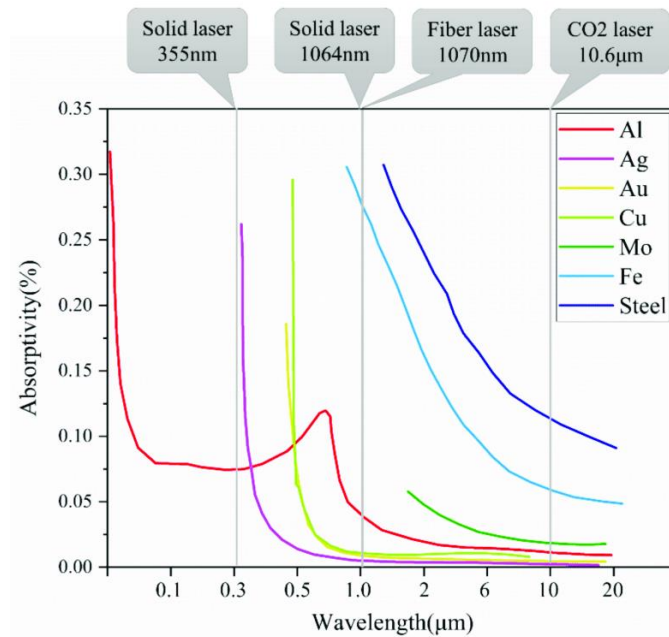
Figure 8: Wavelength dependence on the absorption rate (27)

Solid state sources like Nd:YAG or Ytterbium active fiber as active medium are able to generate laser beam with emission wavelengths of 1.064 μm and 1.070 μm respectively, which are able, as we can see in the picture, to assure a higher value of absorptivity by metallic materials and allow to process highly reflective metals such as aluminium or copper.

Unlike CO_2, fiber laser technology uses a solid gain medium, instead of a gas or liquid. Thanks to its small wavelength, with fiber lasers we can produce an extremely small spot size (up to 100 times smaller compared to the CO_2). This is one of the main advantages of fiber compared to CO_2. (11)

Fibre laser cutter benefits include:

- Rapid processing times.
- Reduced energy consumption & bills – due to greater efficiency.
- Greater reliability and performance - no optics to adjust or align and no lamps to replace.
- Minimal maintenance.
- The ability to process highly reflective materials such as copper and brass
- Higher productivity - lower operational costs offer a greater return on your investment. (12)

Another advantage of fiber lasers is that the laser light is both generated and delivered by a flexible medium, which allows easier delivery to the focusing location and target. In addition, we can obtain high output power compared to other types of laser and support kilowatt levels of continuous output power because of the fiber's high surface area to volume ratio, which allows efficient cooling. (12)

14

2.2.3 Process parameters for laser cutting of Al and its alloys

The capability of the laser cutting technology mainly depends on the optical and thermal properties rather than mechanical properties of the material to be cut. (13)(14)

Aluminium (Al) and its Alloys are considered as difficult-to-cut materials with laser cutting process (15) because it is affected by:

- the high reflectivity that causes the need of high laser power and the problem of the back-reflected beams;

- the high thermal conductivity that produces a large heat-affected zone (HAZ);

- the formation of an aluminium oxide layer on the molten material that prevents the use of reactive laser fusion technique; (13)

- the high viscosity of molten material that makes its removal difficult. (16)

The proper selection of process parameters plays a crucial role to gain the required cut quality in such materials. (13)(17)(18) For that reason, the effects of the different process parameters on the cutting quality were investigated for the detection of the optimal cutting parameters, which obviously depend on various conditions, one of the most important of which is the thickness of the material to be cut, as this leads to the modification of various parameters such as focal position, power, cutting speed or Stand Off Distance (SOD).

The specific mechanism used to reach laser cutting of Al and its alloys is called Melt and Blow cutting, that is a specific Fusion cutting process achieved by continuous laser and thus through continuous removal of material used for materials with low/medium thickness, the main feature is the use of inert gas such as argon or nitrogen at high pressures, which has the task of expelling the melted material away from the laser beam.

2.3 Typical defects during laser cutting of Al and its alloys

Different standards define possible imperfections, defects, and dimensional tolerances and impose survey criteria to quantify the quality of laser cutting.

Defining imperfection as any irregularity with respect to the specified shape of the cut and defect as an imperfection that cannot be accepted.

During the cutting process, the material directly invested by the laser beam will be melted and/or vaporized (depending on the type of material being treated and depending on the energy delivered) while a jet of gas coaxial to the beam will provide for moving the material away from the affected area. A vertical channel called a keyhole will be generated that runs along the entire thickness and ensures the separation of the parts.

The energy supplied by the laser beam will in part allow the phase transition of the material, in part will be dissipated by conduction within the bulk and in part will be absorbed and/or reflected by the plasma that is formed within the keyhole itself, following the vaporization of the material itself.

Given how the mechanism just described takes place, the main defects of this type of cut can include, among others: burr formation, inaccuracies in the creation of the cut, dimensional accuracy problems, thermal degradation, etc.

2.3.1 Striations and Burr formations

Burr formation, which can develop exclusively in cutting by fusion. Burr is formed on the lower edge of the cut edge as a result of the sudden solidification of molten material that is ejected from the groove itself by the gas jet. For this very reason, one of the parameters on which to act to avoid burr formation is precisely the gas pressure; increasing the latter increases the thrust on the spindle and thus its evacuation.

The problem of burr is particularly evident in the cutting of materials like metals and often consists of an extremely brittle metal oxide, easily removed by brushing.

Another typical defect obtained cutting through these methods is the presence of striation, again due to the discontinuity of the re-solidification process on the kerf side.
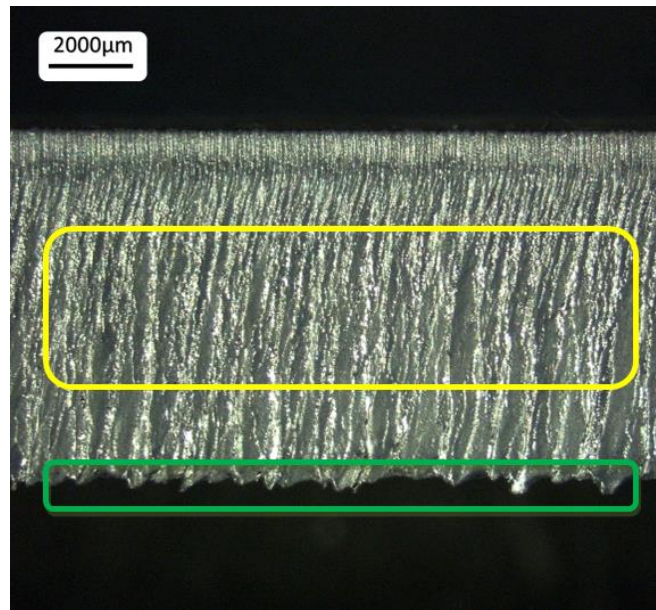
Figure 9: Example of striation (Yellow highlighted zone) and burr formation (Green highlighted zone) on an aluminium sample cut with melt and blow cutting.

As explained by several authors who have analysed these issues previously (15,17,19–21), parameters such as cutting speed, power, focal distance, or gas pressure are critical to the surface quality of the cut workpiece, and their optimization leads to the desired results.

In Leonardo Daniele Scintilla's work, for example, it is shown how for cutting a 2-mm-thick Al-1050 foil, there are optimal parameters for successful cutting.

For which regard for example the cutting speed, the decrease of cut quality, increasing too much the cutting speed, can be explained considering that the optimal cutting speed giving the best cut quality is lower than the maximum achievable cutting speed for the particular value of the set laser power. (13) When cutting speed is increased beyond optimal, phenomena such as dross formation and deterioration of cut edge roughness occur, and in order to have a better cut quality, assist gas pressure and laser power have to be increased. (13)

As shown in Sharifi-Akbari's work for example it can be seen that the increase in cutting speed has a beneficial effect on the surface roughness, but overcoming a certain optimal value (keeping the other values fixed), the surface roughness start to increase. (21)

The same reasoning can be made for laser power and SOD values, as can be seen in Figure 10, Figure 11 and Figure 12.

Regarding the increase in temperature during cutting, cutting speed and power have opposite effects.

In fact, by increasing the power we obtain as it is easy to deduce, a considerable increase in the temperature of the workpiece, while by increasing the cutting speed we reduce the laser-workpiece interaction time, and this leads to a reduction in the temperature of the workpiece at the end of the cutting operations.
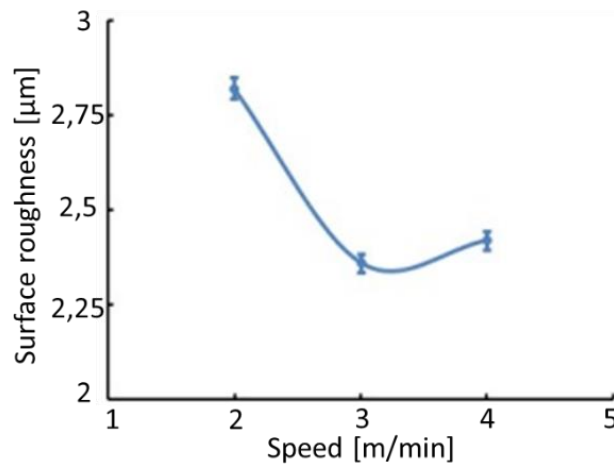
Figure 10: The effect of cutting speed on surface roughness at the laser power of 3000 W, gas pressure of 6 bar and sheet thickness of 1 mm (21)
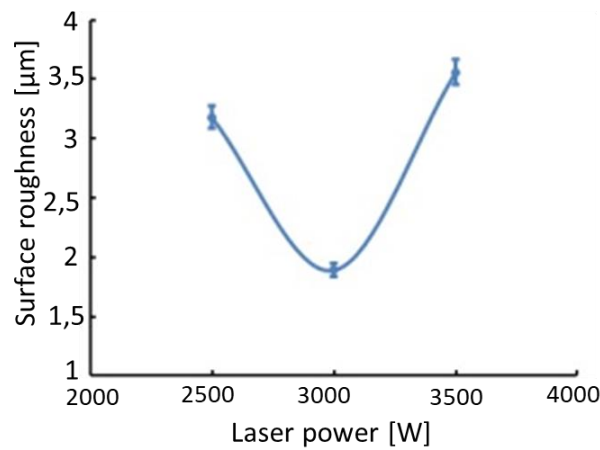
Figure 11: The effect of laser power on surface roughness at laser power of 3000 W, gas pressure of 6 bar and sheet thickness of 3 mm (21)
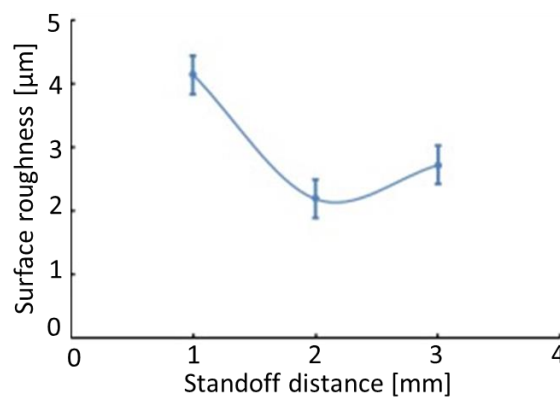

Figure 12: The effect of standoff distance on surface roughness at laser power of 3000 W, gas pressure of 6 bar and sheet thickness of 3 mm (21)

2.3.2 Kerf geometry and HAZ

Another typical defect can be the Taper, calculated as the difference in the cutting width between the top and the bottom surface, that create the so called Taper angle that is defined as shown in Figure 13, or the HAZ (heat affected zone) that represent a region of material being heat treated because of the laser process, that cause grain size changing and property changing of the material.

From the perspective of the material, the most important factor is the coefficient of thermal diffusivity. The diffusivity depends on the thermal conductivity, the density of the material, and its specific heat. The higher the thermal diffusivity, the faster the heat changes propagate.

In other words, the higher the diffusivity, the faster the cooling is and the HAZ is reduced. Conversely, lower coefficients mean that heat cannot be dissipated, and the thermal influence zone is larger.

Aluminium, having a high thermal conductivity coefficient, suffers less than other materials (such as carbon steels) from this issue.

From the perspective of the production process, the extent of the HAZ depends on three factors: the amount of heat applied, the duration of exposure, and the area affected. Providing large amounts of energy, for a long time, and with larger beams generates larger thermal influence zones.
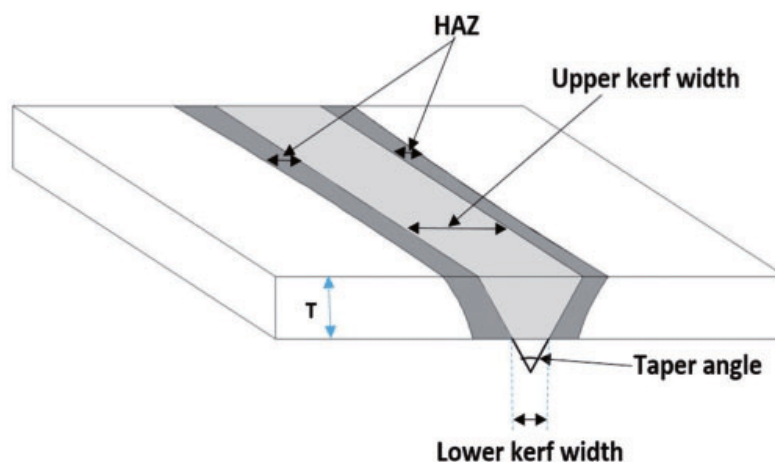
Figure 13: Kerf taper and HAZ (22)

The parameters that most influence the HAZ and the kerf width are laser power and cutting speed, but also other parameters are able to influence these cutting characteristics.

Stournaras, Stavropoulos and Chryssolouris investigated the effect of various parameters on cut quality, HAZ extension, and kerf width in their work, using a CO_2 laser for cutting the Aluminium alloy AA5083 (19)(20).

In their work in fact, we can see that laser power has the biggest effect in the HAZ. Increasing in fact the laser power we give more energy to the material that needs to be cut and as consequence the heat-affected zone becomes larger. Increasing too much the laser power, however, leads to an increase in the kerf width so we want to find as shown before, the optimal value for maximize the quality of the cut.

For the kerf width, instead, the most important parameter is the cutting speed; increasing it in fact we reduce drastically the kerf width and reducing the interaction time we can reduce also the HAZ.

These results can be seen in the following pie charts in Figure 14:
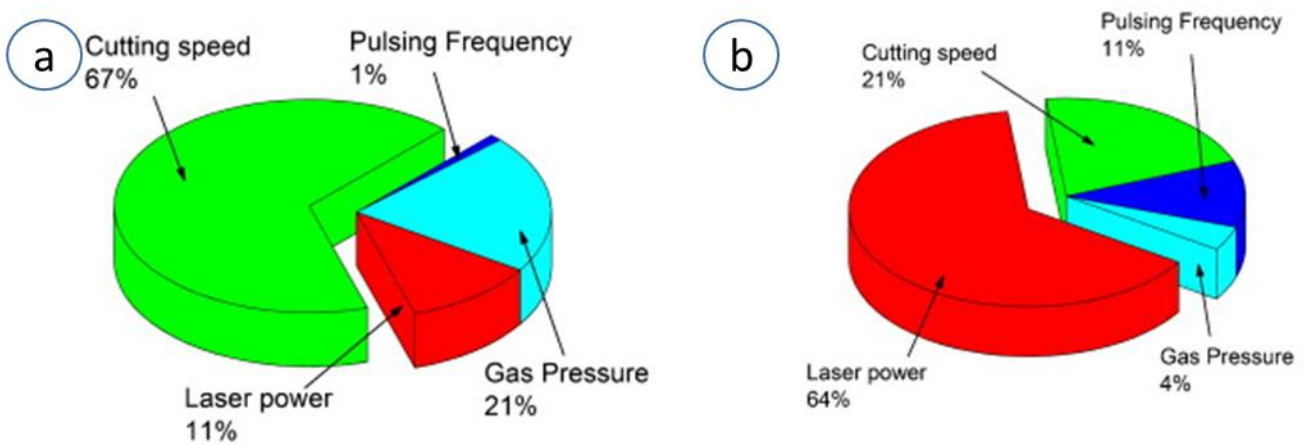
Figure 14: % effect of process parameters on kerf width (a) - % effect of process parameters on HAZ (b) (19)

2.3.3   Geometrical inaccuracies

2.3.3.1   Thermal Expansion

One important aspect that needs to be taken into account for this thesis work, and that would be faced with an experimental point of view in the following part, is an important property of most materials, whether it is solids, liquids or gases and it is that, when the temperature increases, they will expand. (23)

We have three types of thermal expansion: linear, superficial and volumetric expansion. We mention the first one in the case where the material has a fairly linear shape and therefore its expansion will be more noticeable in length (in one dimension). We talk about

the second, when we the body considered as a planar shape and so we need to consider a planar expansion (in 2D). Finally, the third one, when the material is homogeneous, that means that it has the same physical properties at every point and in every dimension. Therefore, the volumetric expansion of the solid or liquid under consideration will be considered (in three dimensions).

This happens because at higher temperatures, objects have higher kinetic energies, so their particles vibrate more. At these higher levels of vibration, the particles aren't bound to each other as strictly, so the object tends to expand.

For all solids, the change in length with temperature follows, with good approximation, the experimental law of linear expansion:

$$\text{\textit{Linear expansion}} \qquad L_f - L_0 = L_0 \times \alpha \times \left(T_f - T_0\right) \qquad (2.10)$$

$$\frac{\Delta L}{L_0} = \alpha \times \Delta T \qquad (2.11)$$

The elongation of the bar, ΔL , is given by the difference between the final length L_f at the new temperature and the initial length L_0. The coefficient of linear expansion (α) depends on the material of the bar.

The thermal expansion coefficient α is equal to the expansion of a bar of length equal to 1 m heated up of 1 Kelvin.

The product $L_0 \times \alpha \times \Delta T$, which is equal to ΔL, has the physical dimensions of a length. Thus, the product $\alpha \times \Delta T$ must be a pure number and, therefore, the physical dimensions of α is the reciprocal of those of ΔT. That is why it is measured in $°C^{-1}$ or in K^{-1}.
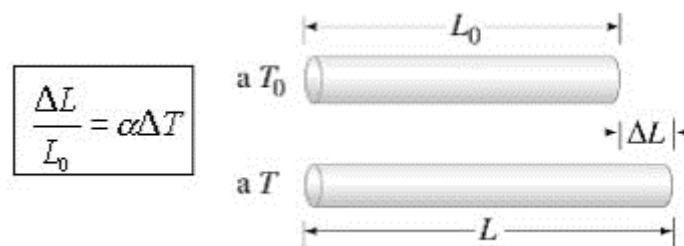
Figure 15: Linear thermal expansion (24)
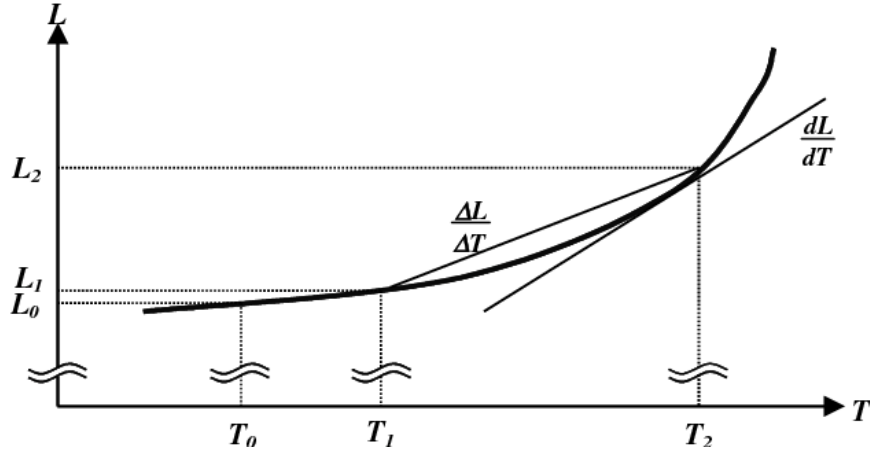
Figure 16: Sample change in length as function of the temperature (25)

As opposite to the previous definitions, we need to define the true coefficient of linear thermal expansion (26) (also referred to as thermal expansivity (27)) is related to the derivative $\frac{dL}{dT}$ at a specific temperature. (25) This represents the slope of the tangent to the curve of length against temperature in figure. The true coefficient can thus be defined as follows (25):

$$\text{Thermal expansion coefficient} \qquad \alpha_t = \frac{1}{L_0}\frac{dL}{dT} \qquad\qquad (2.\,12)$$

This represent the limit of the previous equation when $\Delta T \to 0$ and is the most appropriate definition for the thermal expansion coefficient (25).

For what concern the superficial expansion, which is basically an expansion of the linear law, we have:

$$\text{Superficial expansion} \qquad A_o = L_0^2 \qquad\qquad (2.\,13)$$

$$A_f = L_f^2 = (\Delta L + L_0)^2 = L_0^2 + 2 \times \Delta L \times L_0 + \Delta L^2 \qquad (2.\,14)$$

Where A_o and A_f represents the initial and the final area of the piece before and after the increasing of temperature.

Since the term ΔL depends on α that is a very little term, its power can be neglected and so also the term ΔL^2 can be neglected.

So:

$$A_f = L_0^2 + 2 \times \Delta L \times L_0 \qquad (2.15)$$

$$\Delta A = A_f - A_o = 2 \times \Delta L \times L_0 = 2 \times L_0 \times \alpha \times \Delta T \times L_0 \qquad (2.16)$$

$$\Delta A = 2 \times A_0 \times \alpha \times \Delta T \qquad (2.17)$$

$$\frac{\Delta A}{A_0} = 2 \times \alpha \times \Delta T \qquad (2.18)$$
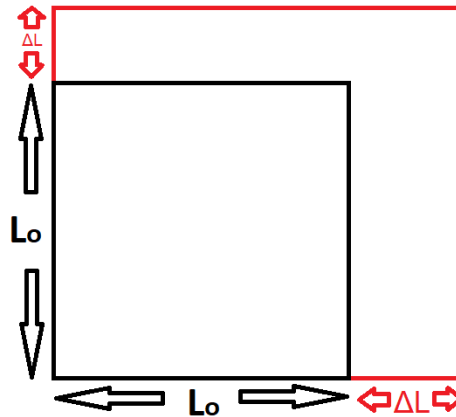
Figure 17: Superficial thermal expansion

In the case of volumetric thermal expansion, we can obtain by induction the experimental formula:

Volumetric thermal expansion $\qquad \Delta V = 3 \times V_0 \times \alpha \times \Delta T \qquad$ (2.19)

$$\frac{\Delta V}{V_0} = \beta \times \Delta T \qquad (2.20)$$

Where $3 \times \alpha = \beta$ is the volumetric thermal expansion.

For liquids and gases it does not make sense to talk about linear or superficial expansion since, they consider only the value of β for volumetric expansion.
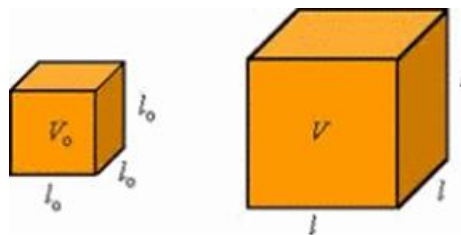
Figure 18: Volumetric expansion (28)

In Table 3 we can see some materials with their corresponding values of the coefficients of linear and volumetric expansion:

Table 3: Approximate Coefficient of Thermal Expansion at 20°C (29)

Approximate Coefficient of Thermal Expansion at 20 °C		
Material	$\alpha(10^{-6}/°C)$	$\beta(10^{-6}/°C)$
Aluminium	23	69
Concrete	12	36
Diamond	1	3
Glass	9	27
Stainless Steel	17	51

2.3.3.2 Industrial problems due to thermal expansion

Up to 75% of the overall geometrical errors of machined workpieces can be induced by the effects of temperatures (30).

For this reason, the thermal stability of the machine tool and the processed material is of critical importance.

The dimensional error parameters are calculated from the difference between the nominal and measured length, taking an adapted machine model into account (31,32).

A change in temperature from the reference temperature causes, in the case of isotropic materials, a linear change in space. In case, however, we were in the presence of an anisotropic material, the length variations can vary in space.

Temporal temperature variations cause varying length changes in time. Spatial temperature variations cause deformations depending on the position (30).

Hence the need to compensate for this geometric error, where in conventional manufacturing it is common practice to numerically correct linear length changes due to constant temperature deviations for both workpieces and machine scales, while for advanced manufacturing processes it is still under investigation.

Of course, an even more difficult challenge to overcome lies in the determination and correction of non-linear length changes.

Today, the ambition of every designer of highly efficient machine tools, particularly the ones to be used for precision machining, is to be able to accurately predict thermal errors through numerical simulations. Accurately predicted errors are the basis for their effective and easy compensation (30).

Continuous usage of a machine tool generates heat, which leads to thermal errors due to thermal expansions of structural linkages.

The heat generated causes the thermal deformation of the pieces we are working on, whether it is a foil, tube or object of another form.

In the last 20 years great advances in the modelling of thermal errors have been made.

The knowledge achieved through improved measurements and simulations is used with new methods for the compensation of thermal errors. A lot of models to compensate for the thermal errors via readjustment of the axes positioning by the machine tool's control are developed (29,32–34). Several indirect compensation procedures based on linear expansion models, rigid body models, neural networks, or other models have been developed. (30) These approaches are based on auxiliary values like temperature measurements. Other types are direct compensation approaches where the thermal displacements, e.g., of the tool relative to a fixed measuring probe in the working envelope, are measured periodically. (30)

Another way to correct this problem is, instead of compensating the thermal expansion, trying to avoid it, controlling the temperature of the tool or the workpiece through the use of cooling flows.

To control temperatures, e.g., temperature of coolants (35), ambient temperature, different techniques are used. In recent years, temperature control techniques have been improved and cooling strategies have been developed. (30)

The only problem is that the energy used for temperature control is not negligible, sometimes is even higher of the energy used for operation itself.

2.4 In-situ temperature measurement approaches during laser-based process

2.4.1 Thermo-couple measurements

A thermocouple is a sensor for measuring temperature. It consists of two different metals joined at one end. When the junction of the two metals is heated or cooled, a voltage is produced that can be related to temperature using a thermometer suitable for the purpose.

This is the Seebeck effect and is the basis of thermocouple operation. The Seebeck effect describes how two metals of different temperatures, when joined together generate a specific electromotive force. Much will depend on the type of metals used within the thermocouple, allowing more precise measurements of temperature and different ranges of it. For this reason, thermocouples are classified according to the pair of metals used.

Known for their versatility as temperature sensors, thermocouples can be made in extremely variable styles. They can be found as insulated or even bare wire or as thermocouple probes in which the wires are protected in a metal shield.

Thermocouples find use in a wide range of applications, from industrial uses to common temperature sensing in regular equipment. With the wide range of models available, it is extremely important to understand their basic structure and functionality, to better determine which is the best type of thermocouple to use.

We have already mentioned the different types of thermocouples on the market today, created to suit a wide range of application scenarios and environmental challenges and, most importantly, different temperature ranges. Letters of the alphabet are generally used to distinguish the different types; among the most common types of thermocouples are J, K, L, N and T.

Each of these letters indicates a different type of combination of metals of which the thermocouple joints are composed, a combination that is critical depending on the sensitivity needed to measure a given temperature range.

The K-type thermocouple is the most widely used thermocouple in industry and it is in fact, commonly used in several scientific papers to measure and predict the temperature (36). It consists of a combination of nickel-based wires (usually chromel/alumel); inexpensive yet reliable ensuring accurate measurement. Measurement ranges are generally between -200 °C and +1260 °C with a standard deviation of +0.75%. The nickel used (resistant to corrosion and oxidation) allows use in a wide range of applications. Specifically, the type K thermocouple wire includes a positive pole composed of about 90 percent nickel and 10 percent chromium, and another negative pole composed of 95 percent nickel, 2 percent aluminium, 2 percent manganese, and a remaining 1 percent silicon.

26

2.4.2 Pyrometric measurements

A thermal imaging camera is a special type of camera that is sensitive to infrared (IR) radiation radiated by all bodies with temperatures above absolute zero. The characteristics of the radiation emitted are a function of the temperature of the material: the hotter an object is, the greater the thermal radiation radiated. Thermal imaging cameras can perform a mapping of the distribution of infrared energy emitted by the body, constructing an image using conventional colour scale.

Infrared radiation emitted, is converged by the optical components (lenses) to a suitable detection apparatus consisting of an array of sensors, each of which is activated on the basis of the infrared energy striking it. The information thus collected is processed to generate a digital image. This, composed of a certain number of pixels, is grey scale, in which the level of brightness is a function of the energy detected by each sensor. To make it more interpretable, a false-colour map is created, by assigning, in general, red to the warmer parts and blue to the cooler parts, thus obtaining a heat map or thermogram.

Thermal imaging cameras detect thermal radiation and can be used to identify the surface temperature of objects and people. Because of this capability, thermal imaging cameras are commonly used as a noncontact screening tool to detect temperature differences at the surface and changes in heat distribution.

The use of a non-contact method of temperature measurement gives us the opportunity to obviate specific problems such as the difficulty, for example, of welding thermocouples on materials on which it is difficult to weld, but also to the possibility of measuring the temperature of moving parts (as is often the case in a factory), which would make the use of thermocouples extremely laborious and difficult.

Thus, in various works it has been used to assess the temperature of specific parts that are difficult to reach by contact sensing methods, such as in the work developed by Lanc and Zeljkovic (37) in which a piece of AW6082 aluminium alloy was placed inside a furnace to assess the correct emissivity value of the latter as the temperature changes.

2.5 Emissivity ε

Most metalworking processes, and thus also aluminium, are extremely temperature dependent. It is often necessary to reach high temperatures in order to achieve the desired microstructure, improved ease of processing, or higher product quality. This leads not only to the aforementioned expansion of the heated material, but also to another important goal, namely to be able to measure with adequate accuracy, the temperature of the body we want to process.

It is therefore necessary to develop and use techniques for the determination of temperature.

In addition to the more classic method of contact temperature measurement, that is, through the use of thermocouples, properly calibrated, which welded on the surface and connected to a computer, are able to report to us the temperature of the part, in this thesis work we have focused more on the use of another method, that is, that of remote temperature detection through a special thermo-camera that use the intensity of the thermal radiation of the surface of the target to detect the value of temperature.

Radiation thermometry is highly dependent on the surface emissivity. All radiometric methods are sensitive to changes in the spectral emissivity of the material and they also require some knowledge of the surface emissivity. (38) Therefore, complex behaviour of emissivity variability is the major reason behind the limited accuracy of radiation thermometry. (38) Aluminium surface emissivity is known to be influenced by the effects of sample temperature, wavelength, heating time, alloy composition, surface finish (roughness and surface oxidation), environment, and process conditions. (38)

We define emissivity as the ratio of the radiation emitted by the surface to the radiation emitted by a blackbody at the same temperature (39):

$$\textit{Emissivity} \qquad \varepsilon(\lambda, T) = \frac{I_{\lambda,e}(\lambda,T)}{I_{\lambda,b}(\lambda,T)} \qquad (2.\,21)$$

Where $I_{\lambda,e}$ is the radiation emitted by the surface and $I_{\lambda,b}$ is the radiation emitted by the black body, which is an ideal emitter, meaning that no surface can emit more radiation than a blackbody at the same temperature. Therefore, the blackbody represents a reference in describing emission from a real surface. (37)

Because the emissivity of metals depends on several factors, many authors have tried to determine the relationship between emissivity and the parameters mentioned above.

Wen and Mudawar have done several cases where they showed that the emissivity of 4 different aluminium alloys: AW 1100, AW 7150, AW 7075 and AW 2024 manly decreases

appreciably between 2.05 and 3.5 µm, and increases slightly between 3.5 and 4.72 µm. Authors also showed that emissivity decreases between 600 & 700 K and rises between 700 & 800 K, while, generally speaking, emissivity increases with the increase of surface roughness (40,41).

After them, Lanc and Zeljković proved that the emissivity of AW 6082 aluminium alloys decreases with increasing temperature in the temperature range from 50 to 200°C and decreases with increasing roughness from 1.07 to 1.77 µm in the spectral range from 8 to 14µm. The values of the emissivity are in the range from 0.07 to 0.3 (37), in good accordance with other authors.

Because of its complex emission behaviour, determining the temperature of aluminium with the aim of infrared thermography can be problematic. (37) Given the fact that we cannot find the table for the emissivity of aluminium depending on the temperature, roughness and types of alloys in the literature, the issue can become more complicated. (37)

In addition to the above considerations, during thermography tests it must be taken in consideration the influence of other heat sources, because aluminium is highly reflective material. This parasite radiation can lead to significant errors in the measurement. (37)

In the experiment of Lanc and Zeljković they considered the effect of temperature and surface roughness on the spectral emissivity of AW 6082 with its own specific composition.

The surface roughness was analysed in four different cases with a roughness that went from 1.07 [µm] to 1.77 [µm] indicated with G.1, M.1, M.2 and M.3 (one grinding sample and three milling samples).

Here are some graphs of the obtained results:
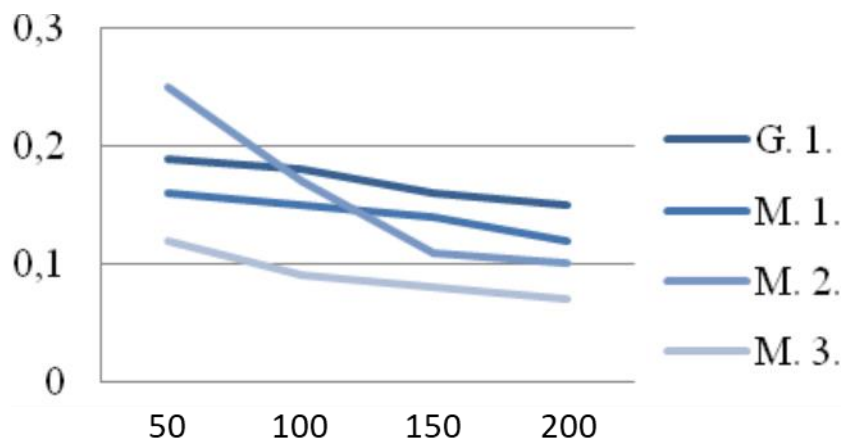
Figure 19: Temperature effect on the emissivity ε (37)
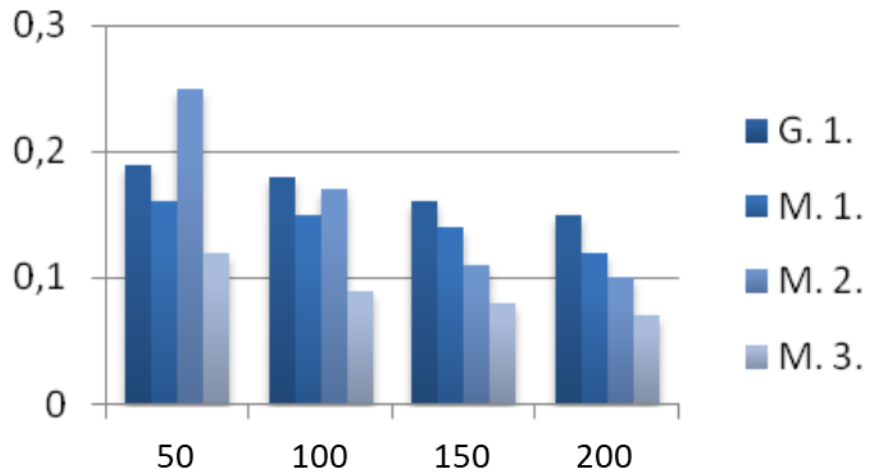
Figure 20: Surface roughness effect on emissivity ε (37)

These figures give us the possibility to observe the obtained results previously mentioned.

With regards to the dependence of the emissivity on the roughness of the surface, Issam Mudawar developed an empirical model to describe this relation:

E*missivity of the rough surface* $\varepsilon_r = \left[1 + \left(\frac{1}{\varepsilon_s} - 1\right) \times R\right]^{-1}$ *(2. 22)*

Where ε_r *and* ε_s are the effective emissivity of the rough surface and the smooth surface, respectively, and where R is called roughness factor and represent the ratio between the area of the smooth surface and the corresponding rough area considering the depression given by the roughness (42):

R*oughness factor* $R = \frac{A_s}{A_r}$ *(2. 23)*
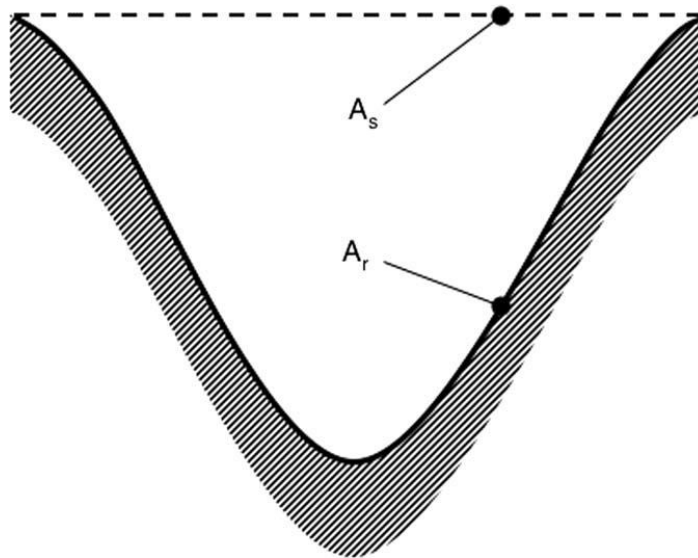
Figure 21: Idealized representation of roughness features (42)

3. Aims of the work

Excessive heating of metal sheets or tubes during laser cutting operations can cause deterioration or even in some cases lead to the failure of the cut itself, thus also causing downtime for the machine and companies.

This is especially true when laser cutting with oxygen as an assistant gas, of fairly thick plates (>10 mm), because the input power is high, and the cutting speed is lowered considerably, which gives the heat much more time to spread and propagate.

However, this problem is also relevant in the laser cutting of aluminium sheets and tubes, where metal sheets are very sensitive to heat due to the high thermal expansion coefficient of this material, which causes it to suffer more from the problem of expansion, and due to the very close cutting geometries that usually are cut, the temperature rises a lot, for this reason sheet and tubes are extremely sensitive to deformation and elongation caused by the excessive thermal load.

However, it is possible to implement certain strategies to deal with deterioration due to heat build-up during laser cutting of sheet metal and pipes of various thicknesses:

- Optimise the cutting process parameters for heated zones
- Generate a cutting path that avoids as much as possible the overheating of the plate or the presence of zones that are significantly hotter than others
- Use an active coolant to remove excess heat
- Make a correction on the machine for dimensional error

For each of these strategies to be implemented, it is crucial to correctly identify where and when heat build-up occurs and at what temperatures we notice the various types of deterioration or expansion.

This can be done using real-time temperature measurements or by simulating the propagation of heat in the metal sheet.

The objective of this thesis work was in fact to investigate the deterioration in the cutting quality of aluminium Al 5753 due to heat accumulation and cutting at high temperatures, carried out for different thicknesses of the aluminium sheet; specifically for the thicknesses of:

- 2 mm
- 5 mm

- 8 mm

and identify a possible critical temperature that would lead to a deterioration that was no longer acceptable.

It was also of considerable importance to experimentally analyse the thermal expansion to which the sheet metal was subjected at various temperatures in order to compare it to theoretical models of linear thermal expansion and to develop a strategy to eliminate or implement this type of problem.

This study, therefore, had to be carried out in several steps:

- identify the optimal cutting process parameters for cutting different thicknesses of the selected aluminium

- study and develop a preheating method to bring the sheet metal to the desired temperature (through the laser itself or through other methods to be studied)

- carry out the experimental activity by varying the preheating temperature and the thickness of the sheet metal

- devise a strategy to ensure a correct cut from the point of view of both the quality of the cut and the dimensions.
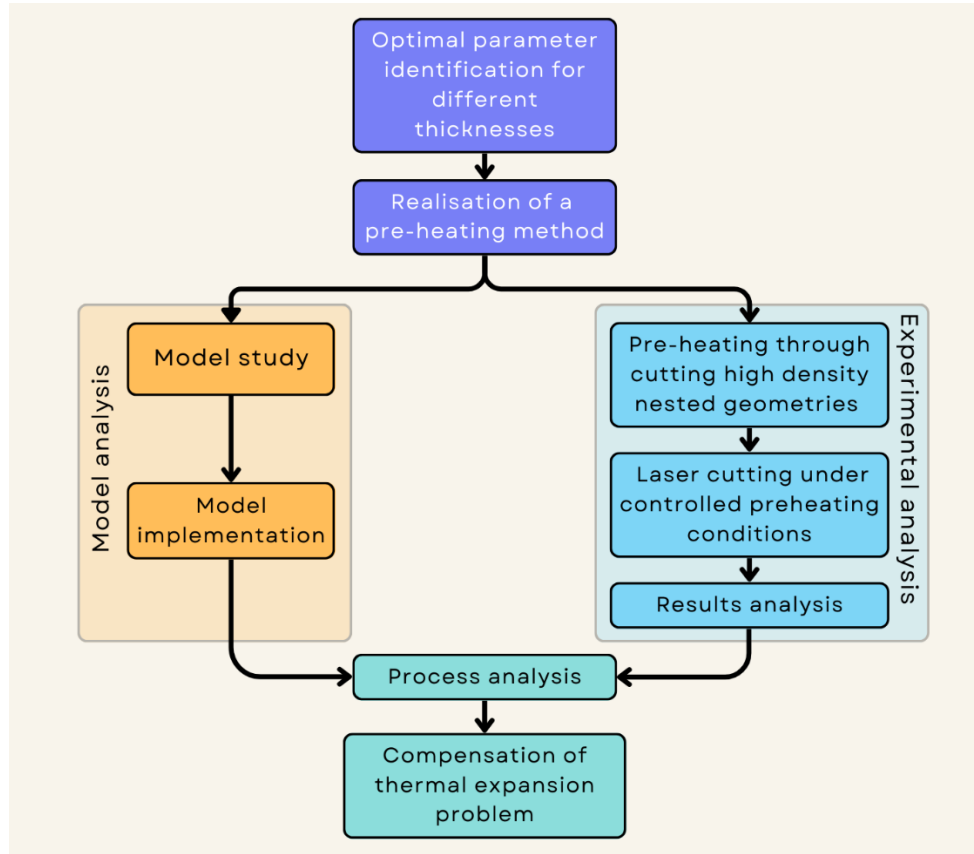
Figure 22: Thesis work scheme

4. Model

4.1 Analytical modelling of the thermal expansion of metals

Thermal expansion is the tendency of materials to change their dimensions in response to changes in temperature.

The amount of thermal expansion depends on the type of material and the temperature change. Some materials, such as metals, have a high thermal expansion, which means that they change their dimensions significantly when the temperature varies by even a few degrees. Other materials, such as ceramics, have a low thermal expansion and change their dimensions very little when subjected to temperature changes.

Aluminium is a metallic material that has one of the highest thermal expansions among metals. The coefficient of linear thermal expansion of aluminium is approximately 23.1 x 10^-6 /°C (43), which means that for every degree Celsius of temperature increase, aluminium will expand by approximately 23.1 micro-meters per meter in length.

The thermal expansion of aluminium is also influenced by the alloy of which it is composed. For example, pure aluminium has a higher coefficient of thermal expansion than aluminium alloyed with other metals such as copper, magnesium or silicon. In addition, the starting temperature and the final temperature to which the aluminium is subjected also affect the thermal expansion.

To minimise these problems, it is important to consider the thermal expansion of aluminium during the design phase and choose aluminium alloys with lower coefficients of thermal expansion for applications where thermal expansion is a critical issue.

As mentioned above, it is possible to consider three different types of thermal expansion, depending on whether the one-dimensional, two-dimensional, or three-dimensional case is to be analysed.

For the simplified case that considers a one-dimensional linear thermal expansion, the equation is as follows (as we can also see in Figure 23):

Linear expansion $\qquad L_f - L_0 = L_0 \times \alpha \times \left(T_f - T_0\right)$ $\qquad$ (2. 10)

$$\frac{\Delta L}{L_0} = \alpha \times \Delta T \qquad (2.\,11)$$
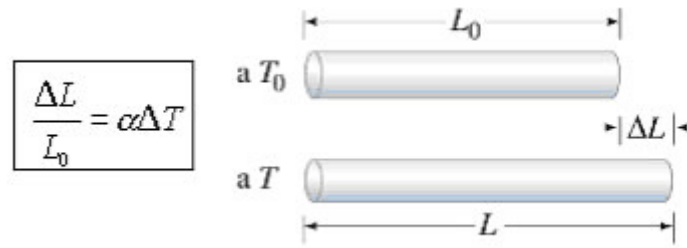
Figure 23: Linear thermal expansion (24)

where ΔL is the change in length of the material, α is the coefficient of linear thermal expansion, L_0 is the initial length of the material and ΔT is the temperature change to which the material is subjected.

The coefficient of linear thermal expansion α is a constant depending on the type of material and is expressed in units of 1/°C. This parameter indicates how much the material expands or contracts per unit temperature change.

The thermal expansion of aluminium is relatively high compared to some other metals, such as stainless steel or copper. However, its high thermal conductivity, low density, and high strength-to-weight ratio make it an ideal material for many applications where dimensional stability is required at high temperatures.

The linear thermal expansion equation can be used to calculate the change in length of a material as a function of temperature. This relationship can be useful in many applications.

It should be noted, however, that the linear thermal expansion equation is a simplification, as it does not take into account any changes in the cross-section of the material or its density.

Considering in fact the two- and three-dimensional cases (see Figure 18), the equations that come into play when analysing thermal expansion in this case regards superficial and volumetric expansion:

Superficial expansion
$$A_o = L_0^2 \tag{2.13}$$

$$\Delta A = 2 \times A_0 \times \alpha \times \Delta T \tag{2.17}$$

$$\frac{\Delta A}{A_0} = 2 \times \alpha \times \Delta T \tag{2.18}$$

Volumetric thermal expansion
$$\Delta V = 3 \times V_0 \times \alpha \times \Delta T \tag{2.19}$$

$$\frac{\Delta V}{V_0} = \beta \times \Delta T \tag{2.20}$$
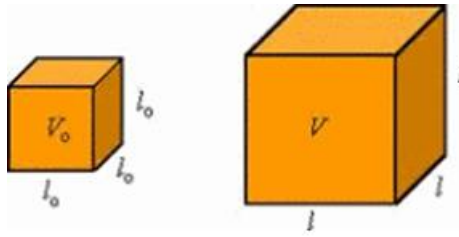
Figure 24: Volumetric expansion (28)

Where again, ΔA and ΔV are the change in area and volume of the material, α is the *coefficient of linear thermal expansion*, β is called *coefficient of volumetric thermal expansion*, and it is three times the linear one, A_0 and V_0 are the initial area dimension and the initial volume of the material and ΔT is the temperature change to which the material is subjected.

For more precise models, more complex equations that take these factors into account can be used.

The most accurate models for describing the thermal expansion of materials depend on the specific material properties and applied loading conditions.

In general, for homogeneous materials with isotropic thermal properties, the most accurate model for describing thermal expansion is the thermodynamic equation of state. This equation takes into account the dependence of thermodynamic properties on the material's stress state, pressure and temperature. However, the use of this model can be very complex and requires advanced knowledge in thermodynamics.

For anisotropic or complex materials, such as composite materials, more sophisticated models based on elasticity theory or material mechanics can be used. These models take into account the material's deformation properties, stress distribution and non-isotropic thermal properties.

In addition, there are also numerical approaches based on computer modelling that can be used to analyse the thermal expansion of materials. These approaches are based on solving partial differential equations that describe the material's behaviour in response to temperature changes.

In general, the choice of the most appropriate model depends on the specific properties of the material, the applied loading conditions and the accuracy required in the analysis.

4.2 Conventional compensation of geometrical errors in laser cutting

The compensation of geometrical errors in laser cutting could be carried out in two ways, i.e. by directly modifying the dimensions of the part to be cut imposed on the machine, obviously taking into account the expansion predicted by the experimental results, or through the use of the tool offset corrector of the machine itself, which through a shift in the position of the cutting point, allowed us to obtain samples of a suitable size.

The tool corrector is already used on the machine also at room temperature, as it allows the dimensions of the sample to be corrected by taking into account that the diameter of the spot with which the cut is made is not in fact perfectly punctiform, so this corrector is usually set equal to the radius of the cutting spot to allow correct dimensioning.

Consequently, the room temperature value of the tool offset corrector will not be equal to zero but will have a specific value depending on the cutting parameters analysed and the thickness of the sheet metal.

This behaviour is well explained in the Figure 25, where we can observe in (a) the imposition of a cutting path equal to the desired one (indicated with a dashed red line), and what happens with a specific laser spot diameter, is that the actual cut will follow a different path to the one imposed (continuous black line).

An offset of the tool corrector, as shown in the figure, must therefore be imposed to compensate for this problem.

In figure (b), in fact, such an offset value is imposed, which will modify the actual cutting path, making it equal to the desired one.

Therefore, using the tool corrector also for the compensation of geometrical errors arising from thermal expansion, gave us greater repeatability, greater freedom of action and greater responsiveness, as we did not have to go and create a different file to set up on the machine with different sample sizes at each temperature, but simply changed the tool offset value according to the expected expansion.
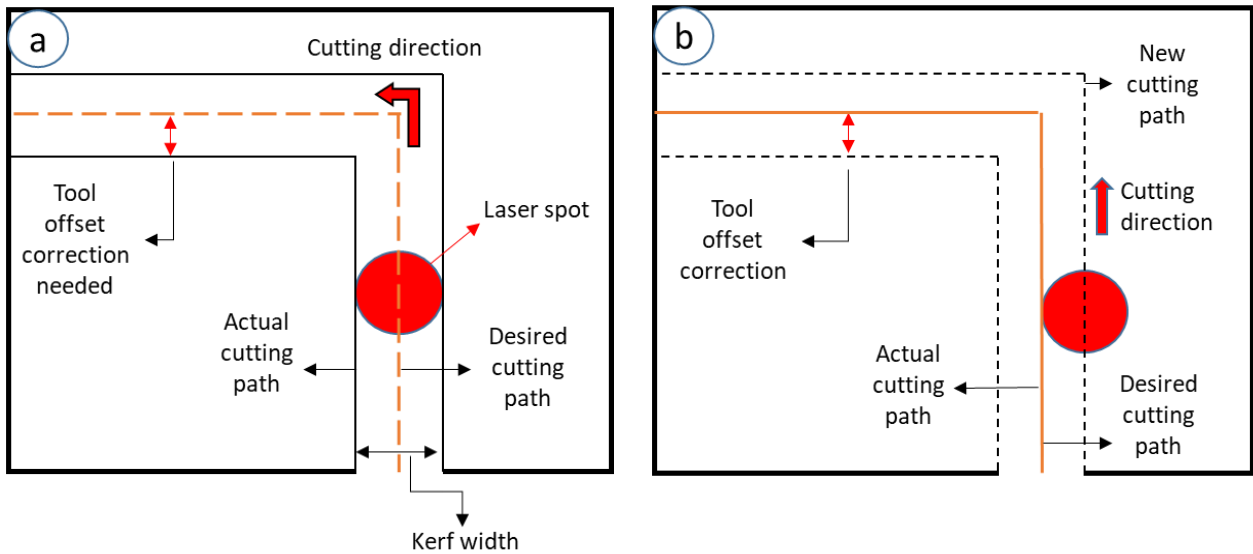
Figure 25: Tool Offset Correction methodology

Furthermore, considering that the samples used for our analysis have a rectangular shape, and that the shrinkage, as well as the action of the tool corrector, occurs along the entire perimeter, we must therefore take this into account, considering that the tool corrector that we have to impose on the machine will correspond to half of the total length variation obtained, as explained in the Figure 26.
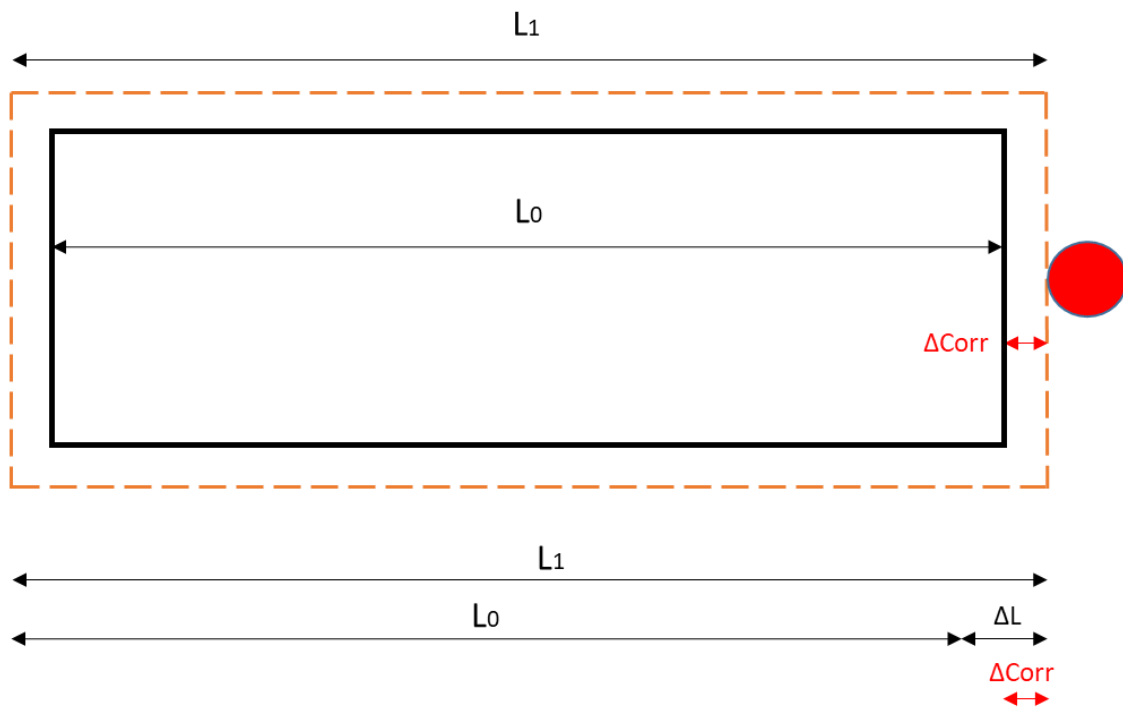
Figure 26: ΔL and ΔCorr comparison to compensate expansion problem

4.3 Predictive compensation of thermal expansion in laser cutting via the analytical model

In the case of this thesis work, the theoretical model of linear expansion was chosen by considering the one-dimensional case and validating its correctness.

What differs from this theoretical model, however, is that in the linear expansion equations we went on to consider an additional term that considerably altered the dimensions of our final sample after cutting, namely the laser cutting kerf, which reduced the size of the sample and had to be appropriately compensated for in order to obtain the nominal sample size even at room temperature.

In the present work, the sample thermal expansion model considered is the linear one, in which only the one-dimensional case has been discussed and validated.

First of all, let's define the engineering (e) and true (ε) deformations as:

$$e = \frac{\Delta L}{L} \qquad (4.1)$$

$$\varepsilon = \ln(1 + e) \qquad (4.2)$$

The two expressions can be considered approximately equivalent when working in the elastic region, so for small values of $\frac{\Delta L}{L}$.

In the following experiments, the conditions for the equivalence of engineering and true deformations are satisfied and, for sake of simplicity, we decide to work only with the engineering deformation (e).

The total expansion of our sample will therefore be represented by two different terms:

$$e_{TOT} = e_{Corr} + e_{\Delta T} \qquad (4.3)$$

Where the value e_{TOT} represents the total relative expansion:

$$e_{TOT} = \frac{\Delta L}{L_o} = \frac{L_x - L_o}{L_o} \qquad (4.4)$$

with L_x the final length of the piece and L_o the nominal length of the piece.

The value e_{Corr} represents instead, the dimensional value that take into account the cutting kerf, which must be compensated for through the use of the tool offset corrector, directly imposed on the machine:

$$e_{Corr} = \frac{2 * \Delta_{Corr}}{L_o} = \frac{2 * (Corr_1 - Corr_0)}{L_o} \qquad (4.5)$$

Where Δ_{Corr} is the increase in the tool offset corrector value due to the increase of temperature, $Corr_0$ is the tool offset corrector value at ambient temperature, and $Corr_1$ is the new tool offset corrector value at higher temperature to compensate for the expansion problem.

Considering that the dimension variation showed also in Figure 26, we can in fact say that:

$$\Delta_{Corr} = \frac{\Delta L}{2} \qquad (4.6)$$

Finally, the $e_{\Delta T}$ represents the expansion due to thermal phenomena and so due to the increase or decrease in temperature values:

$$e_{\Delta T} = \frac{\Delta L_{\Delta T}}{L_o} = \alpha \Delta T \qquad (4.7)$$

Where $\Delta L_{\Delta T}$ is the expansion due to temperature increase.

First of all, it is essential to calculate the value of the tool corrector at room temperature, i.e. $Corr_0$ value.

To do this, we can then consider the temperature variation to be zero, thus cancelling the third term of the Equation (4.3), becoming only:

$$e_{TOT}(25°C) = e_{Corr}(25°C) \qquad (4.8)$$

$$e_{TOT}(25°C) = \frac{L_x(25°C) - L_o}{L_o} = \frac{2 * Corr_0}{L_o} = e_{Corr}(25°C) \qquad (4.9)$$

$$Corr_o = \frac{L_x(25°C) - L_o}{2} \tag{4.10}$$

Or also:

$$Corr_o = \frac{L_o * e_{Corr}}{2} \tag{4.11}$$

Thus, by calculating the length value of our sample at room temperature $L_x(25°C)$, without a temperature increase, we are able to calculate the value of the initial tool corrector, which corrects the cutting width problem.

After that, it is finally possible to go and consider the expansion related to the temperature increase and thus the thermal expansion of our piece, following the previously mentioned linear expansion equation.

The length of the expanded sample after temperature increase will therefore be given by:

$$e_{TOT} = \frac{L_x - L_o}{L_o} = \frac{2 * \Delta_{Corr}}{L_o} + \alpha\Delta T \tag{4.12}$$

$$L_x = L_o + 2 * \Delta_{Corr} + L_o * \alpha\Delta T \tag{4.13}$$

By obtaining the expected value of our final sample, taking into account both the dimensional variation due to the cutting width and that due to thermal expansion due to the increase in temperature, we can finally go on to calculate the tool correction value that we will need for the final task of compensating for this error:

$$\Delta_{Corr} = \frac{L_x - L_o - L_o * \alpha\Delta T}{2} \tag{4.14}$$

and so

$$Corr_1 = Corr_0 + \frac{L_x - L_o - L_o * \alpha\Delta T}{2} \tag{4.15}$$

fundamental equation that will lead us to the final compensation we have set ourselves and which must be analysed and confirmed experimentally.

5. Experimental Set-up

In this chapter are presented all the measurement and analysis instrumentations used in the conduction of this thesis work.

5.1 Temperature measurement equipment

Since the primary objective of this work is to bring the aluminium to high temperatures before cutting it and assessing its condition, whether it is thermal expansion, defects of various kinds, or other, first we must analyse what are the instruments and methods by which the measurement of the plate temperature was carried out.

Specifically, the two instruments used for this purpose were K-type thermocouples, which measure the temperature of the material after being welded onto it and thus with a direct contact method, and then an infrared thermography equipment able to measure the temperature of the material in real time and without contact.

5.1.1 Thermocouple

In general, a thermocouple consists of two wires of different metals. When the two filaments are joined at one end and the junction is heated, a current is generated within the two filaments that induces a voltage between the free ends of the wires: by measuring the voltage, the temperature of the junction can be determined.

The ends of the filaments that make up the junction that will measure the temperature in contact with the metal are soldered together to avoid disturbances in the measured voltage signal, while the other ends are inserted into the acquisition instrument for signal recording.

There are two types of thermocouple measurements: immersion measurement and contact measurement. Immersion measurements are more accurate because they avoid disturbances in the measurement range, which is more controlled and uniform. Contact measurements, on the other hand, are more susceptible to external disturbances such as convection, vibration, or other disturbances that can affect the thermocouple reading.

K-type thermocouple has been used (see Figure 27), formed by Chromel (Cr+Ni) and Alumel (Al+Ni) wires with strand diameters of 250 μm, capable of measuring in the range

-270/1370°C, and Teflon coating resistant in the working range -200/+200°C for prolonged exposures (for short exposures the temperature range can be extended).
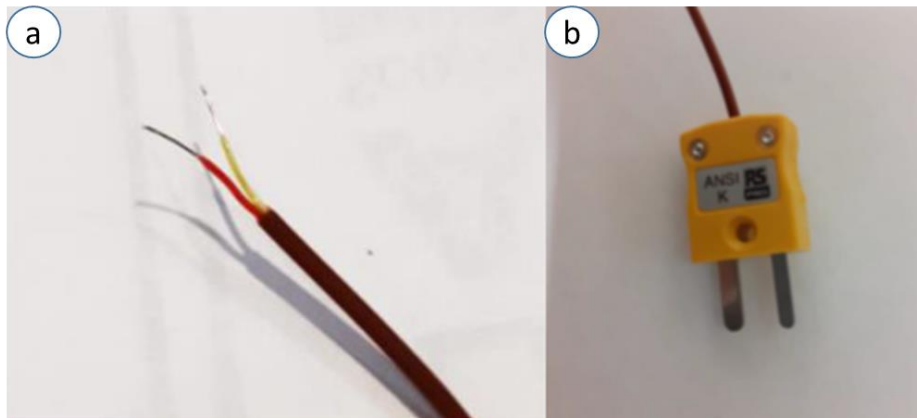
Figure 27: Wire junction to be welded (a) - Thermocouple K-type connector (b)

For the welding of the wires of the junction and for the welding of the thermocouple on the material, the SR48 welding machine in Figure 28, was specifically used for preparing thermocouple leads. The operating principle is based on a capacitor that is charged and then releases an electrical discharge when closing the circuit between thermocouple and graphite electrode, or between thermocouple and metal surface. The graphite electrode is used to join the two wires of the thermocouple, as can be seen in Figure 29.

Figure 28: SR48 Capacitance discharge welder
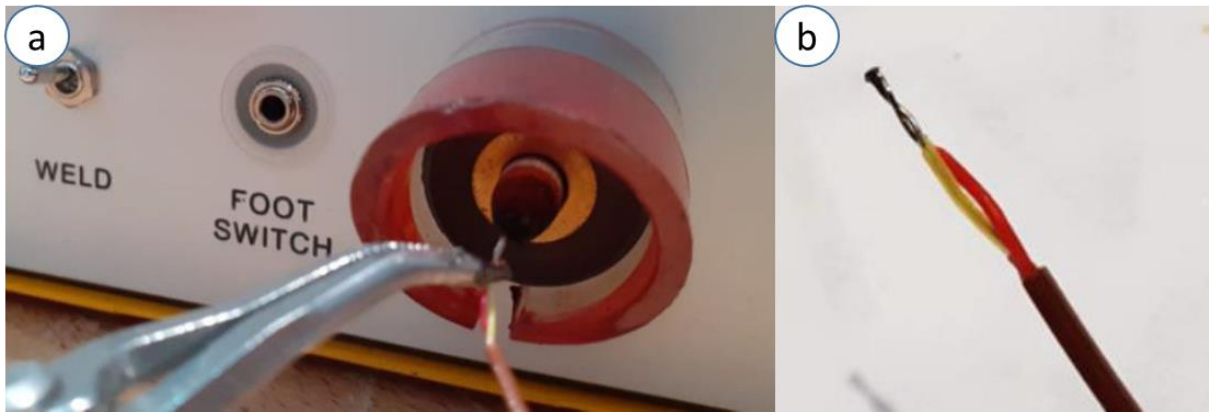
Figure 29: Graphite electrode used for welding the wires (a) - Welded thermocouple extremity (b)

To weld the thermocouple to a metal surface, the same welding machine used to prepare the hot joint is used. This time, instead of closing the circuit with the graphite electrode, we can connect the negative pole to the metal plate and closing the circuit with the thermocouple wire will generate an electric discharge that weld the wire to the metal (see Figure 30).
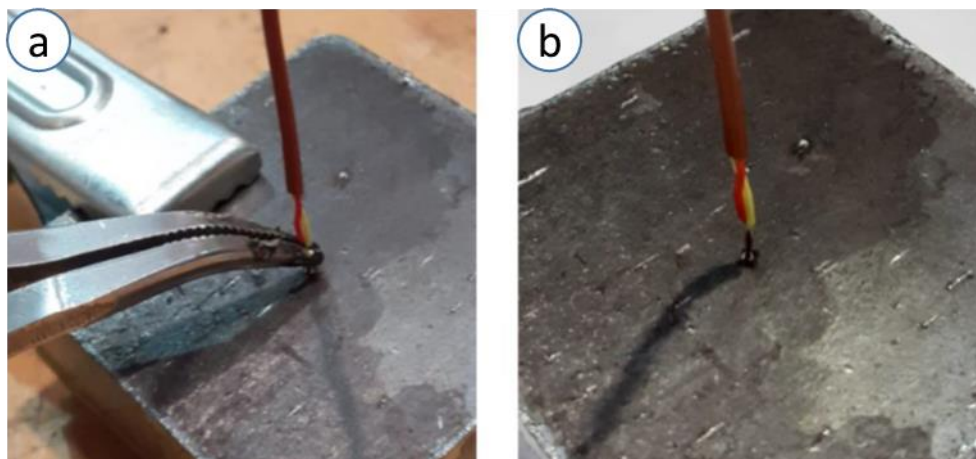
Figure 30: Wire connection, metal plate clamped (a) – Wire connection completed (b)

The instrument for thermocouple signal acquisition is the TC-08 datalogger, manufactured by Pico Technology and supplied through RS Components, capable of acquiring up to 8 channels simultaneously. This datalogger has been connected directly to an elaborator through a simple Type-A USB cable.

For the acquisition of the signal and the visualization of the results, it was used the PicoLog 6 Software, as can be seen in Figure 31 and Figure 32, already installed in the computer, that is able to collect the data and also create a graph with the temperature trend over time as we can see as an example in the Figure 33.

Figure 31: TC-08 datalogger (a) - Thermocouples connected to the datalogger, connected to the elaborator (b)

Figure 32: PicoLog 6 main software screen - multiple connected thermocouple
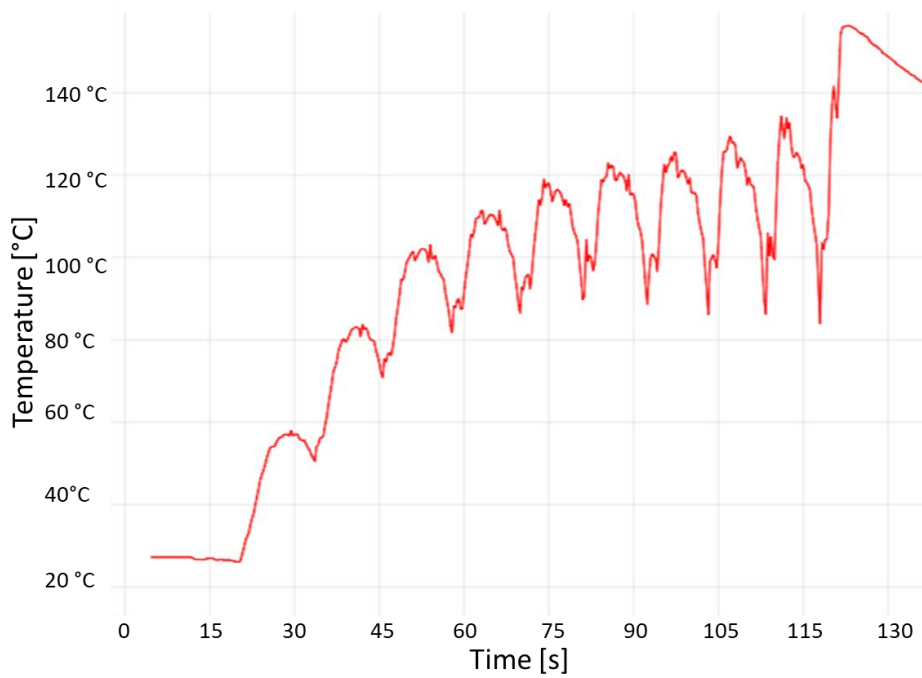
Figure 33: Graph example - thermocouple Temperature over Time

5.1.2 Infrared thermography equipment

Any object that possesses a temperature above absolute zero (0 Kelvin = -273.15 °C) emits infrared rays, which are not perceived by the human eye.

As physicists Josef Stefan and Ludwig Boltzmann pointed out, there is a correlation between the temperature of a body and the intensity of the infrared rays emitted. The thermal imaging camera measures the long-wave infrared rays incident on its field of view. Based on the acquired infrared rays, the thermal camera then calculates the temperature of the object to be measured. The calculation is made considering the emissivity (ε) of the surface of the object to be measured and the compensation of the reflection temperature (RTC = Reflected Temperature Compensation), both quantities that can be set manually in the thermal imaging camera.

Thermography (temperature measurement with a thermal imaging camera) is a passive, non-contact measurement procedure. In this procedure, the thermal image indicates the distribution of temperature on the surface of an object. With a thermal imaging camera, it is therefore not possible to make an analysis inside or through the object.

The infrared thermography equipment at our disposal was the X6900sc camera model, in Figure 34.

The X6900sc infrared camera system has been developed by FLIR to meet the needs of the research, industrial and range phenomenology communities. The camera makes use of FLIR's advanced ISC0804 readout integrated circuit (ROIC), mated to an Indium Antimonide (InSb) detector to cover the shortwave and mid-wave infrared bands. This camera utilizes a large format, 640x512 array with 25μm pixel pitch.

It features a fast pixel clock – 355 Megapixels per second, which enables the camera to output 1004 frames per second at a frame size of 640 x 512 pixels.

The X6900sc camera system is built around high-performance 14-bit A/D converters, preserving the full dynamic range of the FPA.

Higher frame rates are available by windowing down at the Focal Plane Array (FPA) level. Semi-arbitrary sizes and locations of windows are available, limited only by the intrinsic characteristics of the readout.
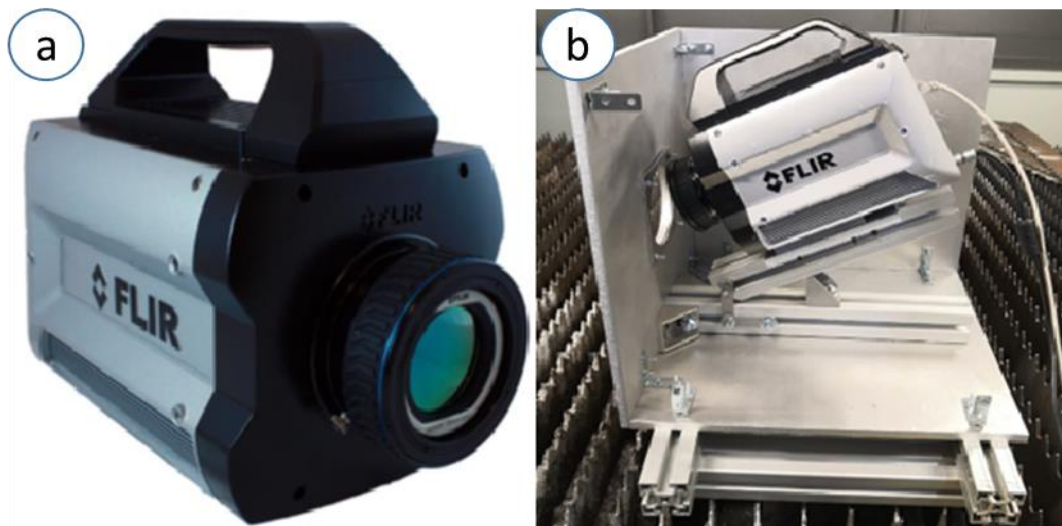
Figure 34: X6900sc thermal camera model (a) – Thermal image camera with support base (b)

As previously mentioned, the radiation acquired by the thermal imaging camera is composed by three elements: emission, reflection and transmission of the infrared rays emitted by objects and detected within the field visual range of the thermal camera.

Emissivity (ε) is a measure of the ability of a material to emit infrared rays and depends on the characteristics of a surface, the material and, for some materials, also on the temperature of the object being measured, as well as the spectral range of the thermal imaging camera used.

The reflection factor (ϱ) is a measure of the ability of a material to reflect infrared rays and depends on the characteristics of a surface, the temperature and the type of material.

As a rule, smooth and shiny surfaces possess a factor of reflection than rough and dull surfaces of the same material.

The reflected temperature coefficient (RTC) can be set manually in the thermal imaging camera, and in many measurement applications, the RTC corresponds to the ambient temperature (especially in thermography acquisition performed indoors).

Finally, the transmission factor (τ) represents a measure of the ability of a material to transmit (pass through) infrared rays, but transmission rarely affects practical measurements.

That is why after measuring the value of the ambient temperature and setting the value of the RTC in the thermal imaging camera, the next and fundamental step is to evaluate the correct emissivity value of the analysed material.

Especially for large temperature differences between the object to be measured and the measuring environment, the correct setting of emissivity is a crucial factor.

In fact, for objects to be measured with temperature above the ambient temperature, with an emissivity set too high, too low value of temperature is displayed; conversely, with an emissivity set too low, a too high temperature of material is displayed.

5.1.3   Experimental set-up for Emissivity (ε)

According to ISO 18434-1:2008 standards, the procedure for determining the emissivity, ε, using the contact method shall be as follows:

a) Place the IRT camera at the desired location and distance from the target to be measured.

b) Measure and compensate for the target's reflected apparent temperature.

c) Aim and focus the IRT camera on the target and, if possible, freeze the image.

d) Use an appropriate camera measurement function (such as spot temperature, cross hairs or isotherms) to define a measurement point or area in the center of the camera's image.

e) Use a contact or mirrored thermometer to measure the temperature of the point or area just defined by the camera's measurement function. Note this temperature.

f) Without moving the camera, adjust the emissivity control until the indicated temperature is the same as the contact temperature just taken. The indicated emissivity value is the emissivity of this temperature target measured with this waveband camera.

g) For greater accuracy, repeat procedures b) to f) a minimum of three times and average the emissivity values.

h) Compensate for emissivity by entering the averaged emissivity value in the IRT camera under the emissivity input (commonly referred to as "ε", "emissivity").

So, with the contemporary use of:

- heat up system to control the temperature
- Thermocouple system to check the real contact temperature
- Thermal imaging camera system

It was possible to confront the temperatures detected by the contact thermocouples and adjust the value of emissivity basing on the thermocouple results.

Since the value of emissivity, as we said, is temperature dependent, it was necessary to check the value of emissivity not only at room temperature but also at higher temperature.
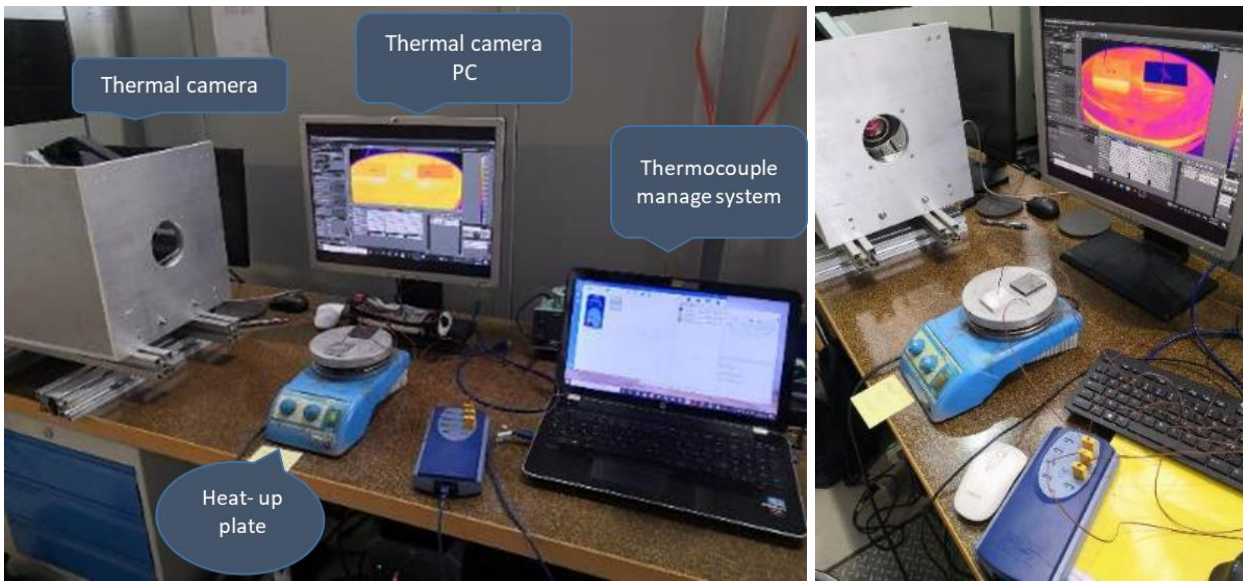
Figure 35: Set-up for emissivity calculation for Al5754
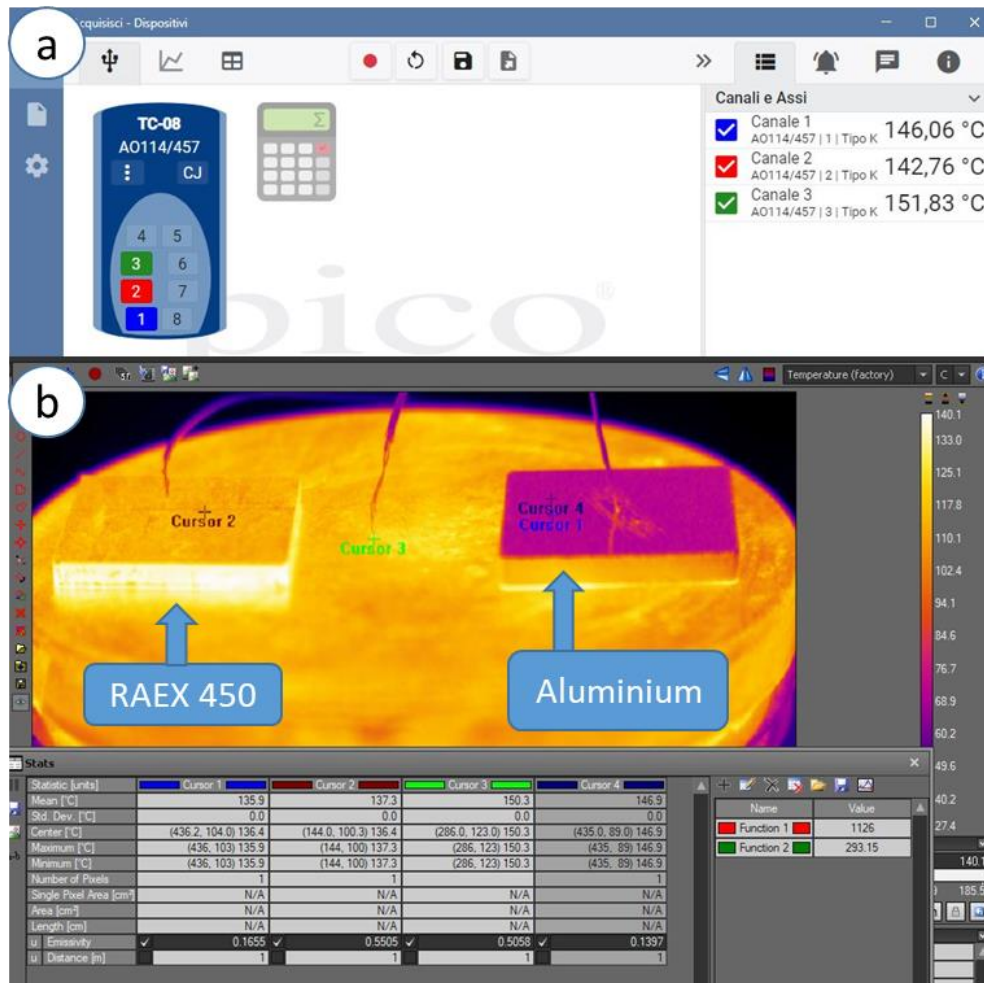
Figure 36: Double temperature checking (at 150°C) – Thermocouples value (a) – Thermal camera (b)

Different thermocouples were placed as shown in Figure 35 and Figure 36, connected to an aluminium sample, a RAEX 450 sample with known emissivity and the base of heat-up plate, to check that the temperature was correct for all the pieces and the emissivity value fixed accordingly to the thermocouples value.

Finally, the subsequent results were obtained as in the graph below, that give us the possibility to see how the emissivity value decrease with the increase in temperature.

At ambient temperature, in fact, the emissivity value seems to be higher, but we can see a rapid decrease of the emissivity when increasing the temperature of the pieces.

After that, we have a more or less asymptotically stable value for temperatures higher than 100 °C.

Table 4: Emissivity values at different Temperature

Material	Test Temperature [°C]	Thermocouple [°C]	Thermal camera [°C]	Emissivity (ε)
Aluminium	27	27	27	0,7340
	50	50	50	0,21
	70	70	70	0,1588
	100	100	100,1	0,1397
	150	146	146	0,1397
	200	188	187	0,1397
	250	241	243	0,1397
	300	273	269	0,1397
	350	333,2	332	0,1397
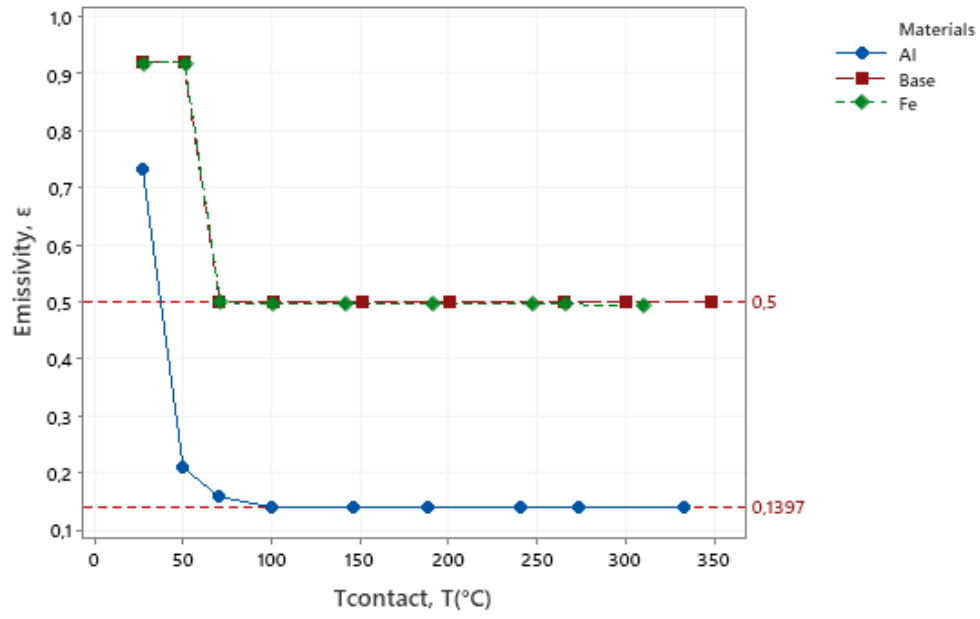
Figure 37: Scatterplot of Emissivity vs Temperature (°C) graph

5.2 LC5 Laser cutting system

The laser cutting machine used in this thesis project is a customized version of the LC5 machine (LC5, Adige-SYS S.p.A., BLMGroup, based in Levico Terme (TN), Italy), which is a combined machine for metal sheet and tube cutting. It can work on a maximum area of 3000 mm×1500 mm for sheet metal cutting and can also cut tubes with a maximum external diameter 125 mm (44).

The LC5 works with a fiber laser source of power up to 6 kW and 1.070 μm emission wavelenght (44) (YLS-6000-CUT, IPG Photonics Coorp., Oxford, Massachussets).

The transport fiber is a graded-index optical fiber having a core diameter of 100 μm.

The cutting head (HPSSL, Precitec GmbH & Co., Gaggenau, Germany, Figure 3.2) has a collimation lens of 100mm and a focal lens of 200 mm, while the laser spot has a theoretical waist diameter equal to 200 μm.

Machine characteristics, optical configuration and laser parameters are reported in Table 5.

For the cut of aluminium, we used a Nitrogen inert gas with high pressure to perform the melt and blow method for cutting.
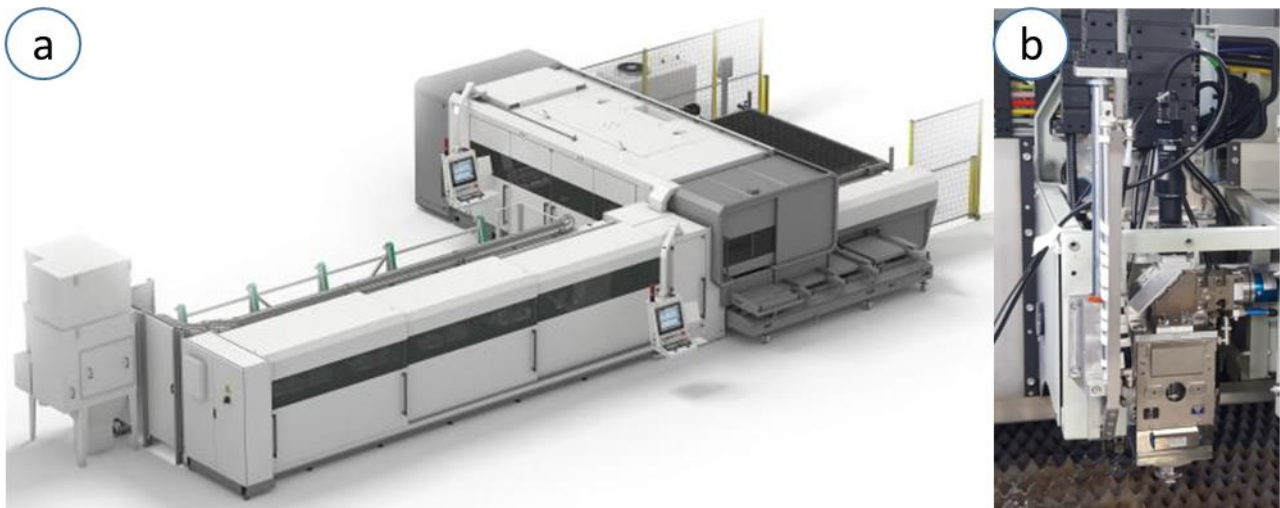
Figure 38: Combined Laser cutting machine (a) – HPSSL, Precitec Laser cutting head (b) (44)

Table 5: LC5 machine information and laser characteristics

MACHINE	
Constructor	BLM Group – Adige Sys S.p.A.
Model	LC5 (Combined machine for sheet and tube cutting)
HEAD CONSTRUCTOR	Precitec
Process Gas	N2 or O2
Focal lenght, f_{foc}	200 mm
Collimation lenght, f_{coll}	100 mm
Focal waist diameter , d_0	200 μm
Core diameter, d_{core}	100 μm
LASER SOURCE	
Constructor	IPG Photonics
Model	YLS – 6000 – CUT fiber laser
Active medium	Ytterbium
Maximum power	6000 W
Emission type	Continuous or modulated
Wavelenght, λ	1070 nm

5.3   Material properties

The material used for this thesis work was Al 5754, with three different thickness for the metal plate of 2-5-8 mm and the initial frame dimensions was 500x500 mm.

The mechanical properties of the 5000 series increase with increasing Magnesium content. The alloys used industrially contain up to 5% of it. The alloys in this series contain other additive elements such as Manganese, Chromium, and Titanium that have the 'effect of increasing corrosion resistance, weldability and, of course, mechanical properties. Good weldability, good behaviour at low temperatures, and corrosion resistance (even at weld points) are the main characteristics of this product.

Due to its high formability, it is often used in the form of thin sheets.

The 5454, 5754 and 5154, which contain from 2.5% to 4% of Magnesium with minor additions of Manganese and Chromium, are widely used in 'construction industry and mechanical industry.

Table 6: Chemical composition of Al 5754 (45)

CHEMICAL COMPOSITION (% present)									
Denomination	Si	Fe	Cu	Mn	Mg	Cr	Zn	Ti	Others	Al
5754	0.40	0.40	0.10	0.50	2.6 to 3.6	0.30	0.20	0.15	0.05	94.3 to 95.3

Table 7: Physical properties of Al 5754 (46)

PHYSICAL PROPERTIES	
Specific weight $\left[\frac{Kg}{dm^3}\right]$ at 20°C	2.67
Young Modulus E $[GPa]$	70
Electric conductivity $[S/m]$	1.9140×10^{-7}
Thermal conductivity $[W/(m \times K)]$	132
Specific heat $[\frac{J}{Kg \times °C}]$	891.2
Fusion interval $[°C]$	590 − 645
Thermal expansion coefficient $\left[\frac{10^{-6}}{K}\right]$	23.8

Table 8: Mechanical properties of Al 5754 (47)

MECHANICAL PROPERTIES	
Hardness [Vickers]	80
Tensile strength, Ultimate [MPa]	270
Tensile strength, Yield [MPa]	215
Elongation at break [%]	14
Poisson's ratio	0.33
Shear modulus [GPa]	25.9
Shear strength [MPa]	160

5.4 Cutting parameters used for different thicknesses of the Aluminium Al5754

The Al5754 aluminium sheets were cut through the use of the laser machine, with specific, fixed parameters being set that varied only as the thickness varied.

These parameters allowed a correct cut and an optimisation of quality, i.e. reducing possible defects in the finished cut.

In the following table (Table 9) it is possible to see the specific parameters used for cutting Al-5754 with respectively 8-5-2 mm thickness:

Table 9: Process parameters for laser cutting of Al 5754 at different thicknesses

Fixed process parameters for cutting Al 5754							
Thickness [mm]	Power [W]	Cutting speed [mm/m]	Focal position [mm]	Gas type	Gas pressure [bar]	SOD [mm]	Tool offset (25°C) [mm]
8	5580	2000	-7.5	Nitrogen	15	0.7	0.32
5	5080	6600	-4.5	Nitrogen	14	0.7	0.2
2	5580	8000	+3	Nitrogen	8	0.7	0.35

5.5   Roughness measurement procedure

Roughness measurements are performed as explained in ISO 9013:2017 (48), where the Roughness value, $Rz5$, is one of the parameters that is able to define the quality of the cut edge.

The roughness measurement is performed at three different heights:

- ¼ of the total height from the upper surface (Top)
- ½ of the total sample height (Mid)
- ¾ of the total height from the upper surface (Bott)

as shown in Figure 38.
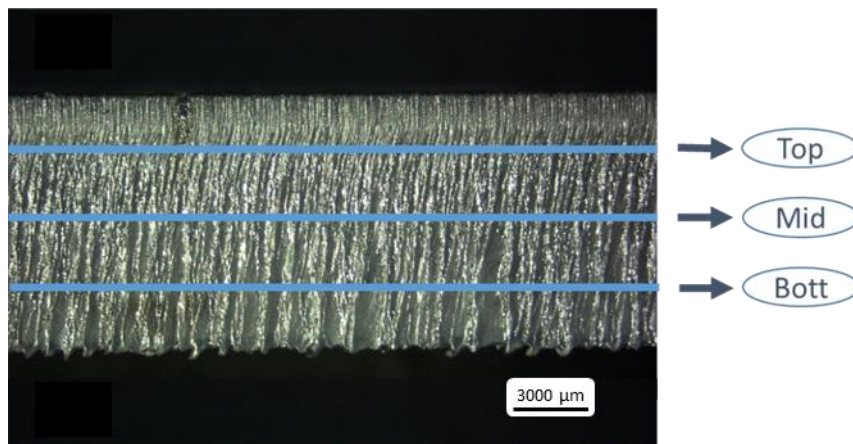
Figure 39: Three different roughness acquisition height

Roughness measurements are performed using a linear profilometer (Perthometer Concept PCMESS7024357, Mahr GmbH, Esslingen, Germany) shown in Figure 40; the instrument has a 2 µm tip (MFW-250) and a measuring arm with an available range of 50 µm (6851805).

The acquisition length for the roughness parameter is 5 mm and the cut-off wavelength is set to 0,8 mm as explained in ISO 4287:1997 (Rev. ISO 21920-2:2021) (49).

Surface roughness is measured approximately at the middle of the two long sides of each specimen, far enough from the corners.
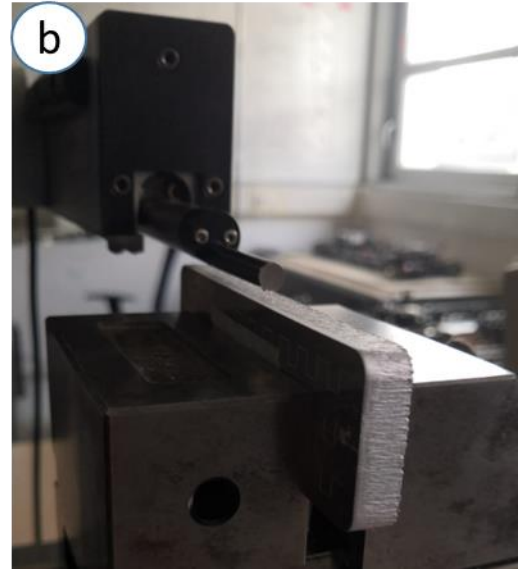
Figure 40: Mahr Perthometer PGK (a) – Contact stylus with 5 μm tip MFW-250 (b)
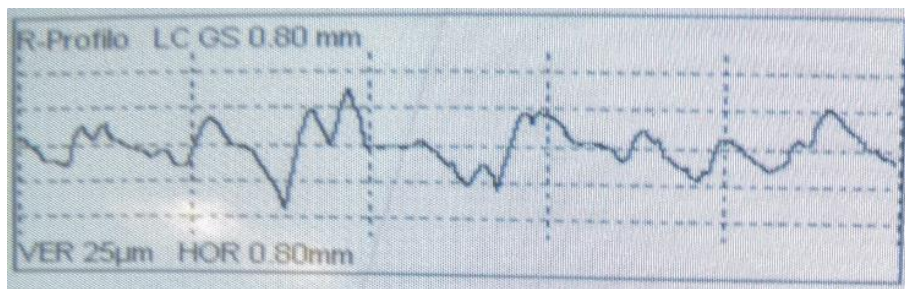
Figure 41: Example of profile acquisition through Perthometer Concept PCMESS7024357

5.6 Dross measurement procedure

The procedure to determine and quantitatively estimate the dross obtained during the operation of laser cutting is not yet completely defined in the literature.

According to ISO 13705:2000 (50), dross entities are calculated as the entire length exiting the bottom edge of the sample (see Figure 9).

To have a quantitative value of the dross attachment, several steps were followed:

1. Acquisition of high-contrast images of two different sides of the samples.

   For this step a Microscope (Echo-Lab SM 535 H, Devco S.r.l.) was used (Figure 42), with three different magnifications for the different thicknesses analysed as shown in Table 10.

2. Pictures analysis through a specific MATLAB code, able to binarize the images and extract the upper and lower contour of the samples.

3. Nominal thickness subtraction to the total height calculated to obtain only the dross height.

4. Study of the burr height at different temperatures and different thicknesses.

We went to study such images using an inner MATLAB program capable of binarizing the obtained images, calculating the two upper and lower profiles of the samples, and after subtracting the nominal thickness of our sample went to calculate the average value of burr and the standard deviation.

Then we could also analyze the maximum variation of the burr trend, calculated as the difference between the maximum peak value and the minimum valley value:

$$\Delta Burr_{variation} = Max\ Burr\ Value - Min\ burr\ value \qquad (5.1)$$

Table 10: Calibration table for different magnification

Thickness [mm]	Magnification	Length	Unit length	Total Pixel	Unit/Pixel
2	1.5X	6000	μm	1598	3.7547
5	1X	10000	μm	1728	5.7870
8	0.65X	16000	μm	1792	8.9286

Figure 42: Microscope Echo-Lab SM 535 H, Devco S.r.l.
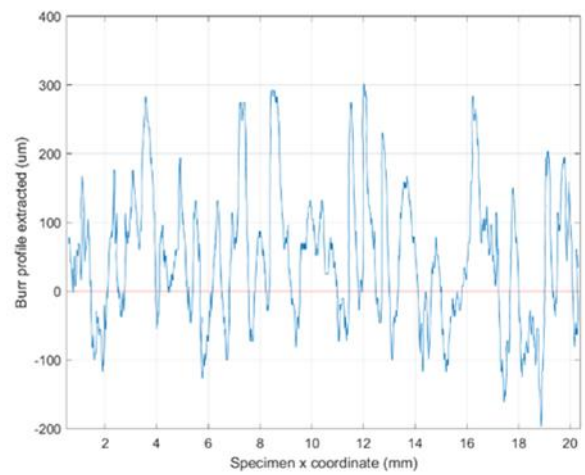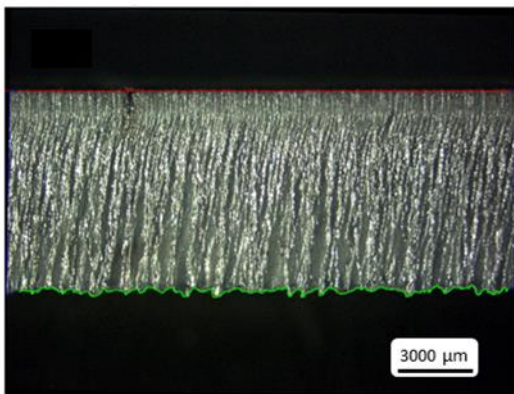
Figure 43: Dross attachment (burr) elaborated through MATLAB Code

5.7   Dimensional measurements

For the dimensional analysis an optical microscope (*Mitutoyo Quick Vision PRO ELF QV-202)* was used, shown in Figure 44.

There were three different magnifications at our disposal, as can be seen in Table 11, and for dimensional measurement purpose it was decided to use the 15X magnification to better define the real dimension of the samples with a dimensional error as lower as possible.

Dimensional measurements were made by placing the specimen on the base under the optical microscope, adjusting the height of the lens and the illumination for better define the images, and defined the reference system for that specimen were then made several measurements; specifically for each specimen, three measurements were made along the X-axis and three along the Y-axis for greater accuracy of measurement data.

These were performed by checking on the available table for X Y and Z values, and we made sure for each measurement that we were only going to vary one parameter until the final sample length was measured.

The procedure is shown in Figure 45.

We were then able to calculate the dimensions of the sample in both X and Y directions. Then, comparing it with the nominal dimensions at room temperature, we could analyse the actual elongation or shrinkage of the sample by calculating the ΔL.

The ΔL in micrometers was calculated using the formula of the equations (5.2) and (5.3) where L_x values are in millimetres:

$$\Delta L_x = [Ref(L_x) - L_x] \times 1000 \qquad\qquad (5.2)$$

$$\Delta L_y = [Ref(L_y) - L_y] \times 1000 \qquad\qquad (5.3)$$
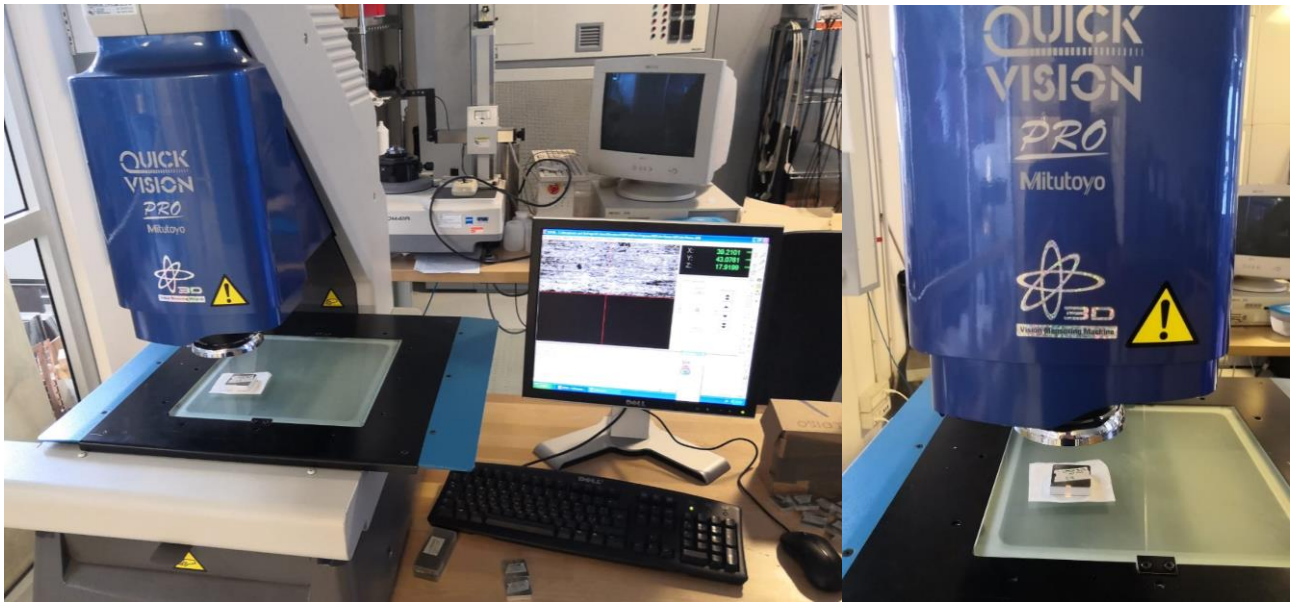
Figure 44: Optical microscope Mitutoyo Quick Vision PRO ELF QV-202

Table 11: Resolution for the different magnifications available

Magnification	2.5X	5X	15X
X (mm/pixel)	0,003895273	0,00193616	0,000647354
Y (mm/pixel)	0,003874953	0,00192628	0,000644048
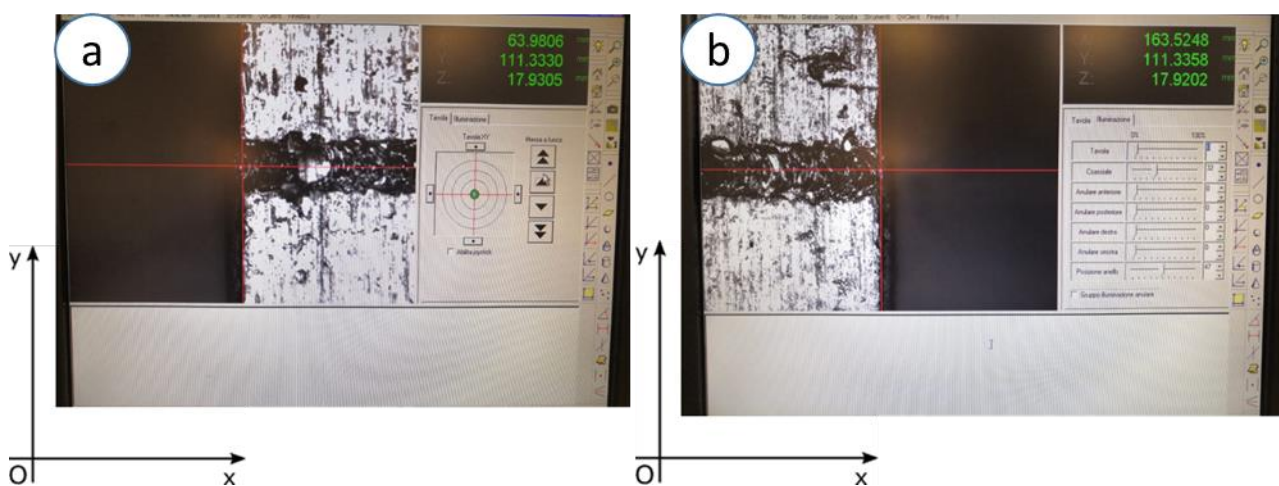
Figure 45: Dimensional measurement procedure. First measurement (a) – Second measurement (b)

5.8 Bimak Milling machine

A Bimak model 45 ACM drill was used to drill the base for the cartridge heating elements described below.

This drill had a base adjustable in the three X, Y and Z axes where the workpiece was clamped. Then the definition of the reference system and the position of the origin was performed, and after having identified the position of the holes by means of coordinates, it was possible to drill.

A special drill with a length of 140 mm and a diameter of 11 millimeters was then installed so that there would be enough space for the insertion of the cartridge heaters.

Information and a photo of the drill under analysis can be seen in Figure 46 and in Table 12:

Figure 46: BIMAK vertical drill (51)

Table 12: Bimak's drill specifications

Bimak's drill specifications	
Construction year	2000
Machine dimensions	1300x1350x2000 mm
Weight	800 kg
Power	3000 W
Voltage	400 V
Drilling capacity	45 mm
Tapping capacity	26 mm

5.9 Electric resistance control unit & cartridge heater

The heat-up of the metal plates in this thesis work was carried out through the use of Cartridge heater (Figure 48), specific resistance heater whit a cylinder shape useful for our purpose.

The resistance heaters were controlled by a two-zone thermoregulation control unit (ELENORM S.r.l., LC 3500 DUAL, Figure 47) in which each zone was able to control two different cartridge heaters with a temperature field that goes ideally from 0°C to 999°C.

The maximum power available per zone was 3500W and each zone had a protection fuse (Extra-rapid FF 16A) to avoid any possible accident.

The cartridge heaters dimensions and characteristics are presented in Table 13.

Figure 47: ELENORM – Two zones thermoregulation control unit – LC 3500 DUAL

Figure 48: Cartridge electric resistance heater

Table 13: Cartridge electric resistance characteristics and dimensions

Diameter	Length	Power	Voltage	Wire length
10 mm	130 mm	800 W	230 V	300 mm

6. Investigating different approaches for the controlled pre-heating of Al sheets

6.1 Overview of pre-heating techniques to conduct controlled experiments

To study the expansion of the samples after cutting, and to evaluate the quality of aluminium cutting at temperatures higher than room temperature, one of the main actions to be done was to develop and implement strategies to preheat the material so as to perform the cutting later when the material was hot.

Therefore, several preheating strategies were devised:

- Induction coil method

- Electric resistance method

- Use of a back reflection conveyer

- Heat-up of the material through the laser itself:

    a. Laser cutting of specific geometries

    b. Laser marking of specific geometries

    c. De-focalised laser beam

The Induction coil method was taken into consideration due to its ability to heat-up materials to high temperatures and in a fast way.

The biggest problem was that any of these systems need to be implemented internally in the LC5 laser cutting machine itself and due to high physical encumbrance and due to the high risk of this method (possibility of short circuit, high currents at play) it was discarded.

The use of a de-focalised laser beam was easily discarded due to the high reflectivity of the aluminium since it was risky for the laser head and also very poorly affected the final temperature of the metal plate.

For what concern the use of a back reflection conveyer, it was thought linked to the contemporary use of the laser itself with a de-focalised laser beam. Since aluminium is a highly reflective material, the idea was to use the energy "wasted" during the operation of marking and conveying it again on the piece that we wanted to heat.

Unfortunately for physical encumbrance (the SOD is really small during cutting), the "Dome" that needed to act as a back-reflection conveyer was impossible to perform without an adaptive method that allows to remove the dome before cutting.

Figure 49: Induction "Pancake" coil example (to be implemented in the laser machine)
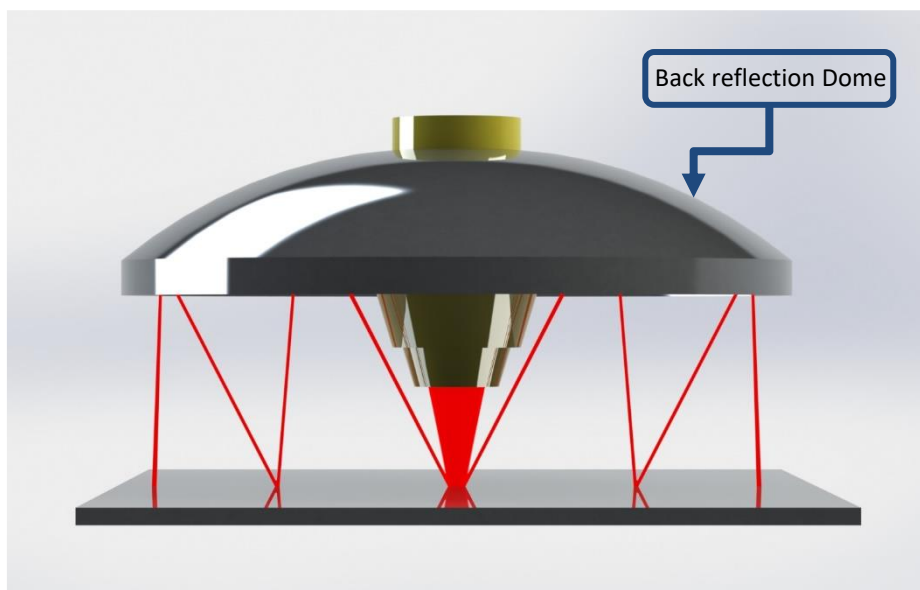
Figure 50: Back-reflection conveyer idea setup

The use, of course, of the method of preheating by the laser itself turned out to be the most convenient since it did not involve the use of external equipment that was difficult to operate or control; consequently, the first method developed and carried out as a strategy for preheating aluminium was this one.

Various methods of preheating by using the laser were then developed and subsequently tested.

Also, the heat-up through electric resistance method was analysed and developed and both this method and the heat-up through laser itself are presented in detail in the following sections.

Here is a tab (Table 14) that allows us to better analyse the pros and cons of every single heat-up method analysed:

Table 14: Comparative table of different heat-up methods

	Induction heating	Back reflection conveyer	Electric resistance	Leser cut of specific geometries	Laser marking of specific geometries	De-focalized laser marking
Advantages	• Simple & fast heating	• Use back reflection as an advantatage	• Good heat-up of the material • Easy to manage temperature values	• Use of LC5 both to heat-up and cut without use of other external system	• Usefull for small thickness • Heat-up without cutting	• No need of external system
Disadvantages	• Physical encumbrance • High risk (possibility of short circuit, high currents at play)	• Difficult to create a rigid and reliable system • Physical encumbrance	• Physical encumbrance	• Difficult to heat-up the material • Difficult to control the temperature	• High reflectivity heats laser head	• High reflectivity of aluminium doesn't allow to heat-up the material

6.2 Heating using marking geometries

The first method used to try to heat the material sample to be studied was through the use of lasers itself, via a marking geometry process.

This process involved the laser beam, through numerous passes made with specific geometry, going to increase the temperature of the part before cutting of the sample was performed.

Therefore, an internal geometry was designed within the specimen of size 30 mm x 100 mm (Figure 51), and this geometry was then repeated with a very small shift, so as to go to recreate the different passes close to each other.

The experimental design was based on fixed marking parameter described in Table 15, and the only variable parameter was the number of the subsequent marking passes shifted by few millimeters.

The temperature was measured through the simultaneous use of a contact thermocouple and an infrared thermal camera.

What was immediately apparent was the sharp increase in the temperature of the nozzle and the laser head, thus becoming dangerous to the safety of the laser itself.

In fact, as can be seen in Figure 53, the temperature measured for the nozzle was several hundred degrees high.

This was due to the high reflection coefficient of the aluminium, which led to overheating of the head and reflection of almost all the incident power.

The part temperature was still relatively low as it's shown in Figure 52, no more than 60°C after one pass and still not increase more also after subsequent passes.

This method was tried both with 8 mm thickness and 2 mm thickness with the same poor results.

This method was therefore discarded and not subsequently analysed further.
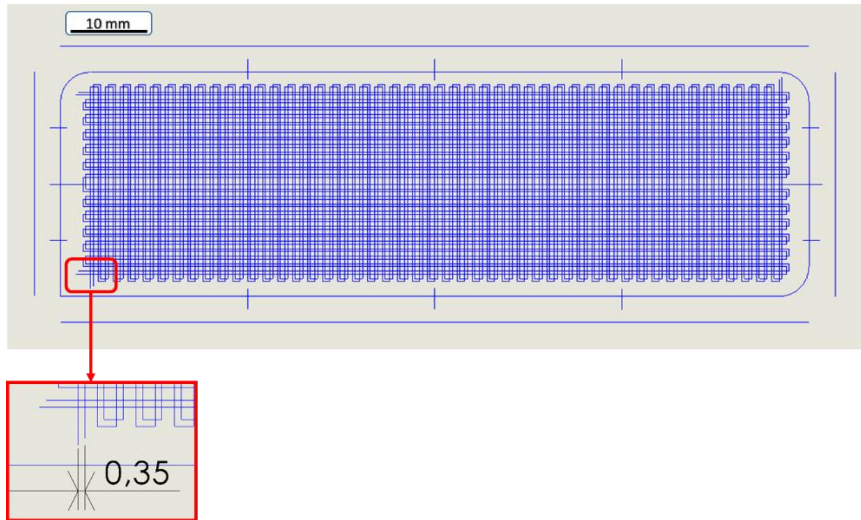
Figure 51: Marking pattern to heat-up the material.

Table 15: Fixed and variable marking parameters

Fixed parameters	
Sample dimensions	30 x 100 mm
External square dimensions	82x152 mm
Marking speed	6000 mm/min
Laser power	3500 W
Stand-off distance SOD	13 mm
Distance between subsequent marking passes	0.35 mm
Variable parameters	
Number of marking passes	1-2-4
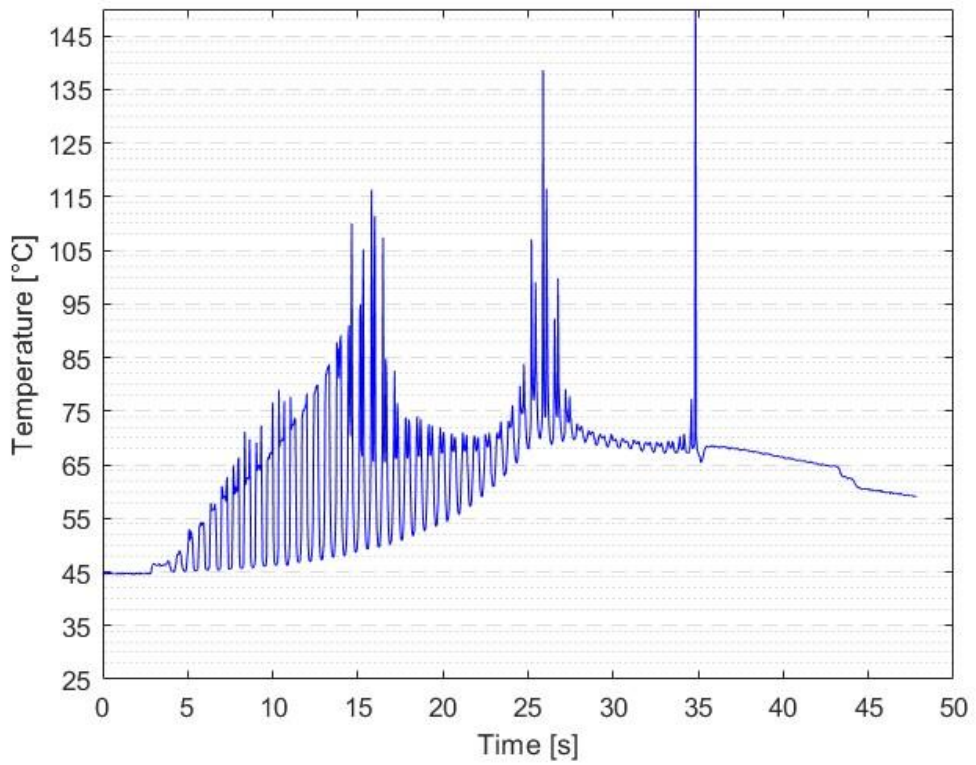
Figure 52: Temperature graph through marking grid heat up method
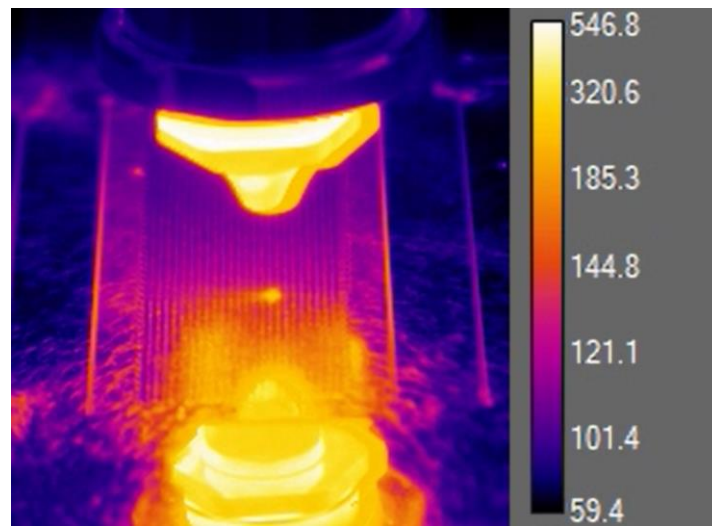
Figure 53: Thermal camera detection of critical temperature of the nozzle during operations

6.3 Electric resistance heating system

The heat source is what each heating element needs. Heating elements work by a process known as resistive heating. In this process, electric current is passed through a conductive material. This channel is known as the heat-releasing resistor. The capacity of the heat produced depends on the heat resistance capacity of the resistor.

Electrical resistors are indispensable elements in the operation of most plants and machines. Widely used in both industrial and domestic settings, these solutions are produced in a variety of shapes and materials to allow perfect adaptation with respect to each specific application.

Technically, they are passive components whose job is to limit the passage of electrical current. In other words, the function for which a resistor is created is to reduce the flow of electrons by opposing resistance during the transit phase of such negatively charged particles.

By opposing the passage of electrons, we thus have the possibility of converting electric current into heat.

There are various types of electric heating resistors that, depending on the category, are perfectly suited to a particular heating mode.

In our specific case, electric heating elements referred to as "contact resistors" were used.

This group of resistors works by transferring heat directly in contact with the element of interest. There are various types, and among those certainly most widely used industrially we find cartridge resistors.

Cartridge heaters (Figure 54) are particularly suitable solutions where high temperatures are present.

Extremely compact, made of stainless-steel and having a tubular form, these models of electric heating elements are ideal in their contact heating function, for example, for heating metal structures.

Figure 54: Example of a typical cartridge resistor

6.4 Realization of the hardware for experiments under controlled heating conditions

In this thesis work, cartridge heaters supplied by Elenorm S.r.l. were used; these heaters were suitable for use with the LC 3500 Dual temperature control unit presented in section 5.

The diameter of these cartridge resistors was 10 mm, the length 135 mm and the length of the cable available was 300 mm.

These developed a power of 800 W and were supplied with 230 V direct current.

All technical specifications are shown in Table 16:

Table 16: Cartridge electric heater characteristics

ELECTRIC RESISTANCE – CARTRIDGE HEATER by Elenorm S.r.l.	
Diameter	10 mm
Length	130 mm
Power	800 W
Voltage	230 V
Wire length	300 mm

Having such resistors available, a device was created for the purpose, an allocation base with cylindrical-shaped holes for the insertion of the cartridge resistor with a depth of 135 mm and a diameter of 11 mm to allow the electrical resistors to enter the base smoothly but without leaking out, which was intended to heat up in an homogeneous way and provide heat to the aluminium workpiece on which the sample would then be cut.
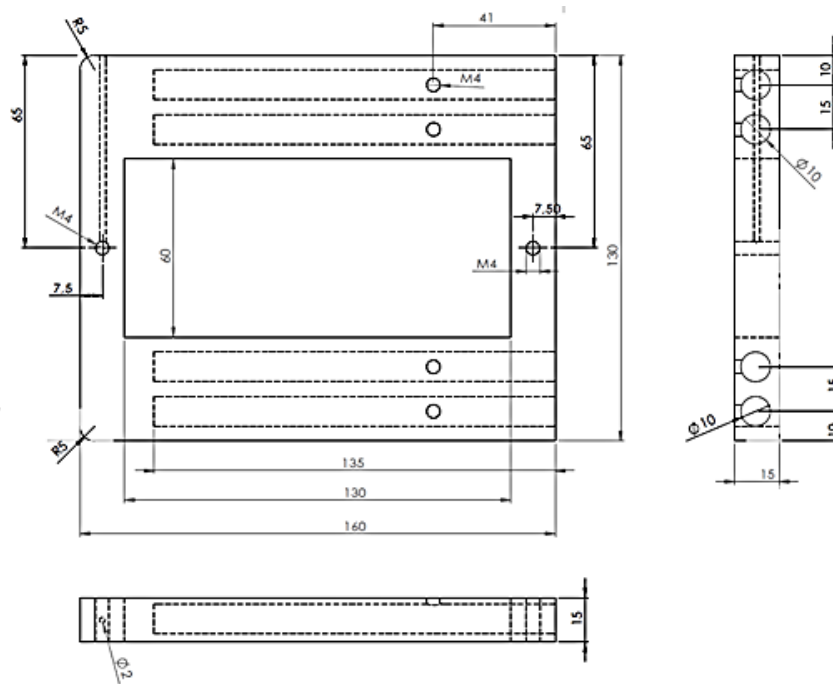
Figure 55: Design of the Cartridge electric resistance allocation base

Therefore, this device was equipped with an M4 screw system both to secure the electrical resistors inside it and prevent them from escaping during the various operations, and to be able to easily mount and dismount an additional aluminium plate of appropriate size on it so as to perform the cutting after heating.

Four housing holes for the heating elements were inserted to be able to give the possibility of choosing the number of heating elements to be used so as to heat the workpiece more or less quickly, and these holes were placed on both sides of the space dedicated to the sample to be cut to ensure an even heating over the entire surface of the plate.

The base was therefore designed using the SolidWorks software, and a model was prepared, also including the plate to be placed on the heating base so as to ensure correct dimensions and attachment.

In the model in Figure 55 as can be seen, a two-millimeter-thick aluminium base of considerably larger size than the heating base itself was also included, this was done to ensure vibration stability and to avoid movement due to high gas pressures during cutting.

As can also be seen from Figure 56 and Figure 57, the underlying 2 mm support base was fastened by means of M4 cylinder head screws with hexagonal recesses and with specific wide rosette to ensure tightness.

Finally, a two-millimeter-diameter side hole was added to provide access for a thermocouple that was responsible for real-time monitoring of the temperature of the base and the part itself.
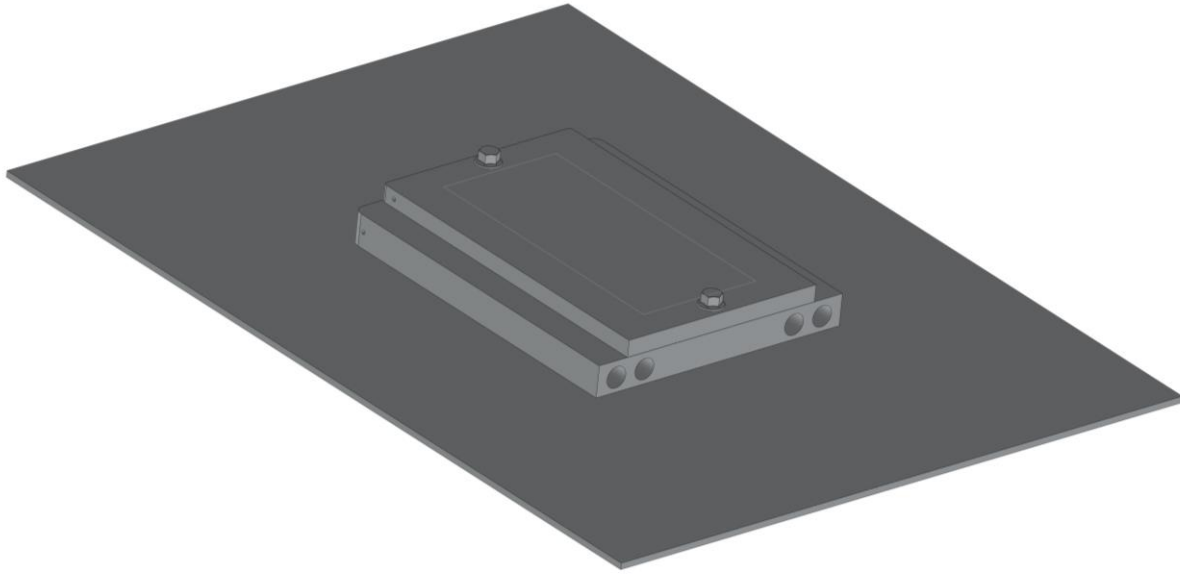
Figure 56: SolidWorks 3D model of the allocation base set-up
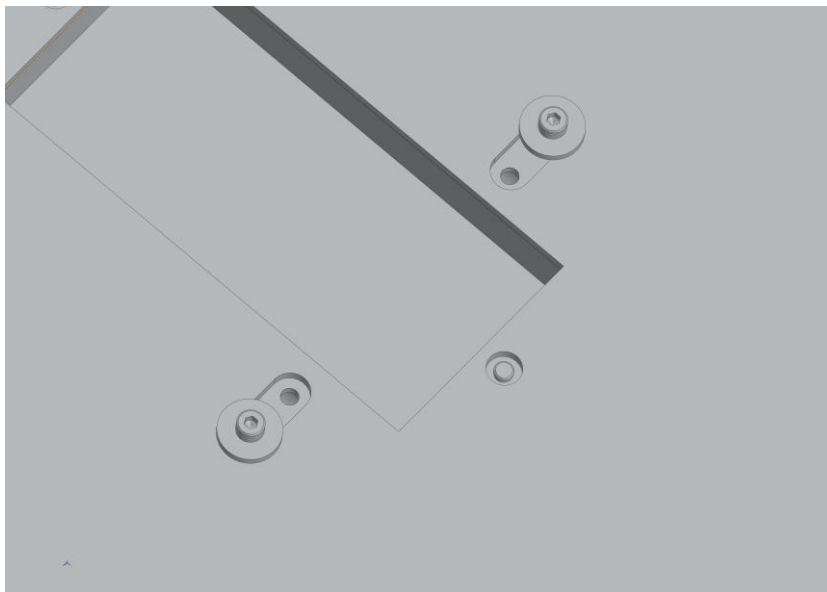
Figure 57: Detail of the fixturing between the allocation base and the support plate

The base for the allocation of the cartridge resistors was therefore cut through the LC5 laser machine, including the holes for the M4 screws later subjected to tapping through a specific tap to make them threaded. Through the same cutting machine, the 2 mm thick support plate and the various fixed-size plates where to perform the cutting of the aluminium sample were obtained.

What was added next were the four holes for the cartridge resistors, where BIMAK's vertical drill (51), with 11 mm diameter and 140 mm length drill was used for this specific task, and finally the hole for housing the thermocouple with 2.8 mm diameter drill bit and 60 mm length.

Figure 58: Methods for drilling holes

In Figure 59 you can see the finished part after being drilled and tapped, ready to be inserted into the final set-up.

The experimental set-up can be seen in Figure 60 with the block diagram of the layout and in Figure 61 with an example picture. The wires sticking out from the base, show the position of the cartridge resistors properly inserted inside it, the thermocouple positioned inside the side hole, and finally some counterweights to prevent bending of the aluminium foil underneath due to high operating temperatures and any residual stresses within it.
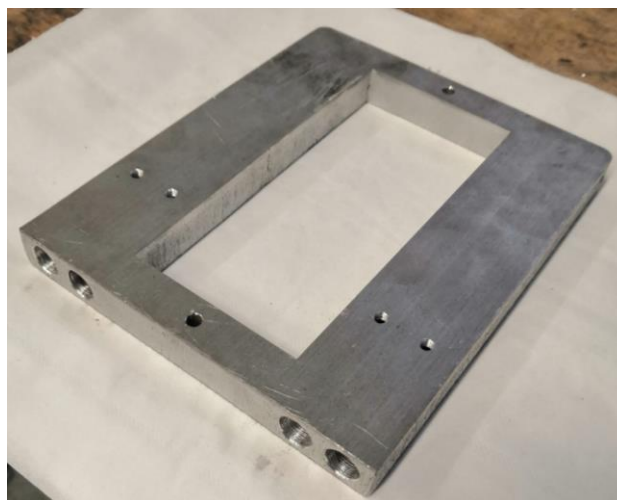
Figure 59: Completed allocation base
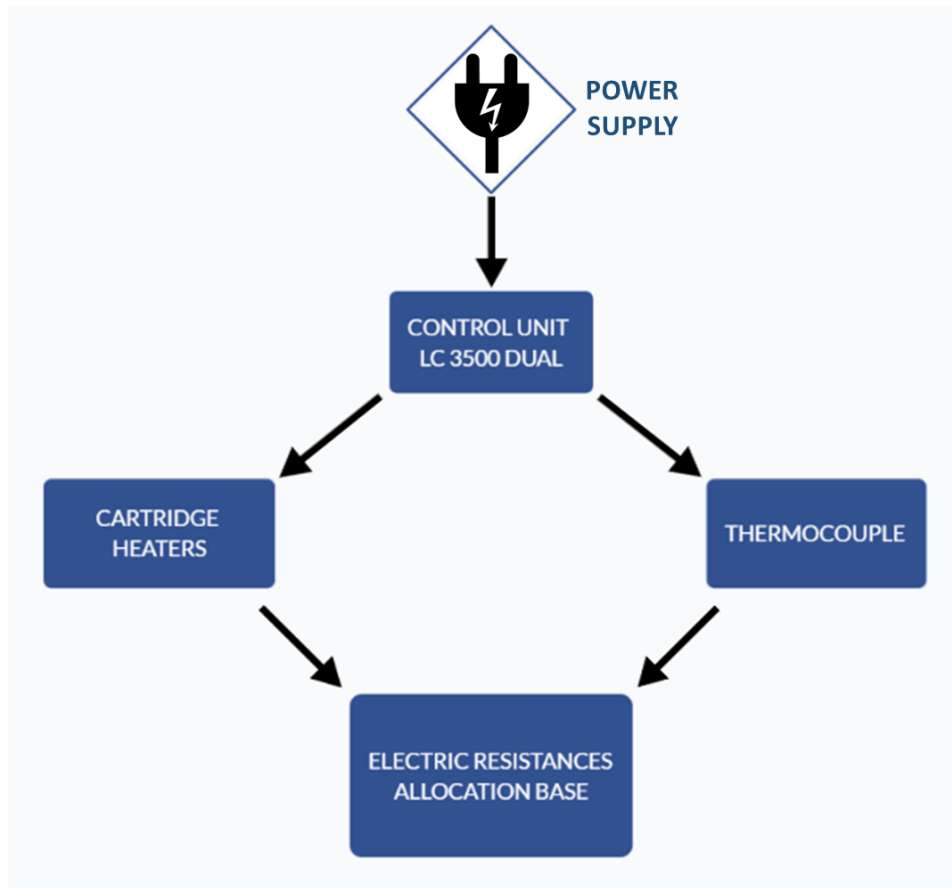
Figure 60: Block diagram of the experimental setup layout
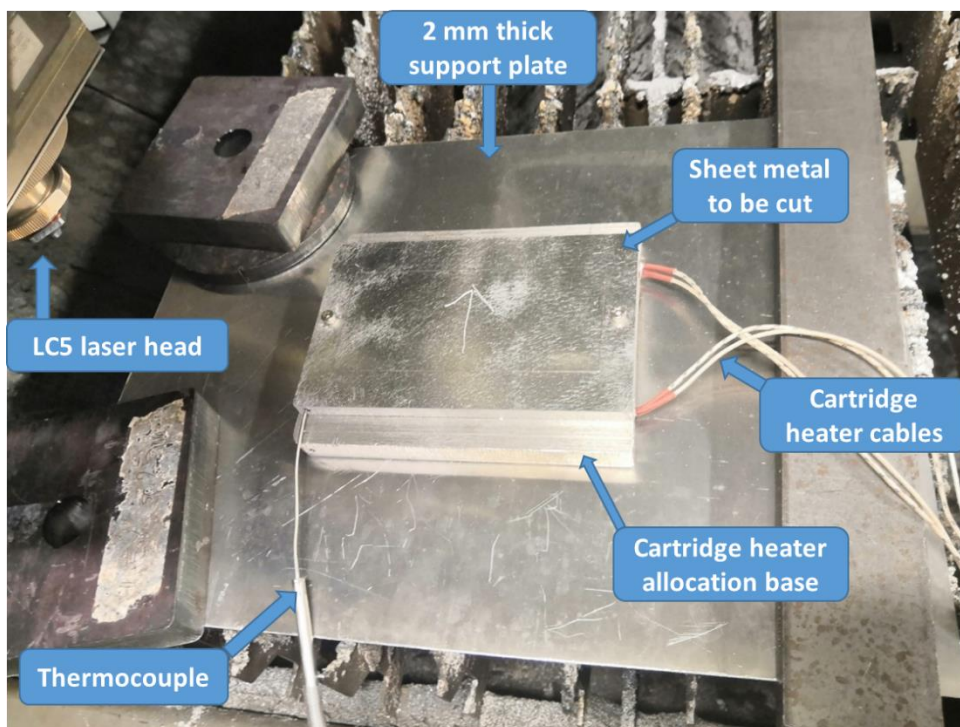
Figure 61: Final layout set-up

7. Preliminary investigation to assess quality issues during the cutting of high density nested geometries

7.1 Experimental design

The cut itself of the aluminium frame increase the temperature of the surrounding material, so it was possible to cut some geometries before performing the final cut of the sample.

Therefore, to increase the temperature of the slab before cutting, a specific design of experiment was developed, starting with the study of the behaviour of the heated and subsequently cut material of 8 mm thick.

This design involved the use of specific parameters for cutting, which can be seen in Table 17-20. The parameters in Table 19, previously optimized, were thus to ensure proper cutting of the material to obtain the lowest possible level of burr and a correct and complete cut of the part.

The only variable parameter was that of the cutting geometry (Table 18).

Therefore, different cutting geometries were devised, aimed at different but efficient heating of the specimen before cutting.

Table 17: Fixed parameters DOE, pre-heating through cutting geometries

Fixed parameters	
Sample dimensions	30x100 mm
Thickness analysed	8 mm
Cutting parameter	See Table 21
Followed path	Greek pattern
Dimensions of the particular geometry	4x4 mm

Table 18: Variable parameters DOE, pre-heating through cutting geometries

Variable parameters	
Geometry	1° Geo – GeoInt - internal
	2° Geo – GeoExt - external
	3° Geo – GeoIntExt - internal&external

Table 19: Cutting parameters for 8 mm thick Al 5754

Cutting parameters – 8 mm thickness	
Cutting speed	2000 mm/m
Power	5580 W
Gas type	Nitrogen (N)
Gas pressure	15 bar
Stand off distance	0,7 mm
Focal position	-7,5 mm

What was devised for the design of these geometries was to provide heating by cutting inside or outside in close proximity to the specimen, or even both inside and outside the specimen. The processed geometries can be seen in Figure 62-Figure 64, with dimensions and parameters specified in Table 19. The pattern that the geometry needs to follow was basically a Greek pattern with the squares measuring 4 mm x 4 mm.

As can be seen furthermore, vertical and horizontal markings were made on the edge that was to be subsequently cut off the specimen, to allow correct dimensional measurements in both X and Y dimensions.

Cuts were also made on the outside of the geometry for heating and on the outside of the geometry to be cut to preserve heat within the cut area.

The heating of the plate was analyzed by the simultaneous use of a contact thermocouple and thermal imaging camera to have proper feedback on the temperature trend. In the

following images, therefore, the three different geometries are presented, and it is also possible to see the images captured by means of the thermal imaging camera that allow us to have an initial visual examination in the temperature distributions and a visual representation of how the pre-heating geometry is cut.

Thus, after cutting the internal and external geometries, we had the cutting of the specimen that was stored for subsequent micro- and macrographic analysis of roughness, burr formation, and finally for a dimensional analysis to see any expansion or contraction of the test piece.

We were in fact able to calculate the dimensions of the samples in X and Y directions and then, comparing it with the nominal dimensions at room temperature, we could go on to analyse the actual elongation or shrinkage of the sample by calculating the ΔL.

The ΔL in micrometers was calculated using the formula of the equations (5.4) and (5.5) already shown in Section 5.7 where L_x values are in millimeters:

$$\Delta L_x \ = [Ref(L_x) - L_x] \times 1000 \qquad (5.4)$$

$$\Delta L_y \ = \ [Ref(L_y) - L_y] \times 1000 \qquad (5.5)$$

Further analysis on sample sizing and its variations are explained in detail in Section 7.2.3.
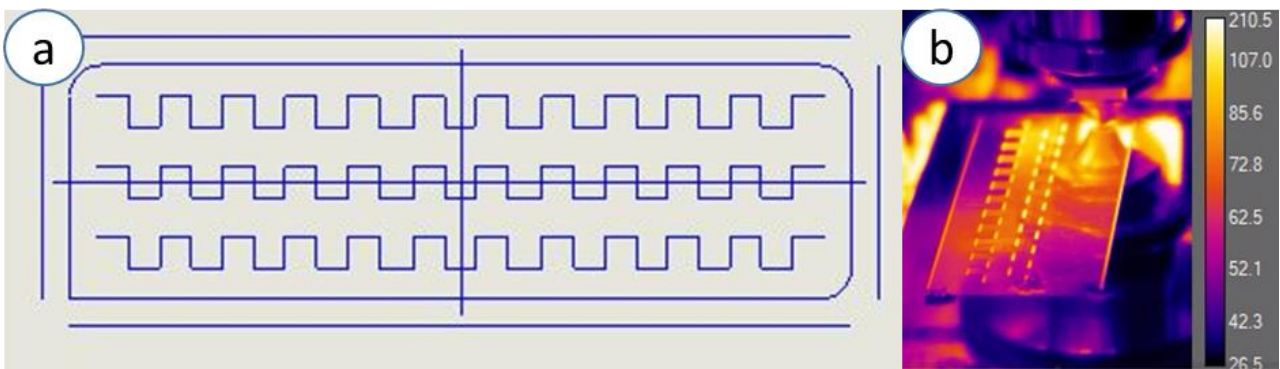
Figure 62: 1ˢᵗ Geometry – GeoInt – Design (a) and thermal image camera preview (b)
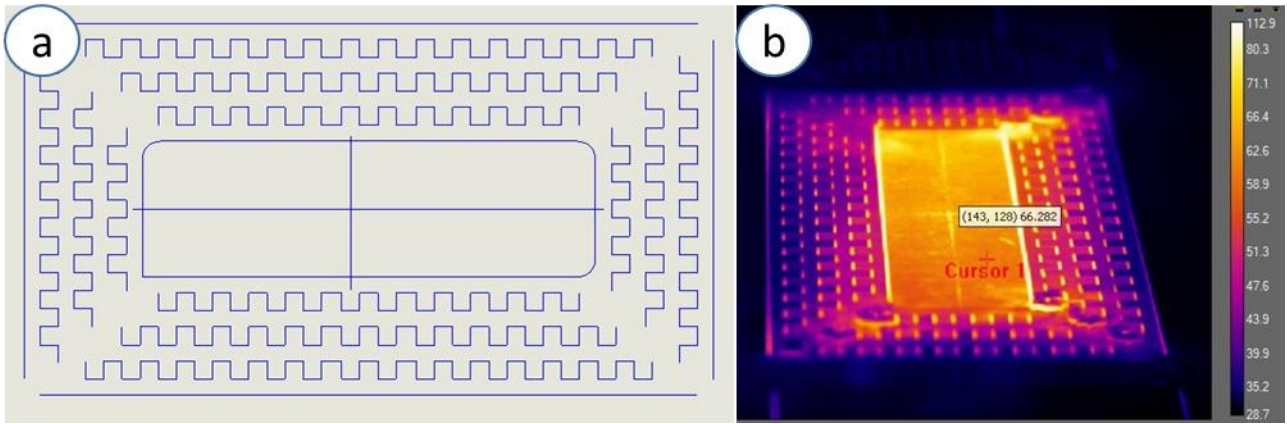
Figure 63: 2nd Geometry – GeoExt – Design (a) and thermal image camera preview (b)
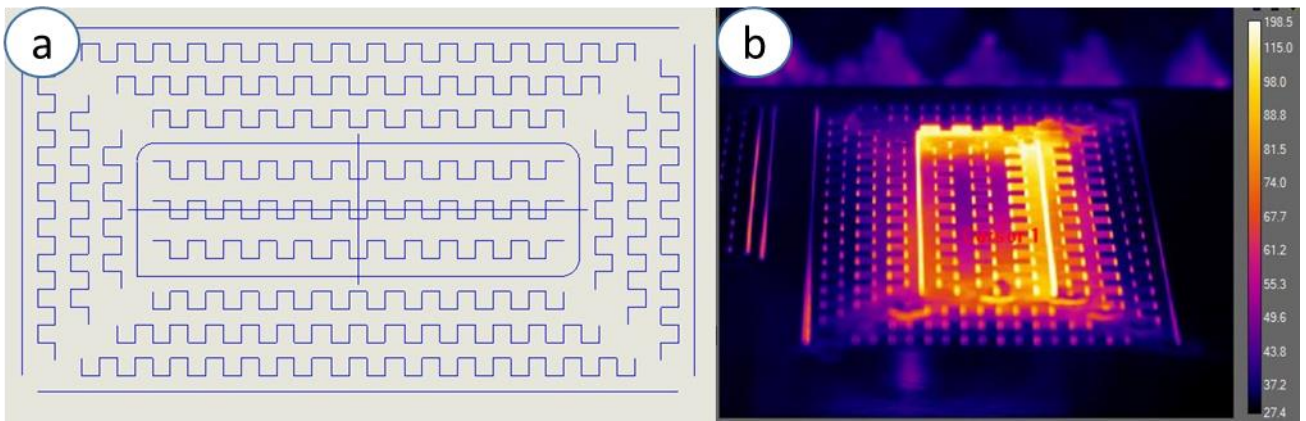
Figure 64: 3rd Geometry – GeoIntExt – Design (a) and thermal image camera preview (a)

7.2 Results

As mentioned earlier, we studied the temperature trends that we were able to obtain by heating through laser cutting of the specific geometries.

Below, in Figure 65-Figure 66-Figure 67, are the temperature trends, captured by thermal imaging camera, of the three different geometries; an indicator was placed on the area of the part whose point temperature we wanted to know over time, taking care to stay as far as possible from the exact points of the cut where the detected temperature would be significantly higher.

As can be seen from the graph in Figure 65, through the internal geometry (Geo_Int) it was possible to reach an average temperature of about 115°C, the last temperature peak, in fact, is related to the cutting operation of our sampler and therefore should not be considered in the calculation of the maximum temperature reached in the pre-heating. The total duration of the operation through this internal geometry was about 44 seconds.

On the other hand, regarding the laser cutting of the second geometry (Geo_Ext), the temperature reached was similar but slightly lower, approximately 100°C, but as can be seen from the Figure 66, the duration of this operation was longer than the previous one, just slightly more than 2 minutes.

Finally, the temperature trend of the inner and outer geometry (Geo_Int_Ext) where we reach a temperature of about 130°C appears to be the heating technique that led to the maximum temperature pre-operation of sample cutting, but with a considerable increase in the total heating time and energy expenditure and cost.

The total time in fact is of course the sum of the inner and outer operation and has a total duration of around 2 minutes and 45 seconds.

What seems to emerge from these initial findings in fact is that a longer heating laser cutting path, with the geometries described, does not lead to a considerable increase in temperature beyond a certain limit and that probably, the thermal dispersion of a highly conductive material such as aluminium, makes the use of internal heating more effective, due to the fact that we obtain similar temperatures but with significantly less time.

Certainly also because of the high time required to perform the heating (for the internal and external geometry we are in fact talking about almost 3 minutes) the result is a non-constant increase in temperature and also there is no certainty that this temperature is distributed within the heated part, homogeneously.

Therefore, after heating our Al 5754 sheet, the objective was to go in and evaluate any changes or damage to the material as a result of cutting the 100 mm x 30 mm sample at elevated temperatures.

Several factors were then examined such as the roughness of the cutting surface at three different heights along the thickness of the part, burr formation on the bottom surface of

the specimen, and finally, any geometric defects due to thermal expansion were investigated.
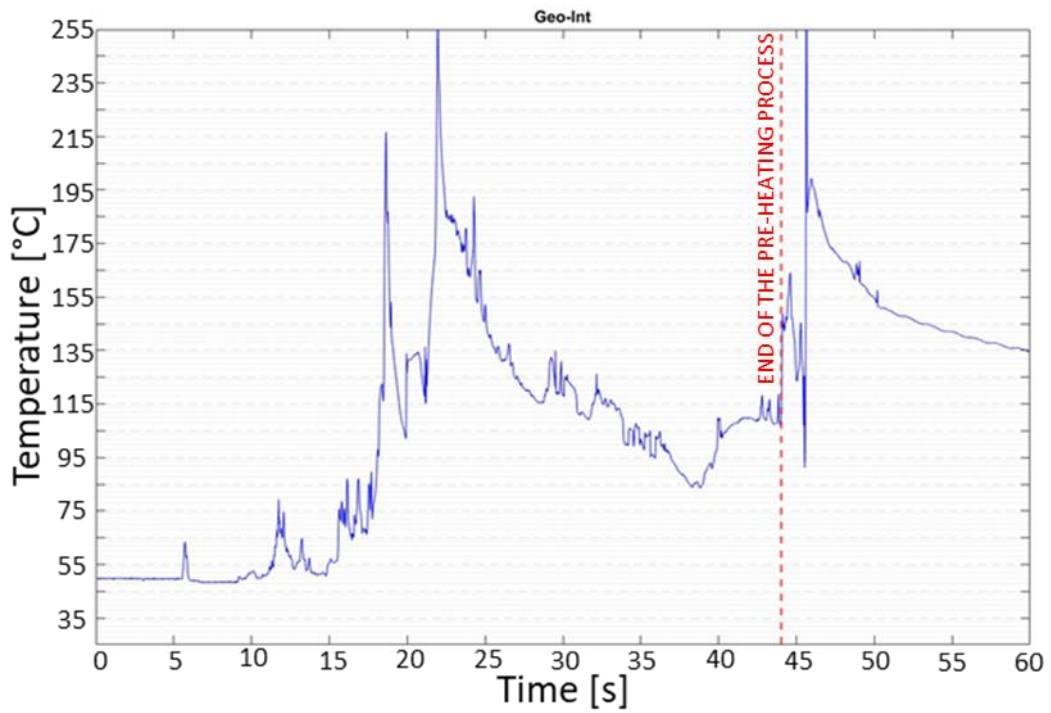
Figure 65: Temperature vs Time graph for Internal pre-heating geometry
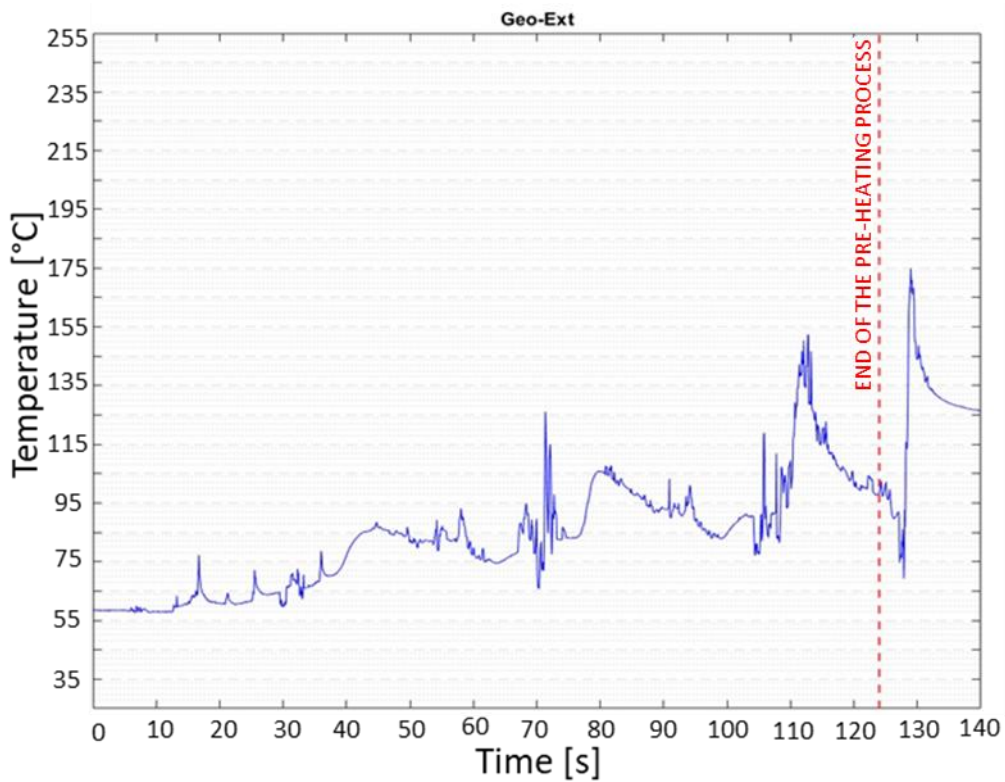
Figure 66: Temperature vs Time graph for External pre-heating geometry
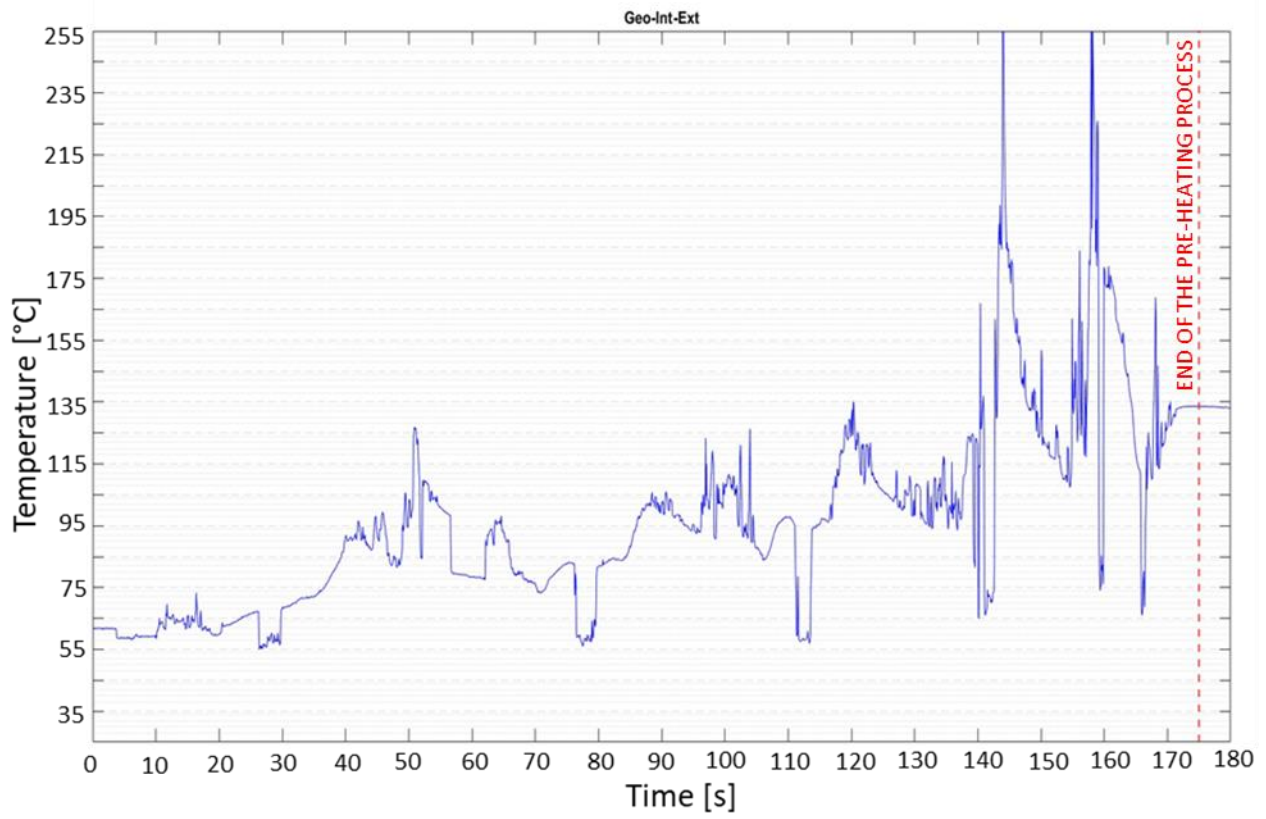
Figure 67: Temperature vs Time graph for Internal&External pre-heating geometry

7.2.1 Profile roughness

For the roughness analysis, several measurements were made using the Mahr Perthometer described in Section 5.4 of Chapter 5 on Experimental Set-up, which can describe the part profile and calculate Rz roughness values useful for our purpose.

For the first part, it was analyzed how the value of Rz changed as the cut geometry and the point of the measurement changed. Three different measurement points were considered based on the thickness of the part, 2 mm from the top surface (Top), in the middle of the piece (Mid) and 2 mm from the bottom surface (Bott). To make sure that the machine was working properly during cutting, measurements were taken on both long sides of the sample, indicated in this case as Side 1 and Side 3; as already explained in Section 5.5 and shown in Figure 39.

As expected from the state of the art, due to the initially laminar and then turbulent motion along the thickness of the part of the melt spillage during cutting, the deeper we go into the part, the more the Rz roughness increased considerably as we can see in the Main effect graph in Figure 68.

We therefore chose to perform an ANOVA analysis even excluding the effect of the measurement location, going to show well in the main effect (Figure 70: Main effect plot for Rz with factor: size, condition) how the measurement side of Rz did not affect its mean value, while we notice a strong dependence of the value of Rz on the heating geometry used.

The results of the ANOVA are shown in Figure 69, where it's possible to see how both Condition and Location are very significant for the Rz value while the Side factor is not significant.

What seems to emerge is that the external geometries cause a greater increase in sample roughness, in slight disagreement with the increase in temperatures that sees Geo_Ext actually reaching slightly lower temperatures than Geo_Int.
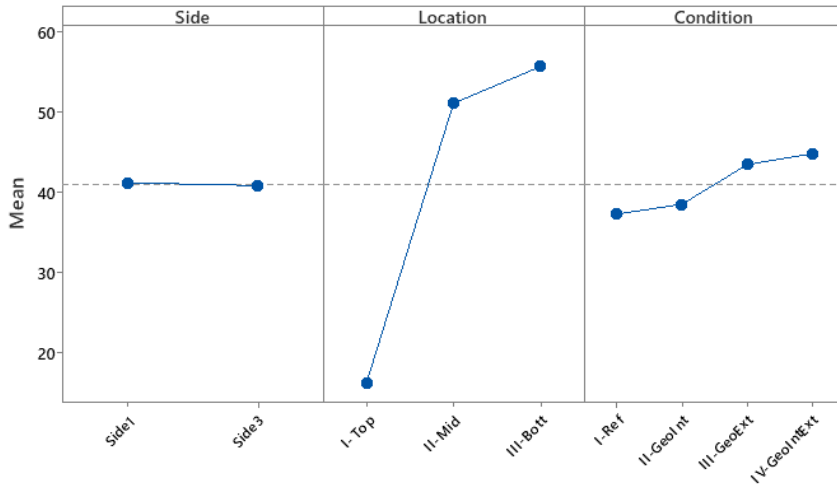
Figure 68: Main effect plot for Rz with factor: side, location, condition

Factor Information

Factor	Type	Levels	Values
Condition	Fixed	4	I-Ref; II-GeoInt; III-GeoExt; IV-GeoIntExt
Side	Fixed	2	Side1; Side3
Location	Fixed	3	Bott; Mid; Top

Analysis of Variance

Source	DF	Adj SS	Adj MS	F-Value	P-Value
Condition	3	733,5	244,5	6,93	0,000
Side	1	2,4	2,4	0,07	0,796
Location	2	22312,8	11156,4	316,33	0,000
Error	65	2292,4	35,3		
Lack-of-Fit	17	689,4	40,6	1,21	0,290
Pure Error	48	1603,1	33,4		
Total	71	25341,1			

Model Summary

S	R-sq	R-sq(adj)	R-sq(pred)
5,93872	90,95%	90,12%	88,90%

Figure 69: Analysis of Variance for Rz with factor: side, location, condition
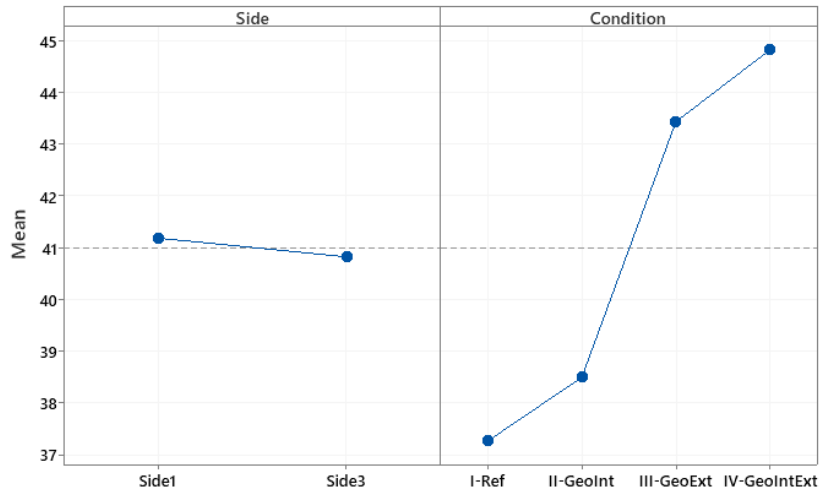
Figure 70: Main effect plot for Rz with factor: size, condition

Let's go specifically to analyze the Rz roughness results obtained at the three different heights of the specimen.

As can be seen from the graphs in Figure 71-Figure 73 and as we also mentioned earlier the Rz values on the top measurement are lower than on the other two measurements because of the initially laminar flow.
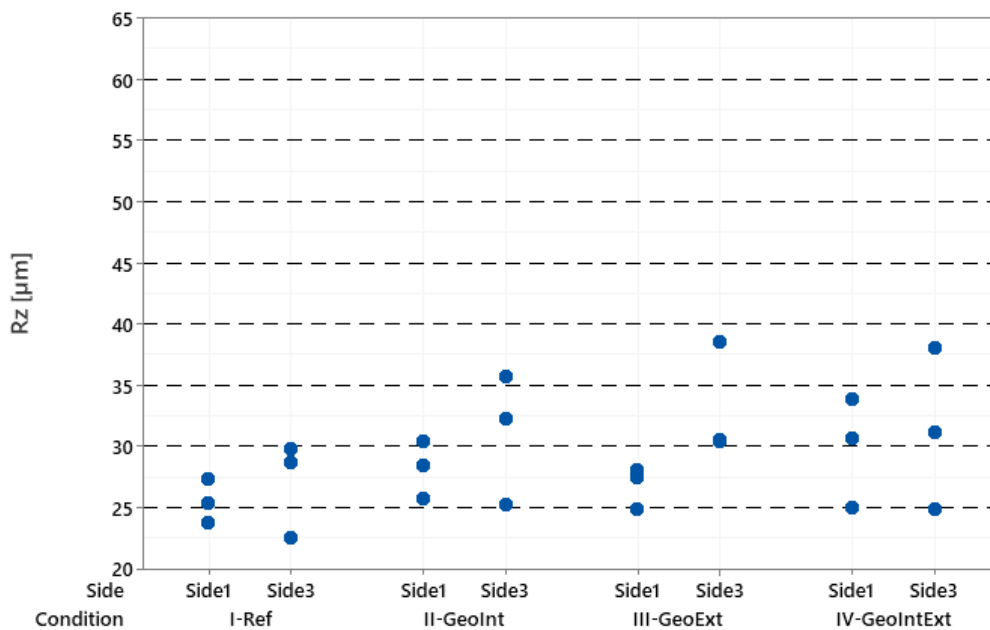
Figure 71: Individual value plot of Rz – Top measurements

We can see in the roughness measurements for the Top measurement in Figure 71 a slight upward trend in Rz roughness depending on the geometry we used.

If in fact with regard to the Rz measurement in the reference sample we had a range of 23 to 30 micrometers, with the other geometries and the different temperatures reached we had roughness measurements varied in a range of about 23 to 40 micrometers.
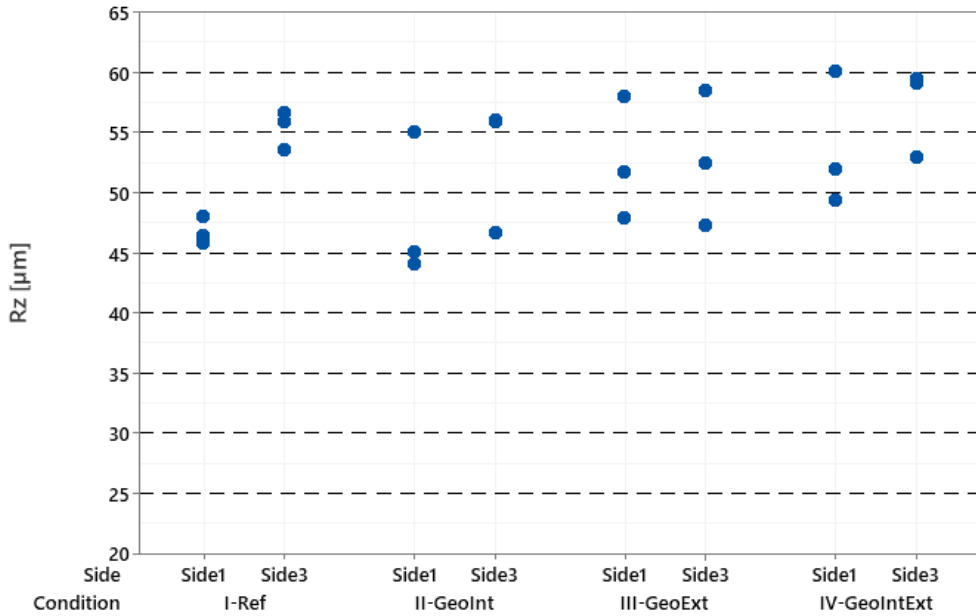
Figure 72: Individual value plot of Rz – Mid measurements
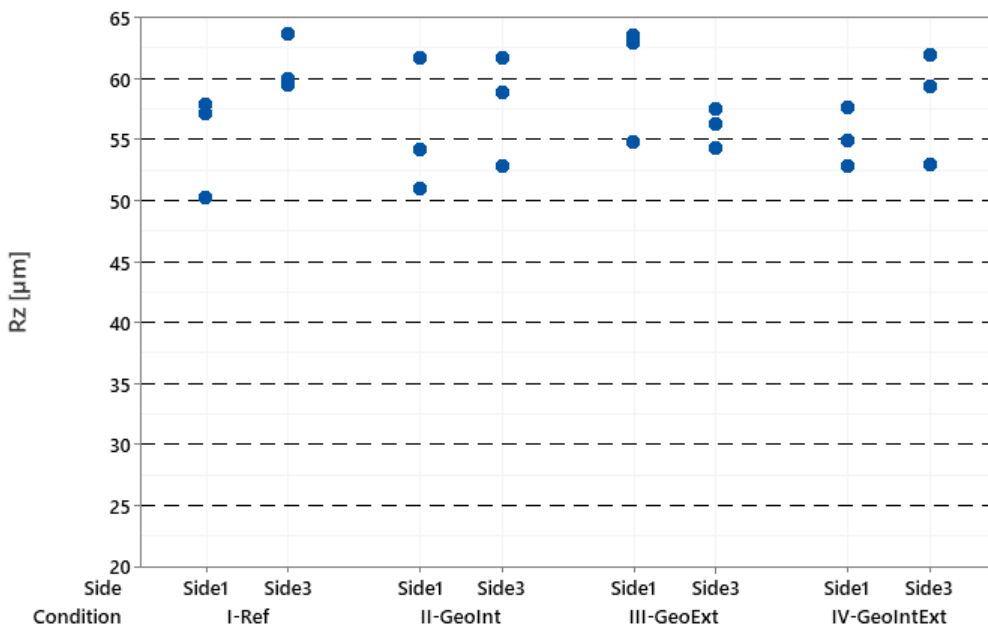
Figure 73: Individual value plot of Rz – Bott measurements

Regarding the Rz values of the Bottom and Middle measurements, there is no trend of increasing or decreasing roughness as the geometry changes and thus as the heating changes; the roughness values in the Middle measurements vary in a range of about 44 to 60 micrometers, while those in the Bottom measurements vary in a range of 50 to 65 micrometers.
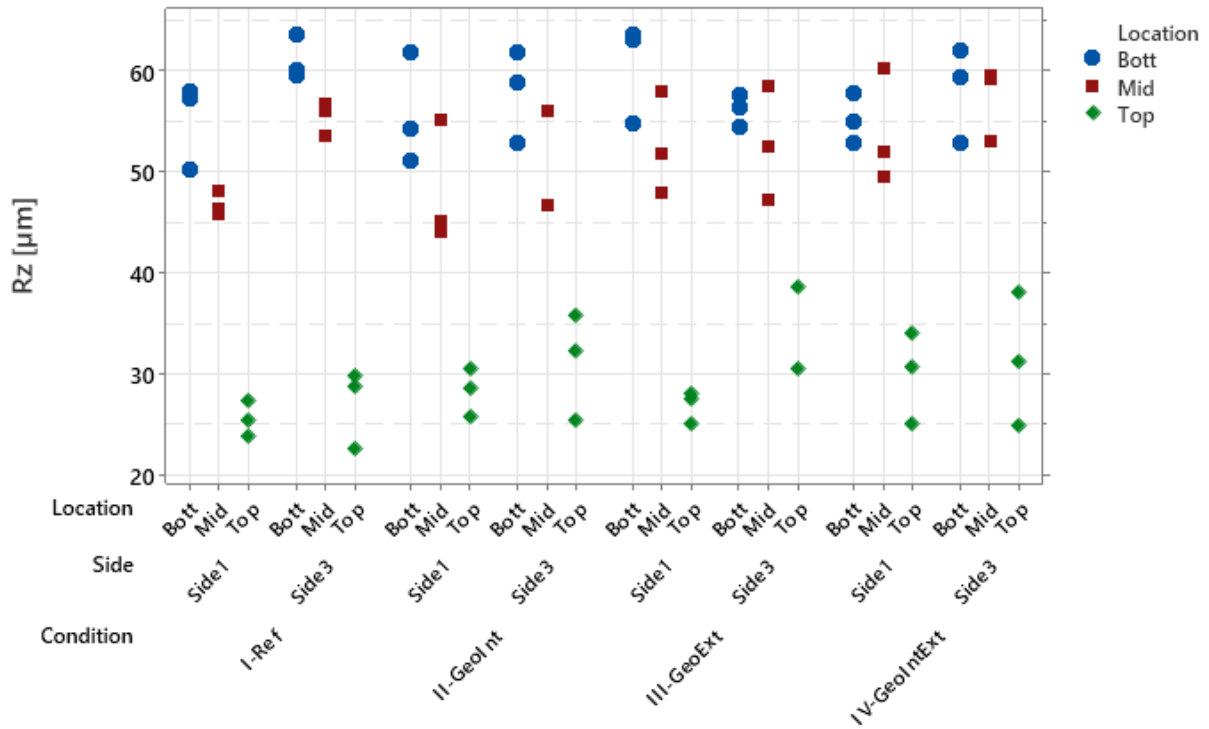
Figure 74: Individual value plot of the roughness measurements, for all three locations superimposed

Finally, in Figure 74, it is possible to see an overlay of the three graphs described above, to better show the difference between the various measurements, and the strong dependence of the roughness on the measurement point itself. On the right-hand side of this image there is a legend, showing the indicators with which, the three different locations are displayed.

Through analysis of variance, we studied the trend of the residuals to go to make sure of the validity of the data obtained. The graph present in the final Appendix shows a normal distribution of our values; in fact, we do not recognize any particular pattern and our measurements are therefore evenly distributed along a Gaussian.

7.2.2 Burr attachment

Another defect that was studied to understand how the change in preheating geometry, and thus the change in temperature, went to affect it, was the burr formation on the bottom surface of the cut samples.

According to ISO 13705:2000 (50), burr quantities are calculated as explained in Section 5.5.

So, after the high-contrast image acquisition of the different sides of our samples we went to study such images through the use of the MATLAB program already cited.

Also very useful was the possibility of obtaining a graph of the precise profile of the burr, which allowed us, beyond the average value of the latter, to identify the maximum variation between the peak and valley values of it, allowing us to better study its variation.

From Figure 75-Figure 76-Figure 77-Figure 78 we can see an example for each geometry used in which the acquired image of our sample is shown on the left, with a precise definition of the two curves that define the upper profile of the sample (red curve) and the lower profile of the burr (green curve). From this image we also see the values calculated through the program, of the mean burr value and its standard deviation.

The right image, on the other hand, shows the burr profile, with the nominal thickness value at 0 (red solid line).
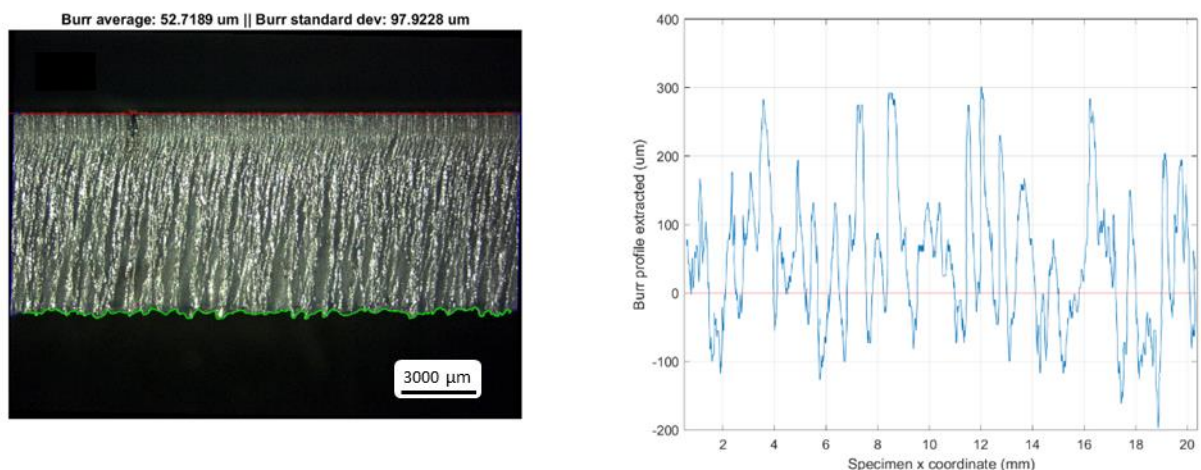
Figure 75: Dross profile (burr) - Reference geometry
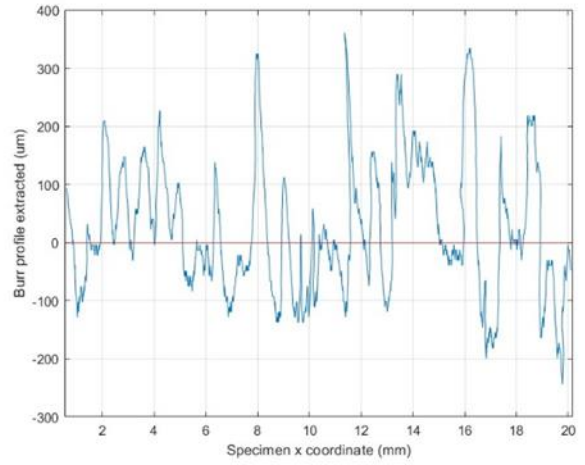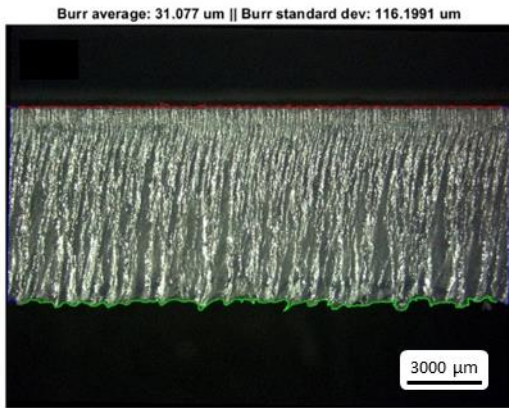
Figure 76: Burr profile - Internal geometry (GeoInt)
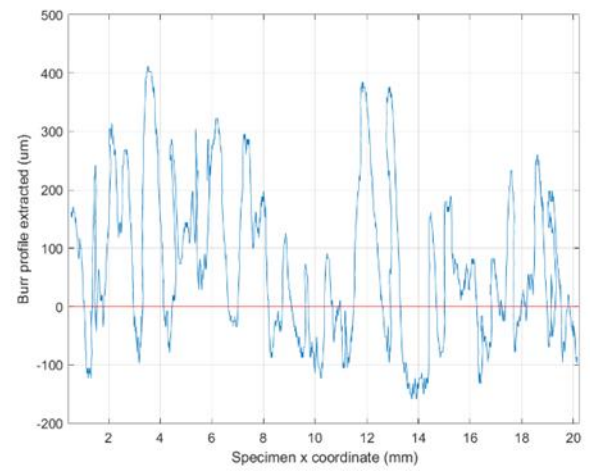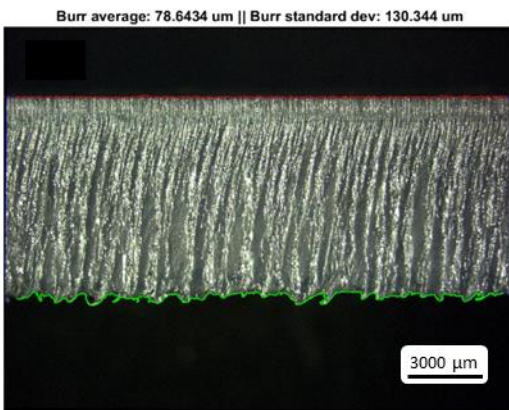
Figure 77: Burr profile - External geometry (GeoExt)
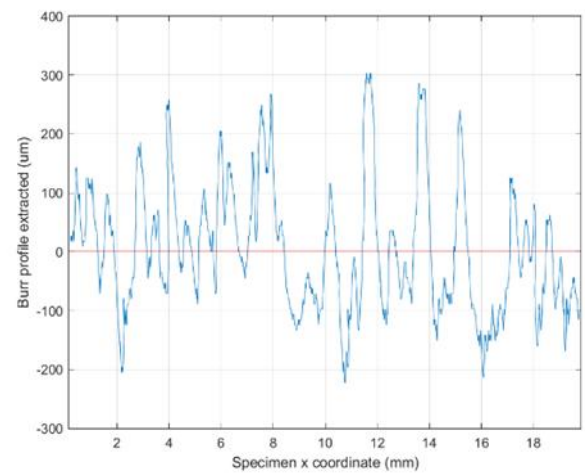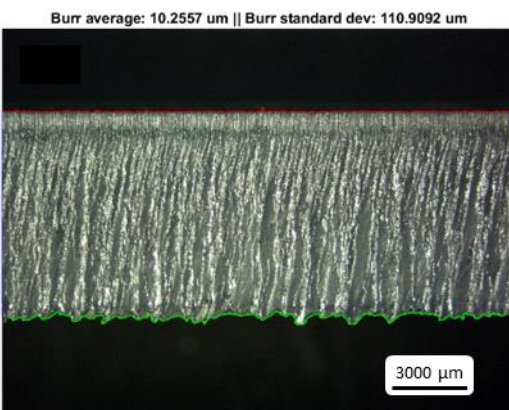
Figure 78: Burr profile - Internal&External geometry (GeoIntExt)

94
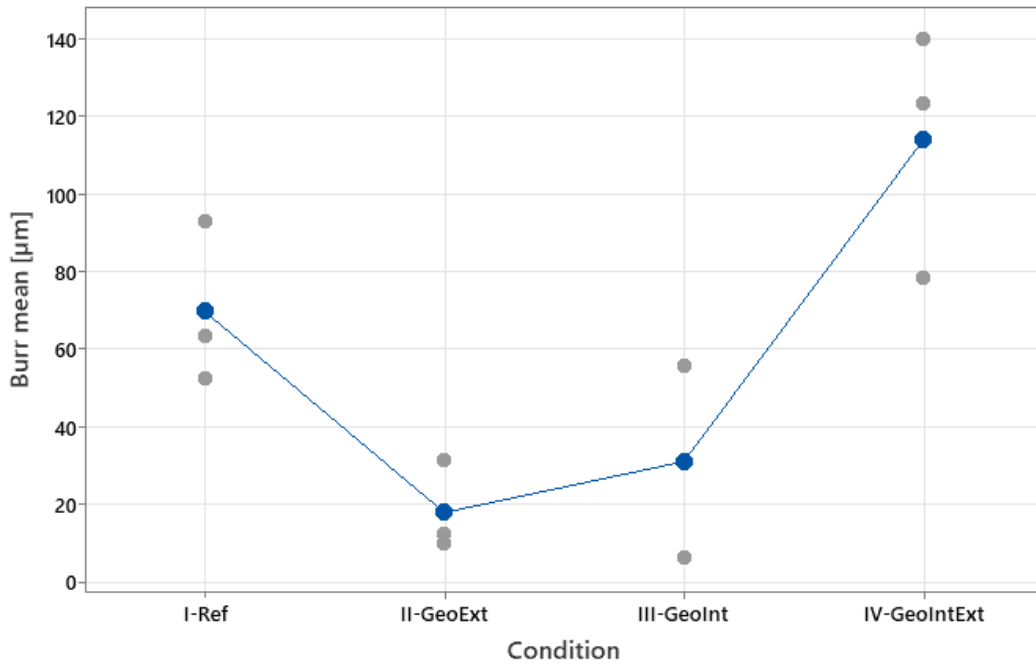
Figure 79: Individual value Plot of Burr means [μm] versus Condition

Thus, analyzing the mean burr values and corresponding standard deviations of the different geometries in Figure 80, the trend does not seem to be well defined. There is in fact an initial decrease in the mean value, but it goes up again in the last inner and outer geometry.

In the last graph, however, in Figure 81 we went to analyze the maximum variation of the burr trend, calculated as the difference between the maximum peak value and the minimum valley value.

Indeed, the trend of this variation seems to have an increasing trend as the geometry used changes in accordance with an increase in the preheating temperature, which thus seems to cause an increase in burr formation. However, we are talking about a difference averaging about 60 μm, a difference that cannot be considered significant of a critical increase in burr formation.
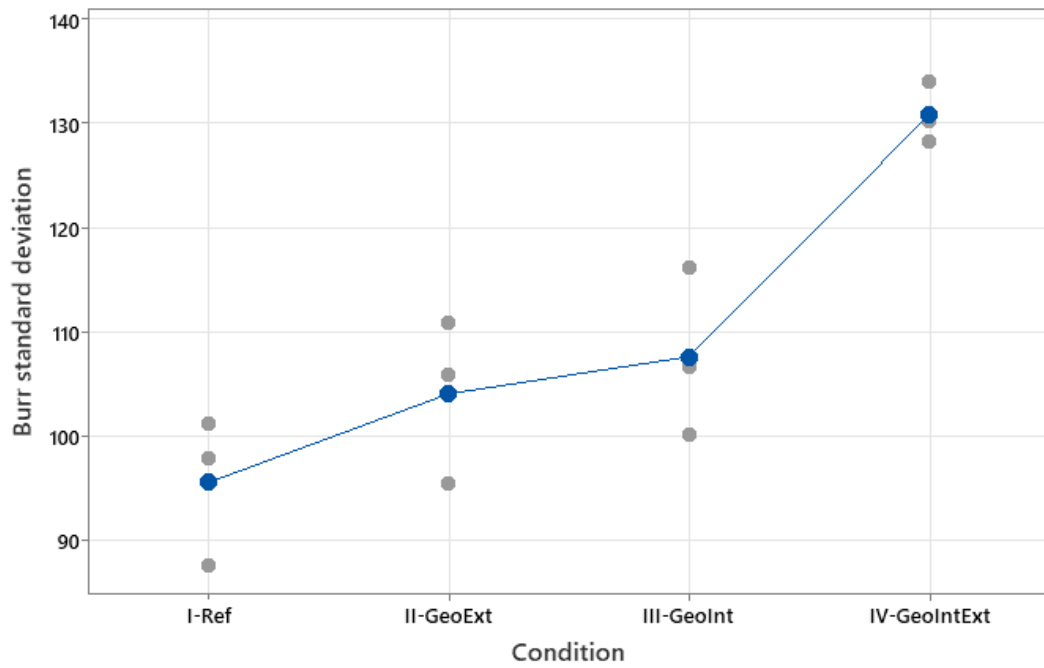
Figure 80: Individual value plot of Burr standard deviation versus Condition
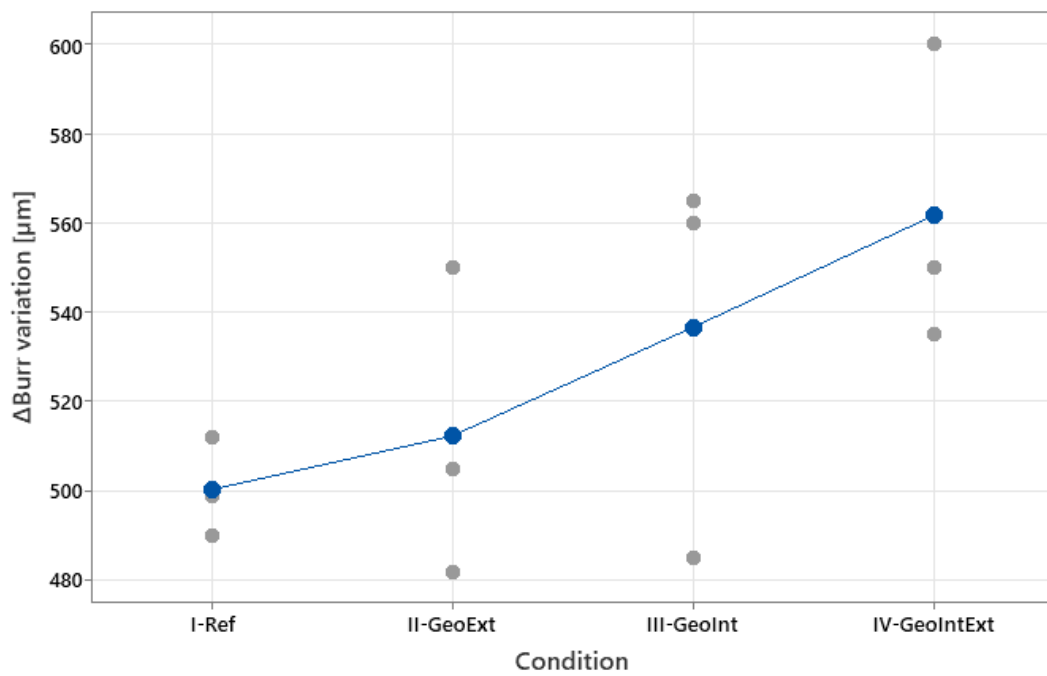
Figure 81: Individual value plot of Maximum ΔBurr variation [μm] vs Condition

7.2.3 Part geometry

A dimensional analysis of the cut samples after heating with the different geometries was performed.

Thus, the length in X and Y of each sample was examined, and these measurements were repeated three times to have more confidence in the value obtained.

In the first two graphs in Figure 82-Figure 83 it is possible to see the length of the samples in millimeter along the two different directions of analysis.

Starting, then, with noting that the average length for the reference samples, thus at room temperature, was 99,35 mm in X and 30,02 mm in Y, what emerges from the first two graphs is that we have an elongation of our sample along X direction while we have a shrinkage along Y direction.

More specifically, it seems that heating by only external geometry did not make any substantial changes, while for the two geometries Geo_Int and Geo_Int_Ext, it is possible to note this trend of size increase along X and a shrinkage along Y.
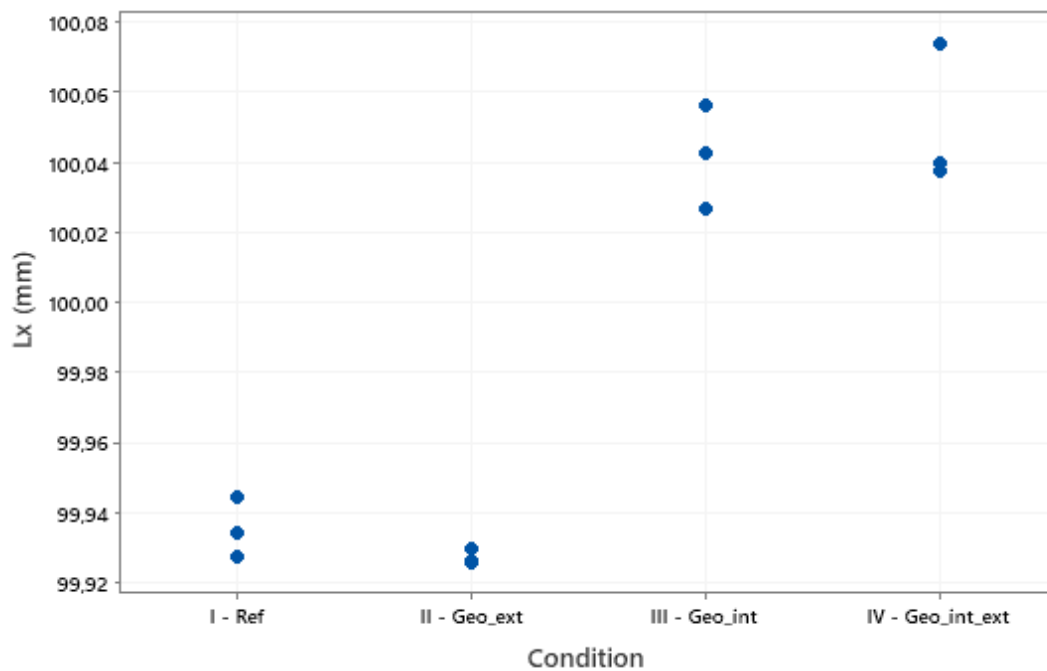
Figure 82: Individual Value Plot of the length of the samples in X direction [mm] at different conditions
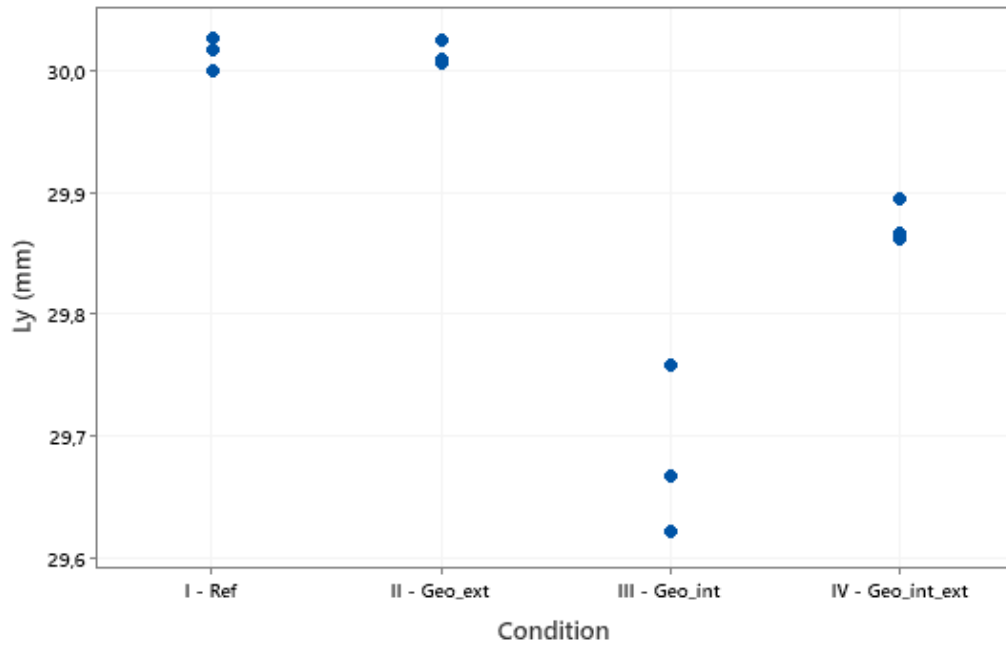
Figure 83: Individual Value Plot of the length of the samples in Y direction [mm] at different conditions

The ΔL in micrometers was also calculated using the formula of the equations (5.2) and (5.3). An Analysis of Variance was performed using of course as a factor the different condition analysed and so the different pre-heating geometries. The Condition factor is clearly significant on the changing in the dimensions of the samples.
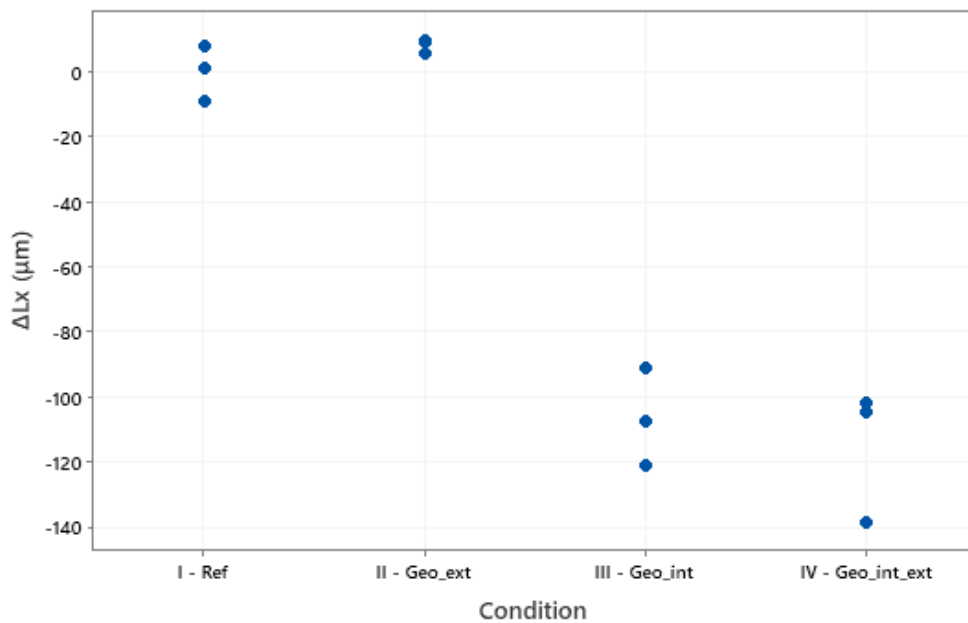
Figure 84: Individual Value plot of ΔLx – Elongation along X direction
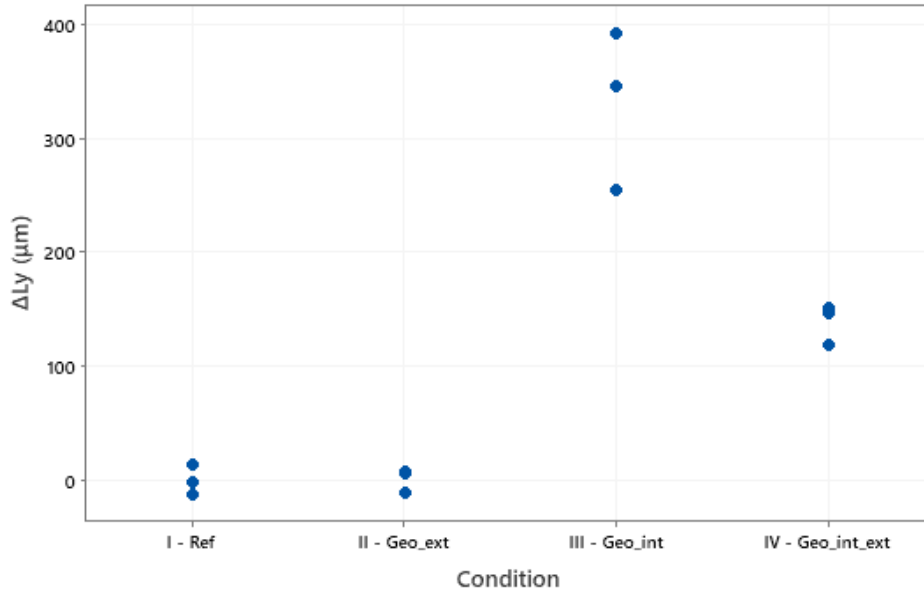
Figure 85: Individual Value plot of ΔLy – Elongation along Y direction

So it was also performed a comparison analysis through Tukey Comparison (Figure 86 and Figure 87) to check the different grouping. As it can be see also from the other graph, the Geo_Ext is in the same group of the Ref samples at room temperature, while the other two geometries are not in the same group.

Model Summary

S	R-sq	R-sq(adj)	R-sq(pred)
0,0133053	96,55%	95,25%	92,23%

Factor Information

Factor	Type	Levels	Values
Condition	Fixed	4	I - Ref; II - Geo_ext; III - Geo_int; IV - Geo_int_ext

Analysis of Variance

Source	DF	Adj SS	Adj MS	F-Value	P-Value
Condition	3	0,039583	0,013194	74,53	0,000
Error	8	0,001416	0,000177		
Total	11	0,040999			

Tukey Pairwise Comparisons: Condition

Grouping Information Using the Tukey Method and 95% Confidence

Condition	N	Mean	Grouping
IV - Geo_int_ext	3	100,050	A
III - Geo_int	3	100,042	A
I - Ref	3	99,935	B
II - Geo_ext	3	99,927	B

Means that do not share a letter are significantly different.

Figure 86: ANOVA and Tukey Pairwise Comparisons in X, for the different geometries

Grouping Information Using the Tukey Method and 95% Confidence

Condition	N	Mean	Grouping		
I - Ref	3	30,0142	A		
II - Geo_ext	3	30,0134	A		
IV - Geo_int_ext	3	29,8751		B	
III - Geo_int	3	29,6832			C

Means that do not share a letter are significantly different.

Figure 87: Tukey Pairwise Comparisons in Y, for the different geometries

Having the linear thermal expansion model available and knowing the value of the coefficient of thermal expansion of aluminum Al 5754, a characteristic value that we are interested in analyzing is therefore the ΔL/Lo, which allows us to understand whether or not in the two directions analyzed, we have a linear type relationship if we relate this coefficient to the change in temperature.

So, we used the following Equations (7.1) and (7.2) to calculate the ΔL/Lo both for the X and Y directions:

$$\frac{\Delta L_x \ [mm]}{Lo_x \ [mm]} = \frac{Lo_x \ [mm] - L_x \ [mm]}{Lo_x \ [mm]} \tag{7.1}$$

$$\frac{\Delta L_y [mm]}{Lo_y \ [mm]} = \frac{Lo_y \ [mm] - L_y \ [mm]}{Lo_y \ [mm]} \tag{7.2}$$

After that we had the possibility to try to analyse this data and try to see if a linear regression model can be applicable and if this model is in accordance with the theoretical model.

What emerges from these data, however, is a result that is inconsistent with what is the theoretical model.

The basic peculiarities that we notice are first of all that we have, as mentioned earlier, an expansion along the direction in X and a shrinkage along the direction in Y, and this expansion or shrinkage also has two different coefficients of thermal expansion for the two directions.

The linear regression model also, as can be seen in Figure 88 and Figure 89, does not describe well the trend of the data and is not able to predict in a consonant way the expansion trend of the analyzed sample.
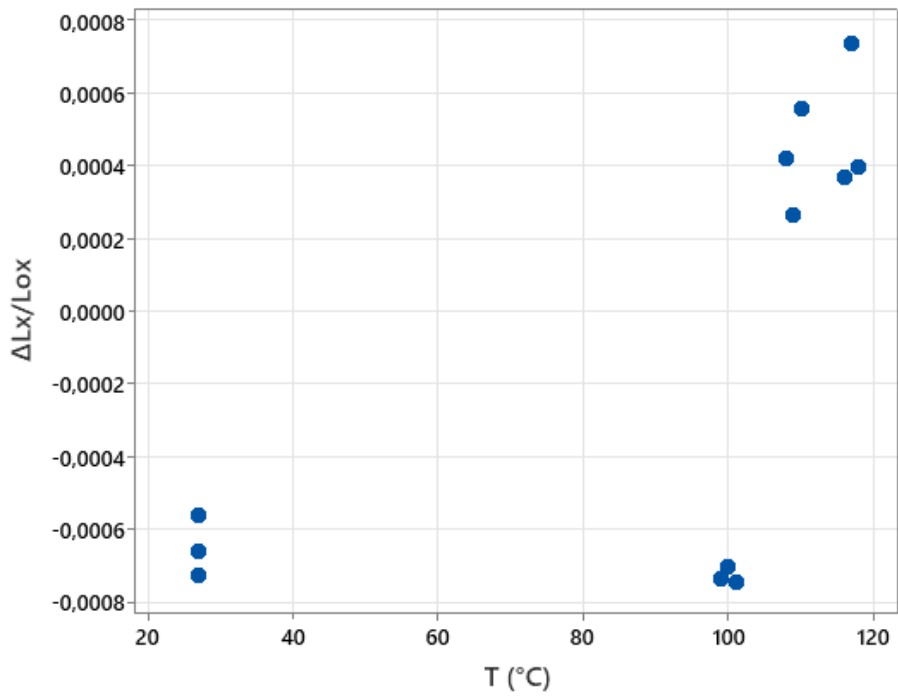
Figure 88: Scatterplot of $\Delta L_x/Lo_x$ versus $T[°C]$
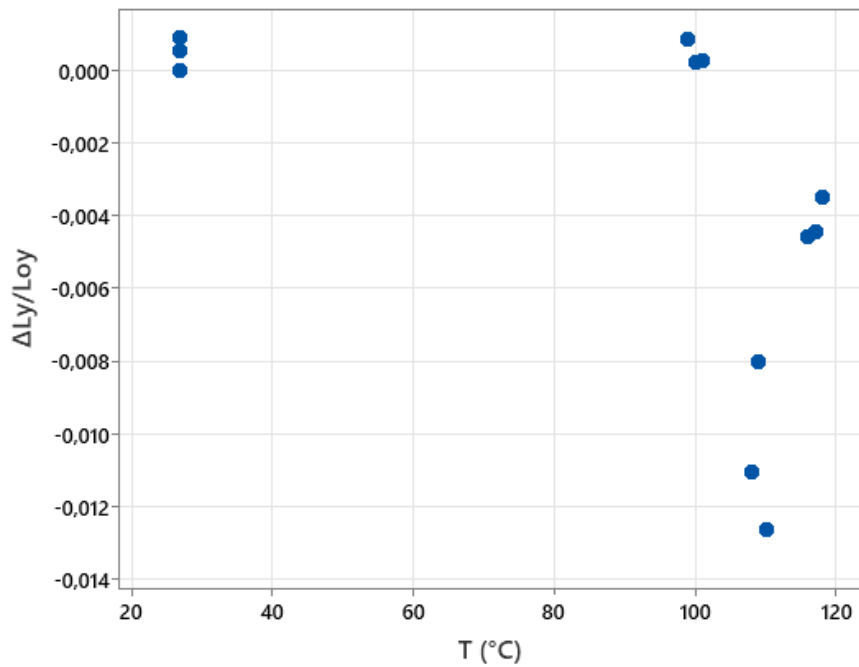
Figure 89: Scatterplot of $\Delta L_y/Lo_y$ versus $T[°C]$

This behaviour of the sample is particularly unexpected, and it is necessary to further investigate the causes of this behaviour.

In fact, if we were to consider the theoretical model of linear expansion, we would have expected an expansion of the sample in both X and Y dimensions, but what happens in this case, through pre-heating of the plates by laser cutting geometries, conflicts with this theoretical model as we have an expansion along one of the two axes and a shrinkage along the other axis.

This could be attributed to the strong inhomogeneity in the heating of our sheets. In fact, we must consider two fundamental things, namely firstly that this pre-heating method takes place in a slow manner and, above all, the heating takes place through a path that varies constantly over time, so the heating of the sheet takes place at different times and at different points of the part.

This heating method also takes a considerable amount of time, which leads not only to uneven heating, but also to a possible partial cooling of the sheet metal in some areas where we are far from the momentary cutting point for heating.

This inhomogeneity of heating and cooling could in fact cause the phenomenon described above by creating disparities along the two axes.

Another reason for such behaviour could be that of the presence of residual stresses in the sheet on which we have performed the cutting of the samples, subject to rolling processes that have probably precisely left residual stresses that have not been removed.

Our concern will therefore be first of all to test a heating system that guarantees with certainty a homogeneous heating of the whole sample, to go and confirm or disprove the influence of residual stresses on the different expansion of the piece in the two different directions and to test precisely if heating homogeneously there is no difference in the expansion in the two directions X and Y.

8. Characterizing part quality after the laser cutting under controlled preheating conditions

8.1 Experimental design

The experimental set-up used for heating the aluminium before cutting using cartridge heating elements was defined in Section 6.4.

An image of the model and the final set-up is shown here in Figure 90 for clarity.
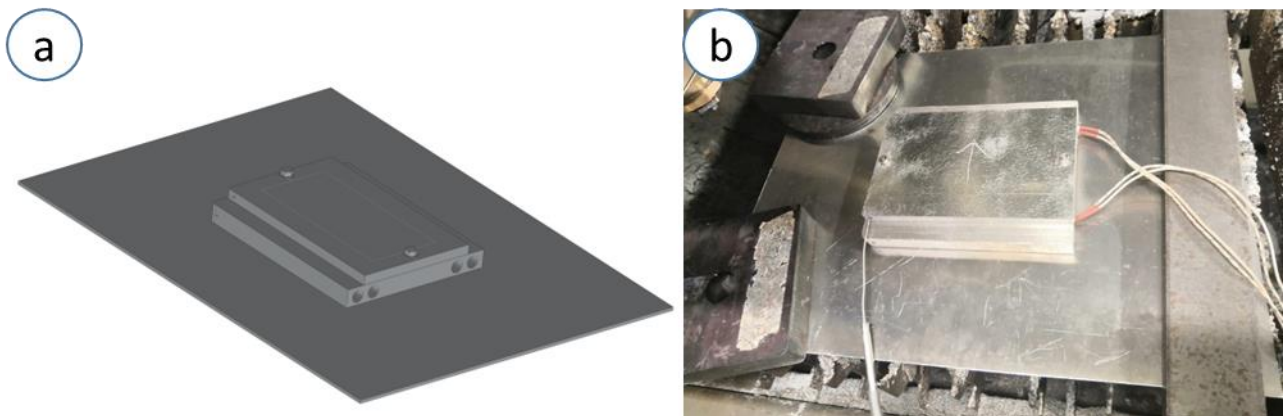
Figure 90: 3D model (left) and final experimental set-up (right) of the cartridge pre-heating method

The objective of pre-heating through this methodology was to solve some of the problems related to the previous methodology where we used laser cutting of different geometries for pre-heating.

Through this method, we aimed to obtain a much more homogenous distribution of the heat along the entire length and thickness of the part, in order to analyse the trend in the two different directions in X and Y correctly.

We also aimed to have greater control of the temperatures both during heating and stabilisation of the same, through control by means of a special thermoregulation unit (described in section 5.8) and a special thermocouple inserted in the part for an even more accurate check.

Finally, this set-up was designed to ensure good repeatability for the various measurements and for any future measurements, by using M4 screws for stability, which are easily removable and manageable.

The design of the experiments for the cartridge pre-heating method was then worked out, where we once again used fixed cutting parameters for each different thickness analysed (parameters in Table 20), and only varied the pre-heating temperature value in a very controlled manner (Table 21).

We will therefore again assess dimensional, roughness and burr defects as in the previous chapter.

As far as dimensional analysis is concerned, we will analyse the total expansion value e_{TOT} (as defined in Equation 4.3), which takes into account both the dimensional error due to shear width and that due to thermal expansion.

Table 20: Process parameters for cutting Al 5754 with different thicknesses

Fixed process parameters for cutting Al 5754							
Thickness [mm]	Power [W]	Cutting speed [mm/m]	Focal position [mm]	Gas type	Gas pressure [bar]	SOD [mm]	Tool offset (25°C) [mm]
8	5580	2000	-7.5	Nitrogen	15	0.7	0.32
5	5080	6600	-4.5	Nitrogen	14	0.7	0.2
2	5580	8000	+3	Nitrogen	8	0.7	0.35

Table 21: Variable process parameter for DOE analysis

Variable parameter	
Temperature	25-100-175-250 °C

8.2   Results

First of all, we went to investigate by means of this cartridge heating method, whether having homogenous heating over the entire workpiece there was still a difference in the thermal expansions along the two directions x and y, and if we could attribute that difference to the rolling direction of the starting plate at our disposal.

For this reason, an analysis of variance was performed using the temperature variation and the rolling direction of the workpiece as variable factors to rule out or confirm such behaviour.

The first analysis of variance therefore included as fixed parameters the cutting parameters of the workpiece (different according to the thickness we were going to cut), while as variable parameters the temperature variation and the rolling direction previously measured on the specific workpiece before cutting were taken into account.

The first of the two variable factors had four different levels, specifically 25-100-175-250°C, i.e. a ΔT of 75 °C for each measurement, while the second variable factor, i.e. the rolling direction had only two levels, rolling in the X-direction and rolling along Y.

The samples were therefore divided according to their rolling direction and length measurements were taken for both directions after the samples were obtained after heating and cutting the part.

Two replicates were performed for each level, so for each temperature under analysis we had 4 samples, two with rolling direction along X and 2 with rolling direction along Y.

After collecting all our samples in the experiment design, we first went to perform the dimensional analysis of the samples. Then using a the Mitutoyo optical microscope, we went to measure the samples obtained, in the two different lengths, measurements performed as described in the Section 5.7.

As can be seen from the analysis of variance in Table 22, as well as from the plot of the Main Effect in Figure 91, it is evident here that the rolling direction factor is not a significant value in the dimensional analysis, i.e. the rolling direction did not significantly alter the variation in sample size.

Consequently, it was decided to only take the temperature as a variable factor in the subsequent analysis, in order to better assess its influence and also to have a larger number of samples and a more accurate analysis.

It was also decided to take only the size in X as it is more reliable because it is larger and easier to study.

The second important variable in the study of this thesis was, as mentioned, the thickness of the plates to be cut and consequently the thickness of the samples analysed.

Three different thicknesses of the same Al 5754 aluminium were analysed, namely 8, 5 and 2 mm.

Since the cartridge heating method is much more homogenous and controlled than the previous one, we were able to carry out our analyses on different thicknesses and temperatures without major obstacles.

A lateral hole for the insertion of the thermocouple was still to be made in each plate to ensure good temperature control.

The thickness parameter, however, was not included in the design of the experiments; instead, three different experiment designs were carried out for each different thickness, with only the temperature being changed as a parameter.

Table 22: Analysis of Variance of ΔL/Lo with Temperature [T] and Lamination direction as variable factor

Factor Information

Factor	Type	Levels	Values
Temperature [T]	Fixed	4	25; 100; 175; 250
Lamination direction	Fixed	2	x; y

Analysis of Variance

Source	DF	Adj SS	Adj MS	F-Value	P-Value
Temperature [T]	3	260424	86808	69,97	0,000
Lamination direction	1	3897	3897	3,14	0,104
Error	11	13647	1241		
Lack-of-Fit	3	4550	1517	1,33	0,330
Pure Error	8	9098	1137		
Total	15	277968			
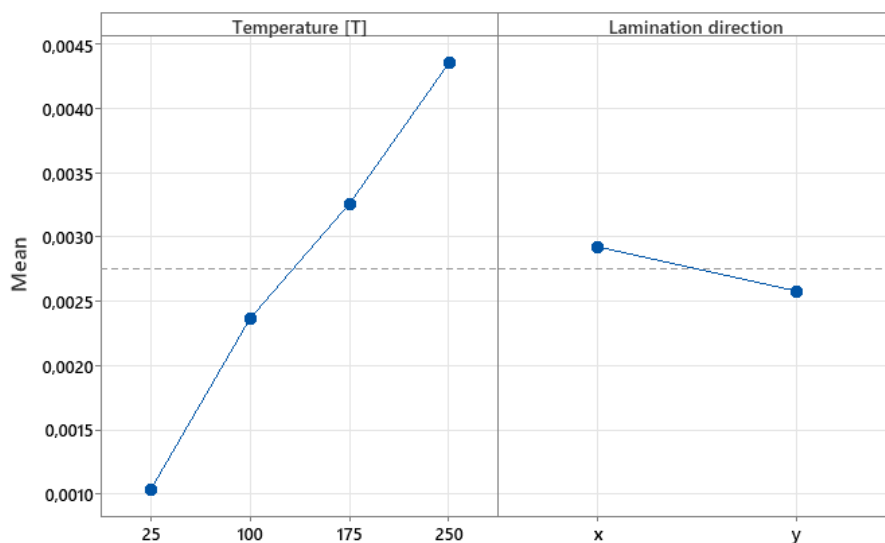
Figure 91: Main Effect Plot of ΔL/Lo with Temperature [T] and Lamination direction as variable factor

8.2.1 Geometrical analysis

Below, therefore, are the data relating to the dimensional analysis performed on the different thicknesses indicated above.

Looking first at the graphs of the individual value plot, we can begin to notice a decreasing trend in the dimension value in X, i.e. a more or less linear shrinkage as the temperature changes.

In all three thicknesses, we started from an average sample length of around 100 mm, i.e. very close to the nominal length considered. Particularly in the case of the 8 mm thickness, we notice an extreme linearity in the shrinkage of the samples, which on average shrink by about 0,16 mm for every 75 °C increase in temperature. What physically takes place when we heat up the metal plate, and then we cut the samples with the dimensions already imposed, is not shrinkage, but rather an expansion of the original sheet, which, however, being cut to the same dimensions imposed in the machine, leads, after cooling, to a shrinkage of the test piece, as explained in Figure 92. For the analysis anyway we need to consider the final shrinkage due to this reason.

a) Metal sheet with imposed sample cut dimensions

b) Metal sheet heated-up and expanded, but with the same imposed sample cut dimensions

c) Cut sample (heated) with the imposed dimension

d) Cut sample (cooled at room temperature) with reduced final dimensions
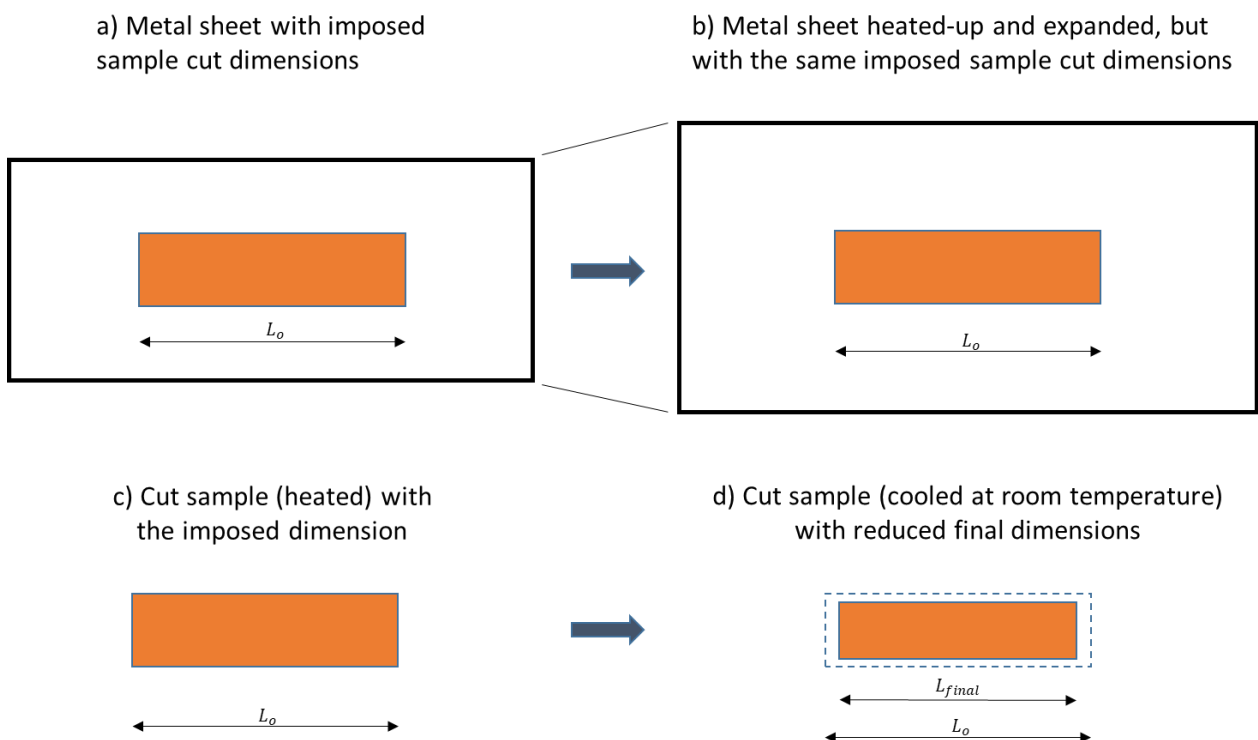
Figure 92: Different steps for the metal plate to be cut

Particularly in the case of the 8 mm thickness in Figure 93, we notice an extreme linearity in the shrinkage of the samples, which on average shrink by about 0,16 mm for every 75 °C increase in temperature.

On the other hand, looking at the two individual value plots of the other two thicknesses, despite the lower linearity, we still have a sustained trend in the reduction of the size in X of the part. In the case of the 8 millimetres, we go from an average length at room temperature of 100,01 mm to a length at 250°C of 99,51 mm, with a total reduction of 0.5 mm on average.
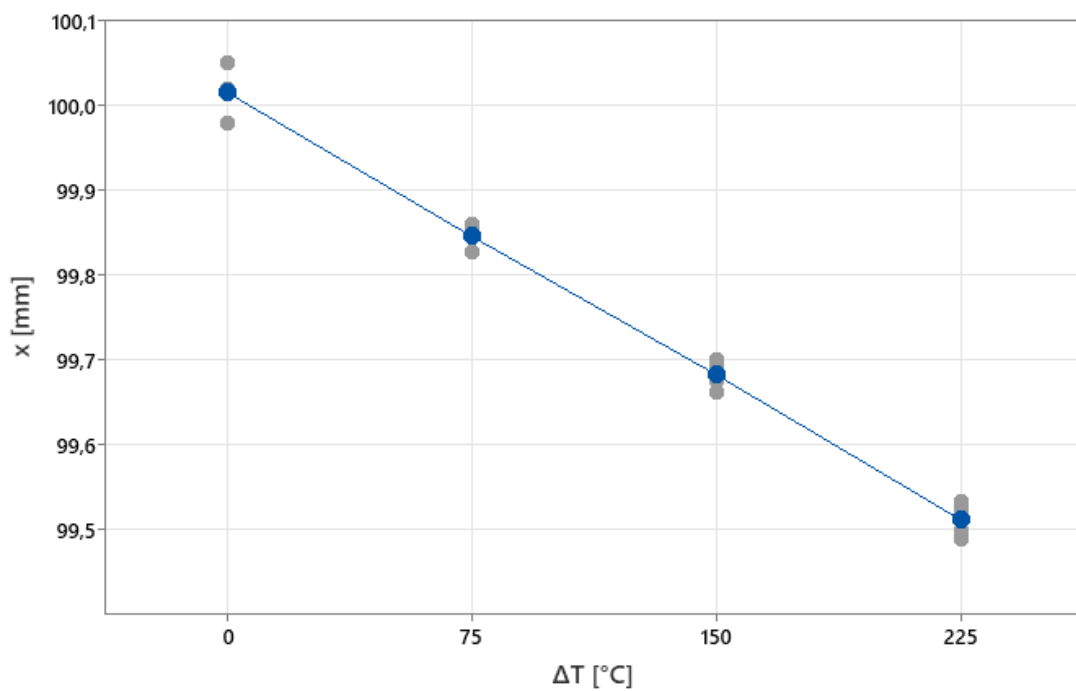
Figure 93: Individual value plot of the length of the samples in X direction [mm] for the different temperatures – 8 mm thickness

In the case of the 5 millimetres (Figure 94), on the other hand, the dimensions of the sample go from 100,04 mm to 99,56 mm, with a total reduction of 0,48 mm on average.
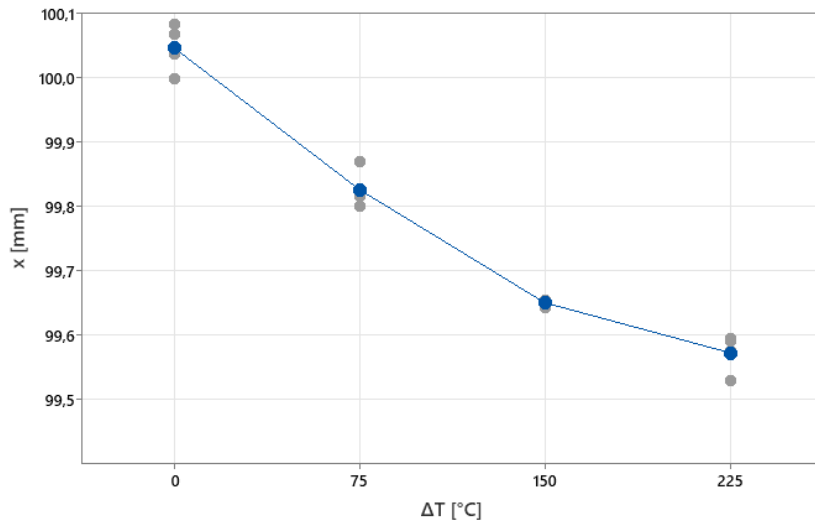
Figure 94: Individual value plot of the length of the samples in X direction [mm] for the different temperatures – 5 mm thickness

Finally, in the case of the 2 mm thickness (Figure 95), the dimensions of the sample go from 99,98 mm at room temperature to 99,51 mm at 250°C, with an average reduction of 0,57 mm.

As can be seen then, despite the slight difference in linearity, the final result at 250°C appears to be extremely similar in all cases for the different thicknesses.
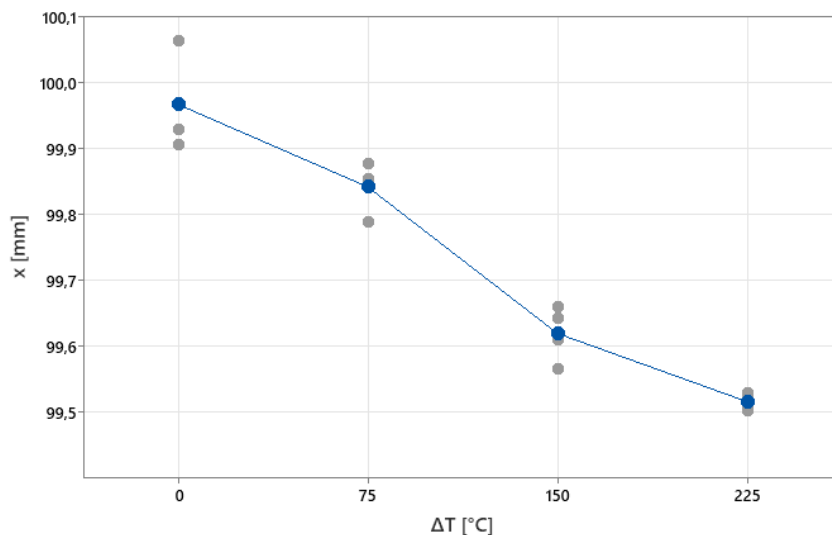
Figure 95: Individual value plot of the length of the samples in X direction for the different temperatures –

2 mm thickness

In order to better analyse the data collected and, above all, to assess whether or not there was a linear dependence between the expansion of our aluminium sheet and the temperature used, and whether or not this dependence could be found at all the thicknesses analysed, three different linear regression analyses were carried out for each thickness under examination.

Let us therefore analyse each case in detail.

As far as the 8 mm thickness is concerned, when analysing the data in the linear regression and ANOVA in Table 23, we can see that the imposed linear regression is significant, as is obviously the variation in temperature for the variation in sample size.

The regression analysis was performed on the e_{TOT} value in order to compare the values obtained as closely as possible with those of the model used and described in Section 4.3.

Regression Equation

$eTOT = 0{,}006398 + 0{,}000023\ \Delta T\ [°C]$

Coefficients

Term	Coef	SE Coef	T-Value	P-Value	VIF
Constant	0,006398	0,000155	41,22	0,000	
ΔT [°C]	0,000023	0,000001	20,66	0,000	1,00

Model Summary

S	R-sq	R-sq(adj)	R-sq(pred)
0,0003710	96,82%	96,60%	95,59%

Analysis of Variance

Source	DF	Adj SS	Adj MS	F-Value	P-Value
Regression	1	0,000059	0,000059	426,94	0,000
ΔT [°C]	1	0,000059	0,000059	426,94	0,000
Error	14	0,000002	0,000000		
Lack-of-Fit	2	0,000001	0,000000	2,85	0,097
Pure Error	12	0,000001	0,000000		
Total	15	0,000061			

Table 23: Regression Equation and ANOVA table – 8 mm thickness

It is immediately evident that there is a constant term, which is also significant in the regression analysis.

In fact, this term is fundamental for the calculation of the tool corrector at room temperature ($\Delta T = 0$), i.e. when the $e_{\Delta T}$ term in the Equation (4.3) is zero, and the dimensional error calculated on the e_{TOT} is to be attributed exclusively to the cutting kerf width.

$$e_{TOT} = e_{Corr} + e_{\Delta T} \qquad (4.3)$$

Considering in fact the expression of the e_{Corr} in the Equation (4.5):

$$e_{Corr} = \frac{2*\Delta_{Corr}}{L_o} = \frac{2*(Corr_1 - Corr_0)}{L_o} \qquad (4.5)$$

We can easily calculate the value of the tool offset corrector at ambient temperature, $Corr_o$, rearranging the last equation and using the Equation (4.11):

$$Corr_o = \frac{L_o * e_{Corr}}{2} \qquad (4.11)$$

The same is valid also for all the other thicknesses analysed.

We then note from the fitted line plot in Figure 96, an extreme linearity of the data, a homogeneous sheet expansion and the data all fall well within the confidence interval of the predicted model, we find no presence of outliers or values significantly different from the model used.

What we are therefore mainly highlighting is the regression equation that results from this model.
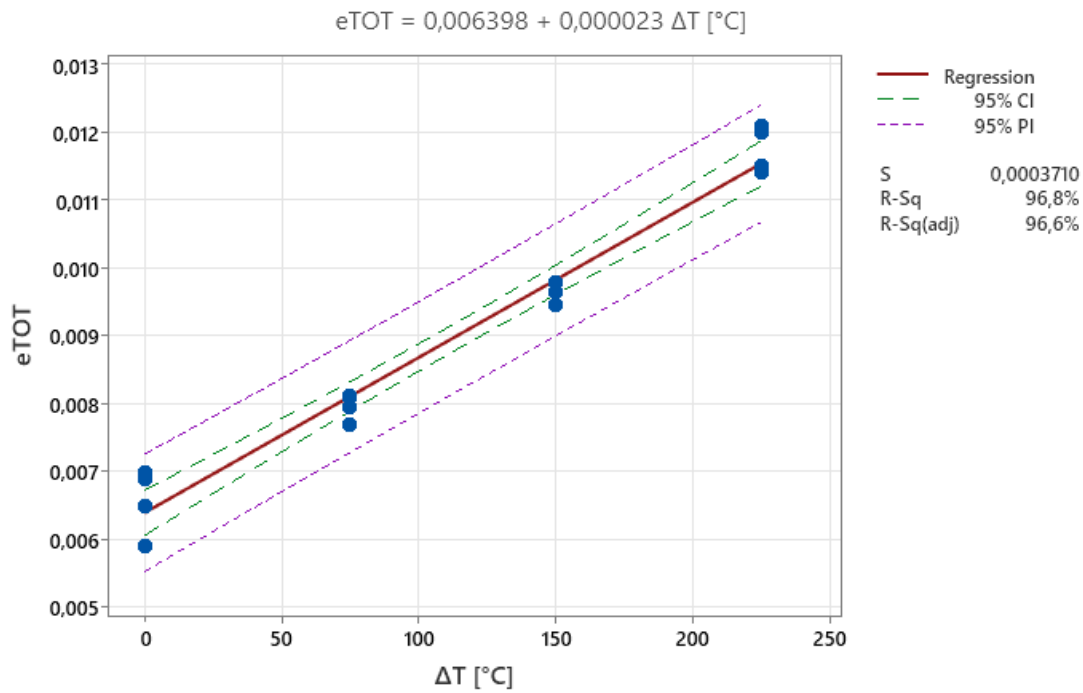
Figure 96: Regression analysis of e_{TOT} versus the variation of temperature ΔT [°C] – 8 mm thickness

What is in fact evident is that for all the three thicknesses under examination, we find a value of the angular coefficient of the regression line of approximately $21/22 \times 10^{-6}$. This angular coefficient, going back to the theoretical linear expansion model analysed in Chapter 4, to which we compare it, is none other than the coefficient of linear expansion of the material under examination, where we note an extreme correspondence between the experimental values obtained and the theoretical value at all the thicknesses analysed.

As we can in fact see from the model in Section 2.2.3.1, and from the Figure 15, the thermal expansion values found experimentally, reflect very well what has been described in the theory.

This indicates that at all the thicknesses analysed we have an expansion value at different temperatures that can be predicted and consequently corrected.

The only case in which the trend is not perfectly linear is found in the case of the 5 mm thickness, where, however, the values fall well within the confidence interval of the linear model and the linear regression model turns out to be the most significant, also with respect to higher order regression models.
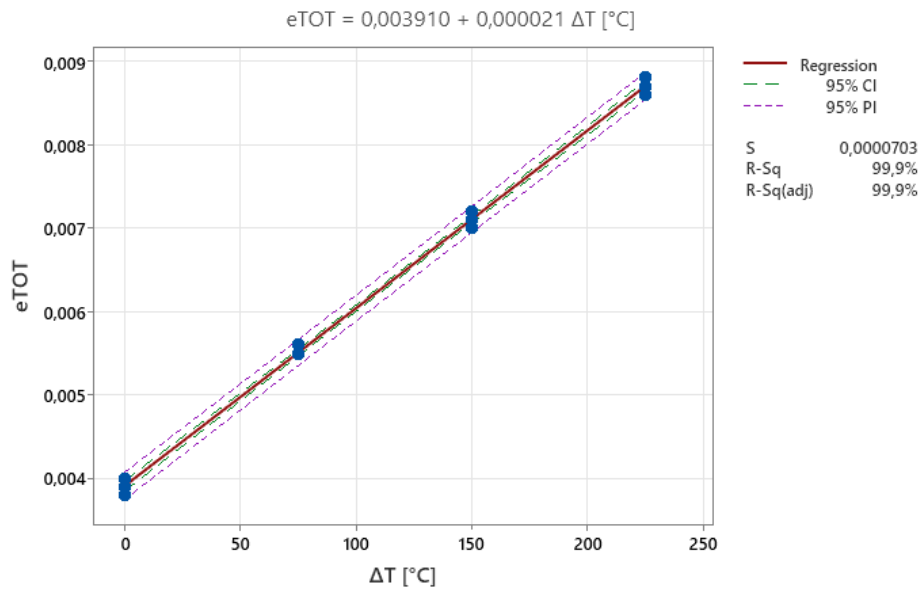
Figure 97: Regression analysis of e_{TOT} versus the variation of temperature ΔT – 5 mm thickness

Regression Equation

eTOT = 0,003910 + 0,000021 ΔT [°C]

Coefficients

Term	Coef	SE Coef	T-Value	P-Value	VIF
Constant	0,003910	0,000029	132,90	0,000	
ΔT [°C]	0,000021	0,000000	101,58	0,000	1,00

Model Summary

S	R-sq	R-sq(adj)	R-sq(pred)
0,0000703	99,86%	99,85%	99,82%

Analysis of Variance

Source	DF	Adj SS	Adj MS	F-Value	P-Value
Regression	1	0,000051	0,000051	10318,58	0,000
ΔT [°C]	1	0,000051	0,000051	10318,58	0,000
Error	14	0,000000	0,000000		
Lack-of-Fit	2	0,000000	0,000000	0,16	0,858
Pure Error	12	0,000000	0,000000		
Total	15	0,000051			

Table 24: Regression Equation and ANOVA table – 5 mm thickness
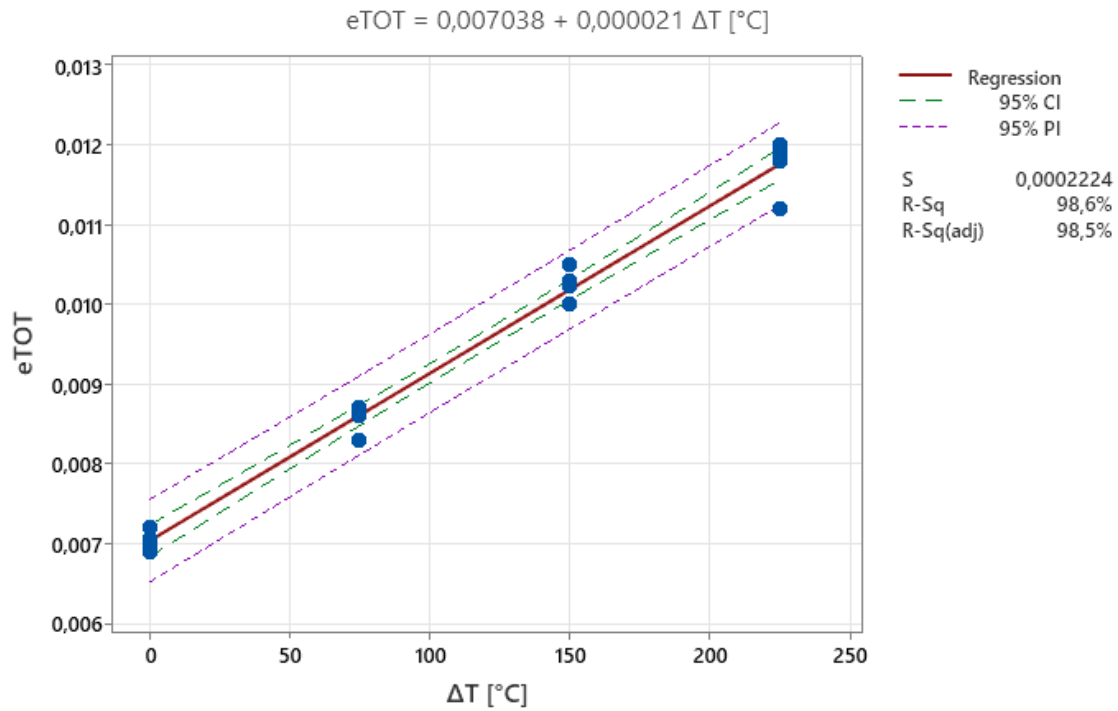
Figure 98: Regression analysis of e_{TOT} versus the variation of temperature ΔT – 2 mm thickness

Regression Equation

$$eTOT = 0{,}007038 + 0{,}000021 \; \Delta T \; [°C]$$

Coefficients

Term	Coef	SE Coef	T-Value	P-Value	VIF
Constant	0,007038	0,000093	75,64	0,000	
ΔT [°C]	0,000021	0,000001	31,62	0,000	1,00

Model Summary

S	R-sq	R-sq(adj)	R-sq(pred)
0,0002224	98,62%	98,52%	98,12%

Analysis of Variance

Source	DF	Adj SS	Adj MS	F-Value	P-Value
Regression	1	0,000049	0,000049	1000,07	0,000
ΔT [°C]	1	0,000049	0,000049	1000,07	0,000
Error	14	0,000001	0,000000		
Lack-of-Fit	2	0,000000	0,000000	0,31	0,741
Pure Error	12	0,000001	0,000000		
Total	15	0,000050			

Table 25: Regression Equation and ANOVA table – 2 mm thickness

114

8.2.2   Profile roughness

In this case, as in the case of heating by cutting geometries, we went to analyse the roughness values by means of the profilometer (Mahr Perthometer PGK described in Section 5.4) at three different heights of the sample under examination.

Using this method, as the temperature control and the cutting control were significantly higher than in the previous case, we were able to study both the case with a thickness of 8 millimetres and the case with 5-mm thick sheets. The heights of the three measurements for the 8-millimeter sheet have already been described above, but with regard to the three different heights of measurement for the 5 mm case, the TOP measurement was taken at 1 mm from the upper surface, the MID measurement as always at half the thickness, and finally the BOTT measurement at 1 millimetre from the lower surface.

In both cases, as was to be expected, "Location" (so the position of the measurement taken into account) turns out to be an extremely significant factor in the variation of the average roughness value.

8.2.2.1   Roughness results - 8 mm thickness

For the 8 mm thickness it is possible to see from the Main Effect Plot in Figure 99 that the only significant factor that affects the roughness values is the Location term, while we can see no significant influence of the other two.
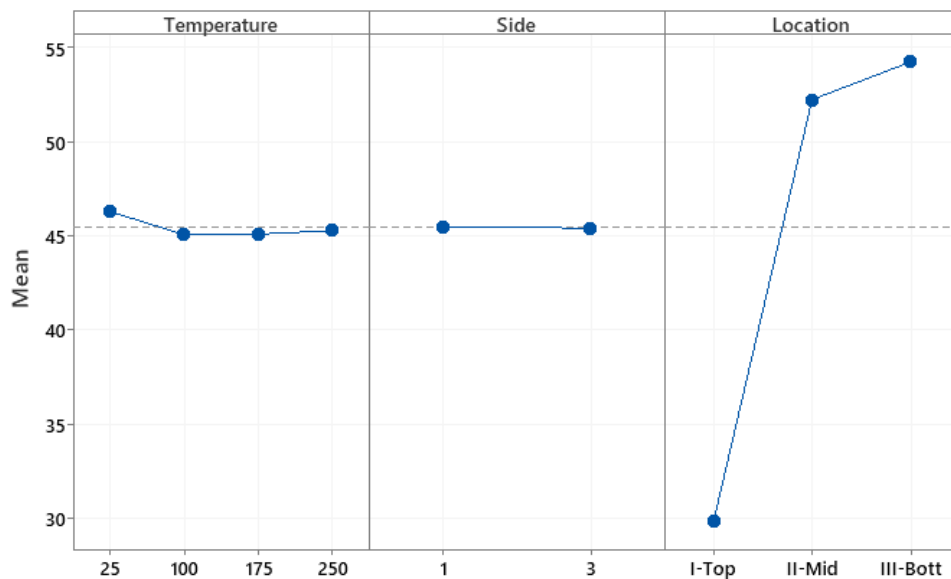
Figure 99: Main Effect Plot for Rz with factor: Temperature, Side and Location – 8 mm thickness

The roughness value in the top measurements varying in a range between about 20 and 40 micrometres, for the middle measurements between 35 and 65 μm and finally for the bottom measurements varying in a range between 40 and 70 μm.

Except in the case of the top measurements, in the other two we recognise no upward or downward trend in the roughness value, which remains extremely constant as the temperature changes.

For the top measurements, on the other hand, we note a very slight downward trend, where we go from an average of 32 μm at room temperature, to a value of 28 μm for the case at a temperature of 250°C, a difference of 4 μm which turns out to be completely irrelevant and whose variability can in any case be due to a not too large number of samples and above all this variability falls well within what can be considered as measurement error of the machine and the operator.
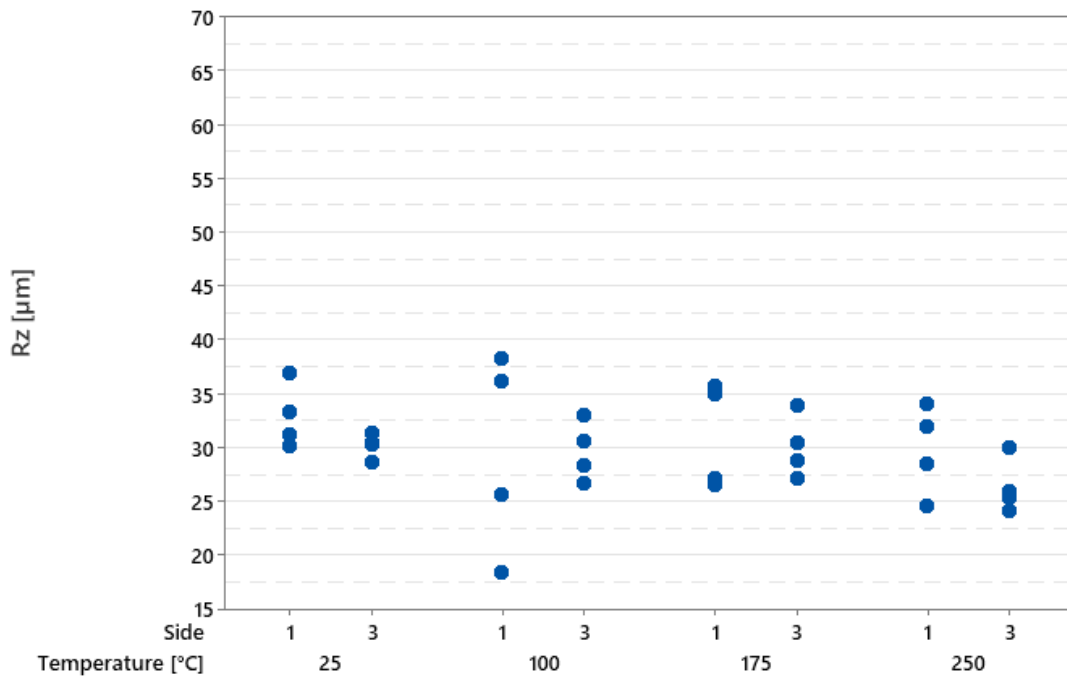
Figure 100: Individual value plot of Rz – Top measurements – 8 mm thickness
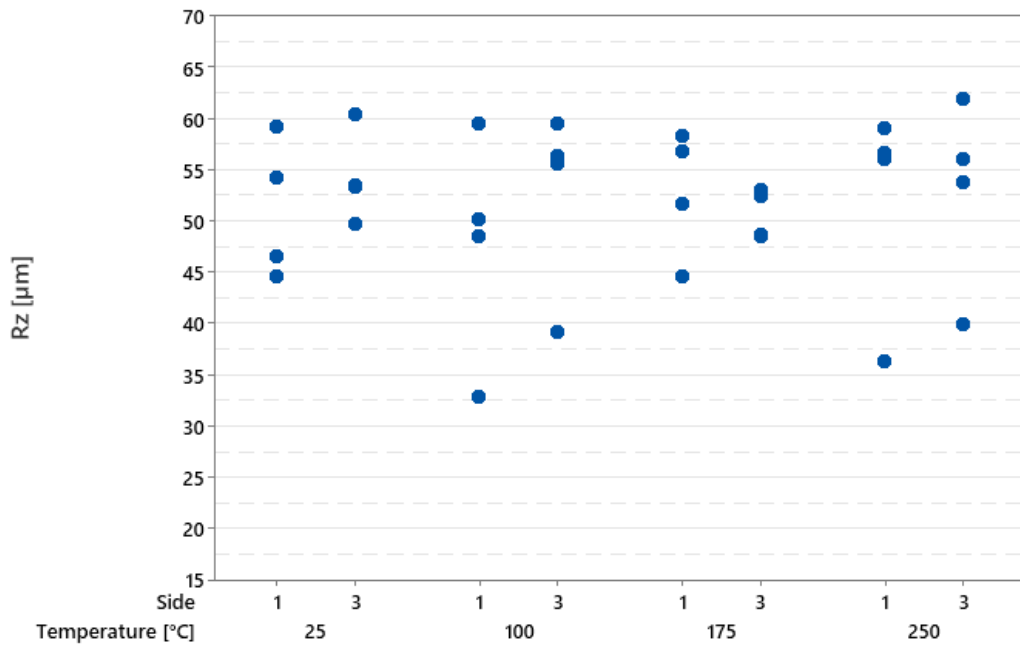
Figure 101: Individual value plot of Rz – Mid measurements – 8 mm thickness
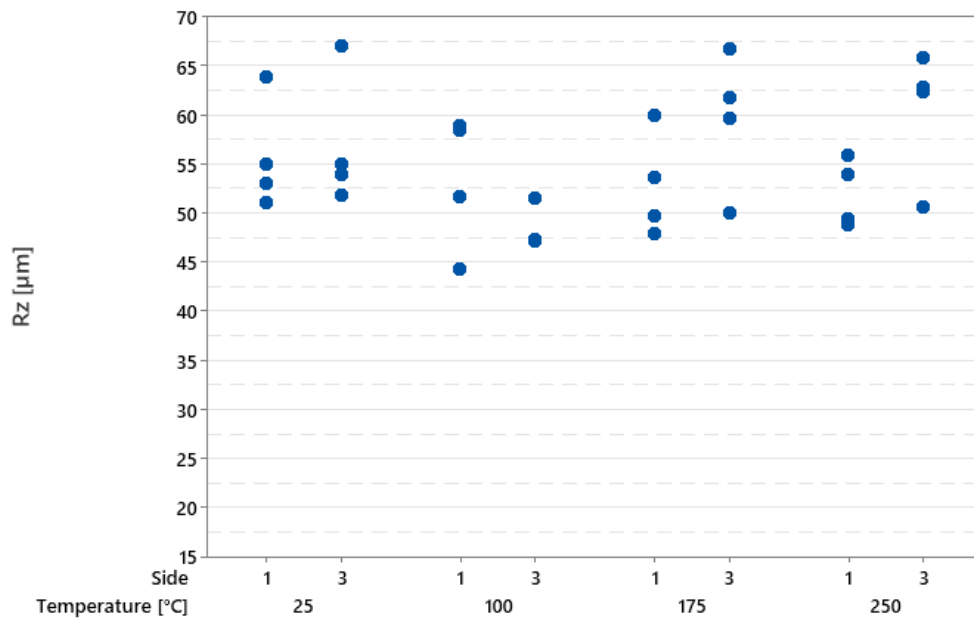
Figure 102: Individual value plot of Rz – Bott measurements – 8 mm thickness

The results of the ANOVA are shown in Table 26, where it's possible to see how both Temperature and Side are not significant for the Rz value while the Location factor is the only very significant.

Factor Information

Factor	Type	Levels	Values
Temperature	Fixed	4	25; 100; 175; 250
Side	Fixed	2	1; 3
Location	Fixed	3	I-Top; II-Mid; III-Bott

Analysis of Variance

Source	DF	Adj SS	Adj MS	F-Value	P-Value
Temperature	3	12,19	4,06	0,17	0,917
Side	1	0,01	0,01	0,00	0,988
Location	2	5876,87	2938,44	122,30	0,000
Error	41	985,07	24,03		
Lack-of-Fit	17	504,02	29,65	1,48	0,185
Pure Error	24	481,05	20,04		
Total	47	6874,14			

Model Summary

S	R-sq	R-sq(adj)	R-sq(pred)
4,90164	85,67%	83,57%	80,36%

Table 26: Analysis of Variance for Rz with factor: Temperature, Side and Location

8.2.2.2 Roughness results – 5 mm thickness

Considering instead the roughness analysis on the 5 mm thick samples, we find a similar trend, but with a few exceptions.

Here again (Figure 103), location is obviously a key factor.
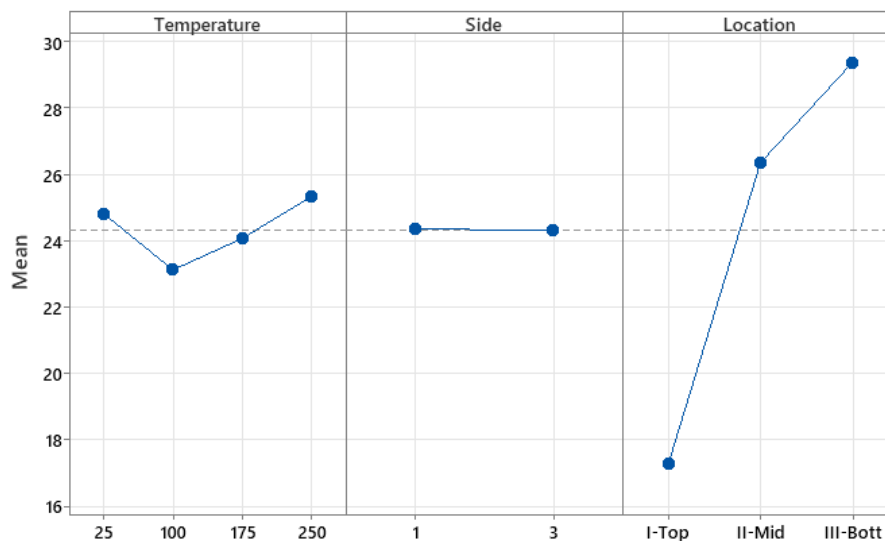
Figure 103: Main Effect Plot for Rz with factor: Temperature, Side and Location – 5 mm thickness

In the Top measurements (Figure 104), we find no upward or downward trend in the average roughness value; all the values of the various replicas and at the different temperatures are evenly distributed over a range of approximately 13 μm to 22 μm.
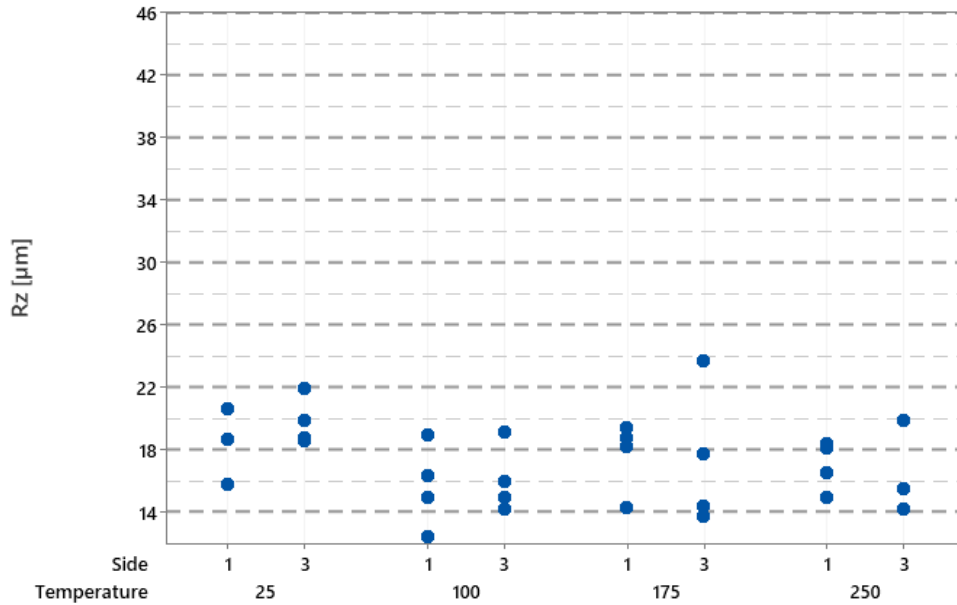
Figure 104: Individual value plot of Rz [μm] – Top measurements – 5 mm thickness

In the Mid values (Figure 105), the average roughness value is increased to a range from 22 μm to 33 μm, with a variation between the minimum and maximum of approximately 11 micrometres and a difference between the averages at the various temperatures of no more than one micron.
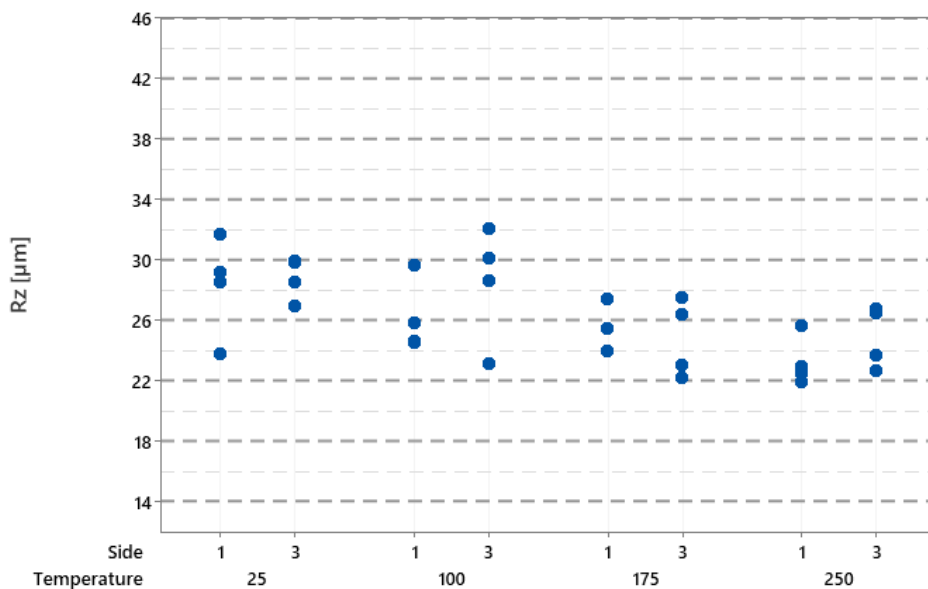
Figure 105: Individual value plot of Rz [μm] – Mid measurements – 5 mm thickness

The only measurement area in which a slight pattern of increasing roughness values is recognised concerns the Bott measurements (Figure 106), i.e. the measurements taken 1 mm far from the bottom surface of the sample.
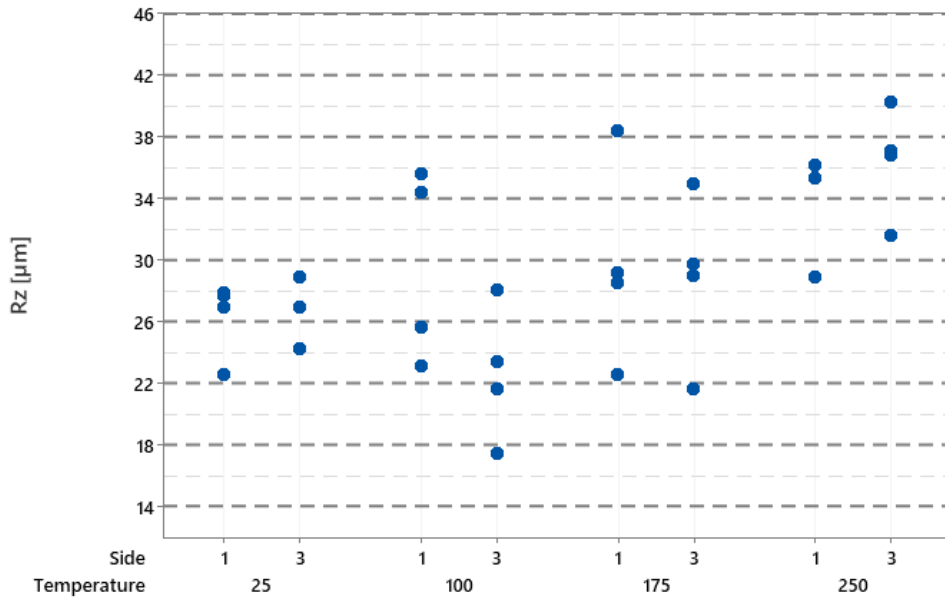
Figure 106: Individual value plot of Rz [μm] – Bott measurements – 5 mm thickness

Here, first of all, we have a range of roughness values from approximately 20 μm to 40 μm, and we notice an increase in the average roughness value from approximately 26 μm at an ambient temperature of 25°C, rising to an average value of 36 μm at 250°C with a total increase of 10 μm, certainly not very high, but nevertheless out of the range of possible machine measurement error.

This increase could be due to the fact that the increase in temperature leads to a different fluidity of the molten material during cutting, which leads to a different ejection of this material and more difficult re-solidification.

However, this difference in roughness could also be attributed to the cutting parameters used that are not perfectly suited to the thickness cut, using a higher cutting speed than necessary. The reasoning will be more deeply discussed in the next section 8.2.3.

The correctness of the cutting parameters used should therefore be further investigated by means of a dedicated design of experiment.

The results of the ANOVA are shown in Table 27, where it's possible to see how both Temperature and Side are not significant for the Rz value.

Factor Information

Factor	Type	Levels	Values
Temperature	Fixed	4	25; 100; 175; 250
Side	Fixed	2	1; 3

Analysis of Variance

Source	DF	Adj SS	Adj MS	F-Value	P-Value
Temperature	3	66,19	22,0624	0,50	0,680
Side	1	0,09	0,0858	0,00	0,965
Error	91	3979,50	43,7308		
Lack-of-Fit	3	28,56	9,5190	0,21	0,888
Pure Error	88	3950,95	44,8971		
Total	95	4045,78			

Table 27: Analysis of Variance for Rz with factor: Temperature, Side and Location

8.2.3 Burr attachment

Again, the other defect that went to study, was the definition and study of burr formation on the bottom surface of the cut samples, to understand how temperature differences went to affect it.

According to ISO 13705:2000 (42), as already mentioned, dross entities are calculated as the entire length exiting the bottom edge of the sample.

As mentioned in Section 5.5, after the high contrast image acquisition of the different sides of our samples using the Echo-Lab Microscope SM 535 H, we went to study such images through the use of the same MATLAB program used for studying the pre-heating through cutting geometries.

This analysis was performed for all the three different thicknesses analysed, 2 mm, 5 mm and 8 mm.

An ANOVA was then performed on the average burr value, using only the temperature as a variable factor, which varied over the four different levels of 25-100-175-250°C, having in this case a controlled temperature variation, which was not possible with the pre-heating through cutting geometries.

As can be seen from the graphs in Figure 107, as far as the average burr value is concerned, in the case of the 2 mm, the average values vary between about 13 μm and 18 μm, therefore extremely unvarying, considering the thickness of the sample, with an average, moreover, that deviates of no more than 1 μm from one to another.
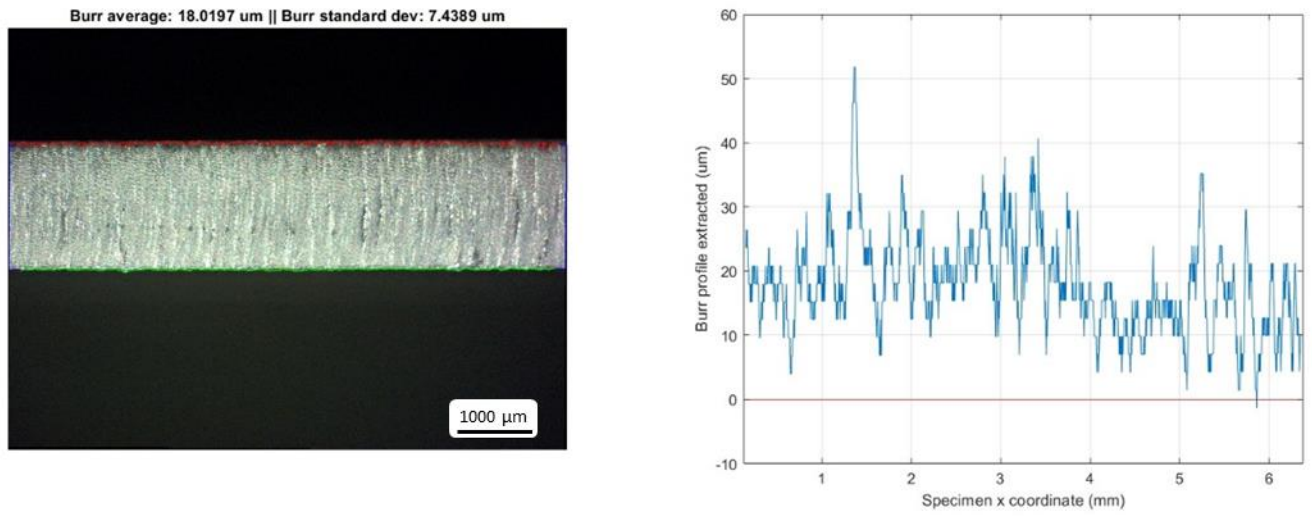
Figure 107:Burr profile with Average and Standard deviation values – 2 mm thickness – 100°C
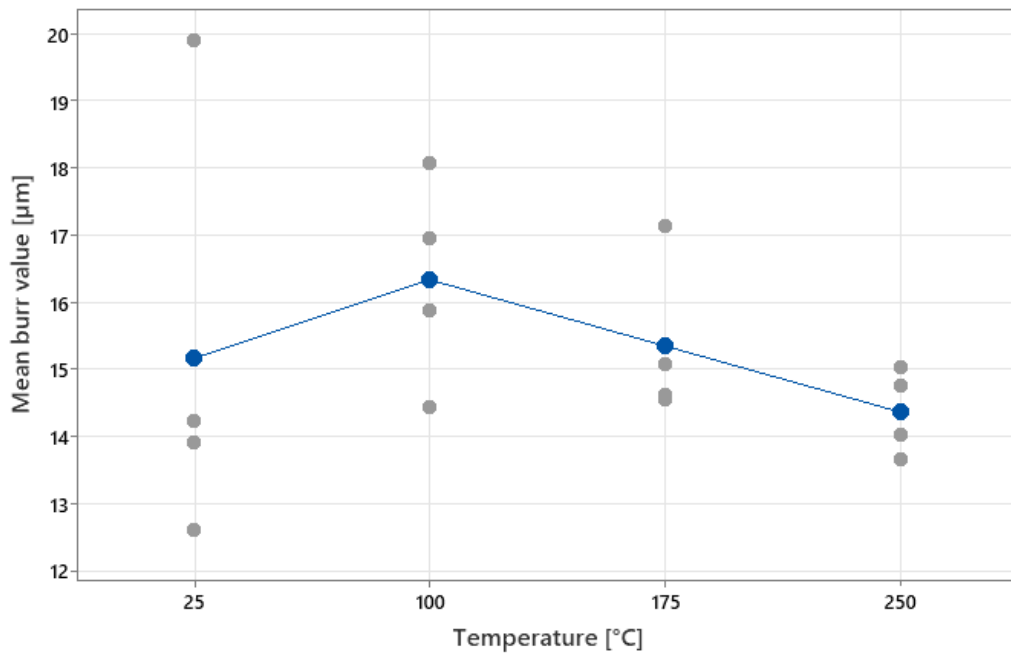
Figure 108: Individual Value Plot of Mean burr value [μm] – 2 mm thickness

Analysing the graph regarding the 5-mm-thick samples in Figure 110, the burr values vary in a range between approximately 32 μm and 40 μm, again with an average value that can be considered constant.
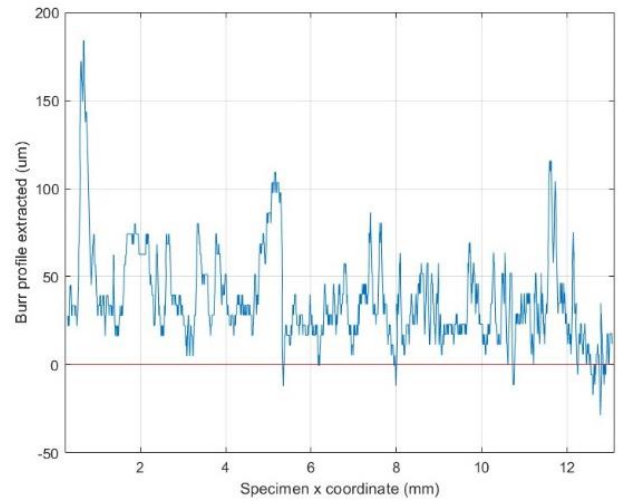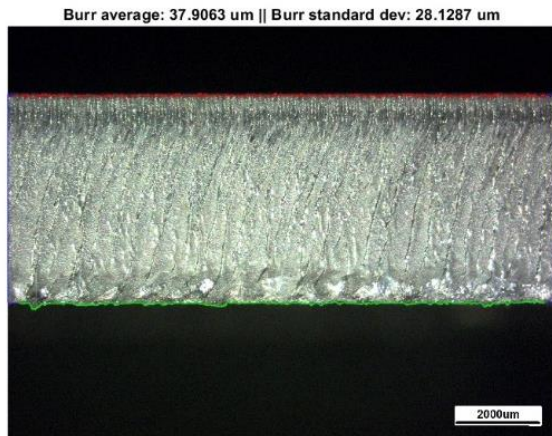
Figure 109: Burr profile with Average and Standard deviation values – 5 mm thickness – 100°C
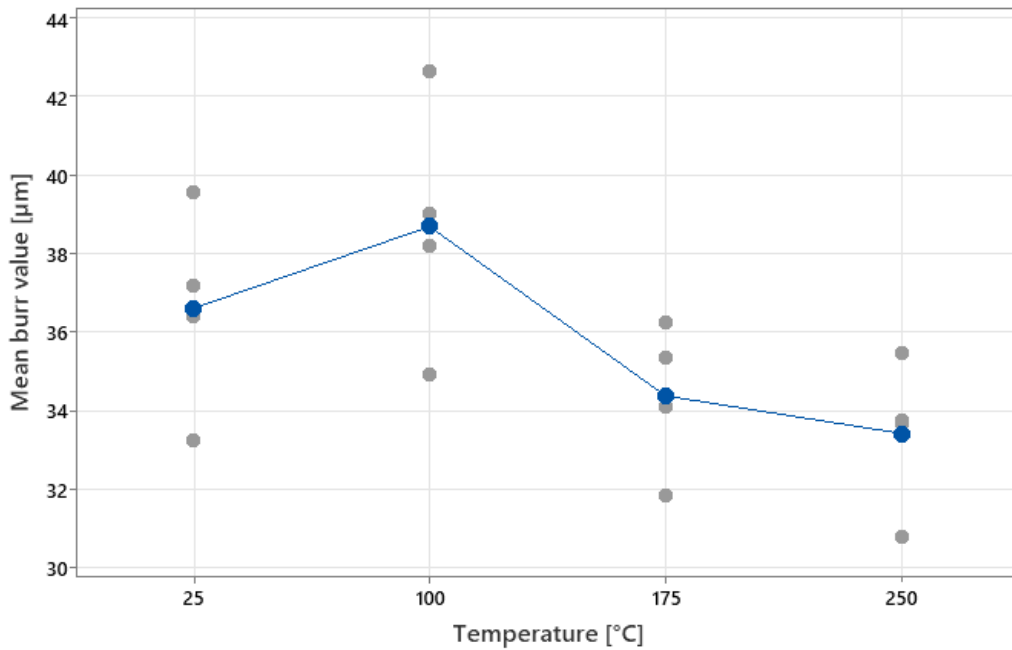
Figure 110:Individual Value Plot of Mean burr value [µm] – 5 mm thickness

Lastly, the graph regarding the 8-mm-thick samples in Figure 112, where the burr value increases to a range of values from about 150 µm to 170 µm, with an average value varying by no more than 5 µm as the temperature changes.
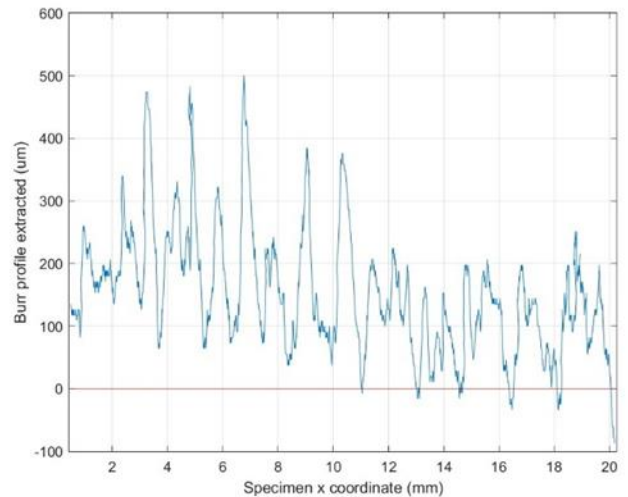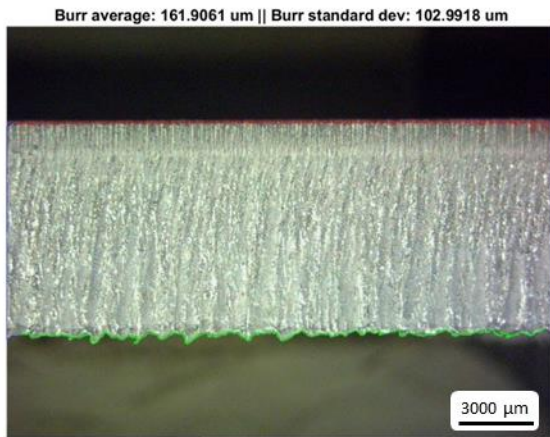
Figure 111: Burr profile with Average and Standard deviation values – 8 mm thickness – 100°C
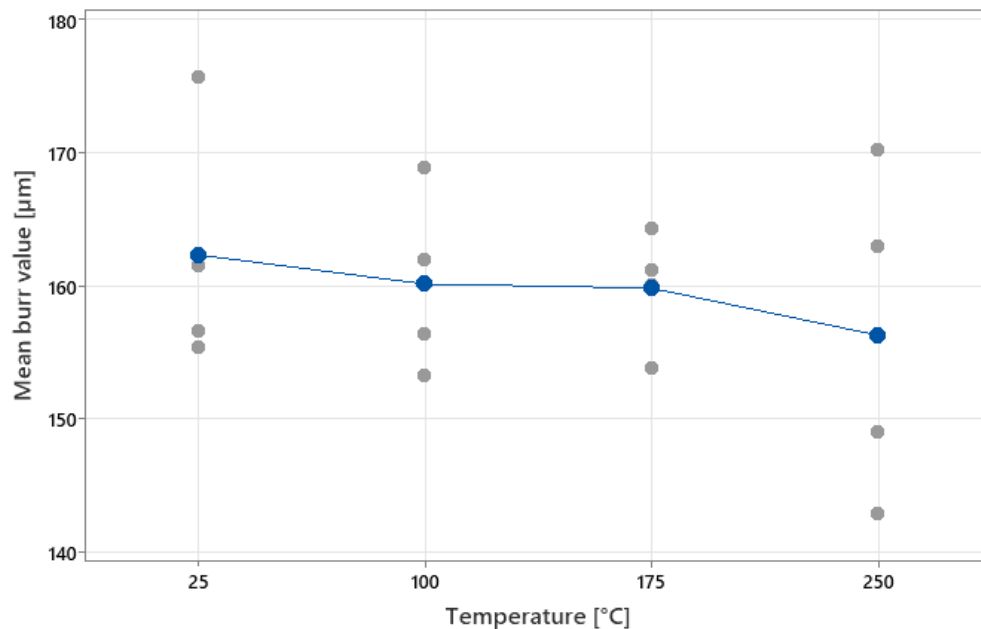
Figure 112:Individual Value Plot of Mean burr value [μm] – 8 mm thickness

As can be seen from the Table 28 of the ANOVA, the temperature factor does not appear to be significant when it relates to varying the size of the burr.

We then took care to analyse that these data had been collected properly and could be considered valid, so by means of the probability plot and the individual plot (that can be seen in the Appendix) of the standard residuals, we ascertained that there was no evidence of any particular pattern followed by the data, that the data were therefore normally distributed following a Gaussian pattern, and that there were no outliers that could alter the analysis of the average burrs values.

Factor Information

Factor	Type	Levels	Values
Temperature [°C]	Fixed	4	25; 100; 175; 250

Analysis of Variance for Transformed Response

Source	DF	Adj SS	Adj MS	F-Value	P-Value
Temperature [°C]	3	0,003183	0,001061	0,35	0,790
Error	12	0,036311	0,003026		
Total	15	0,039493			

Table 28: Analysis of Variance of Mean Burr height [μm] with Temperature [°C] as variable factor

In the following image in *Figure 113*, three examples of high-definition acquisition of samples are shown, one for each thickness under examination. All images show side 1 of the samples heated to 100°C and subsequently cut.
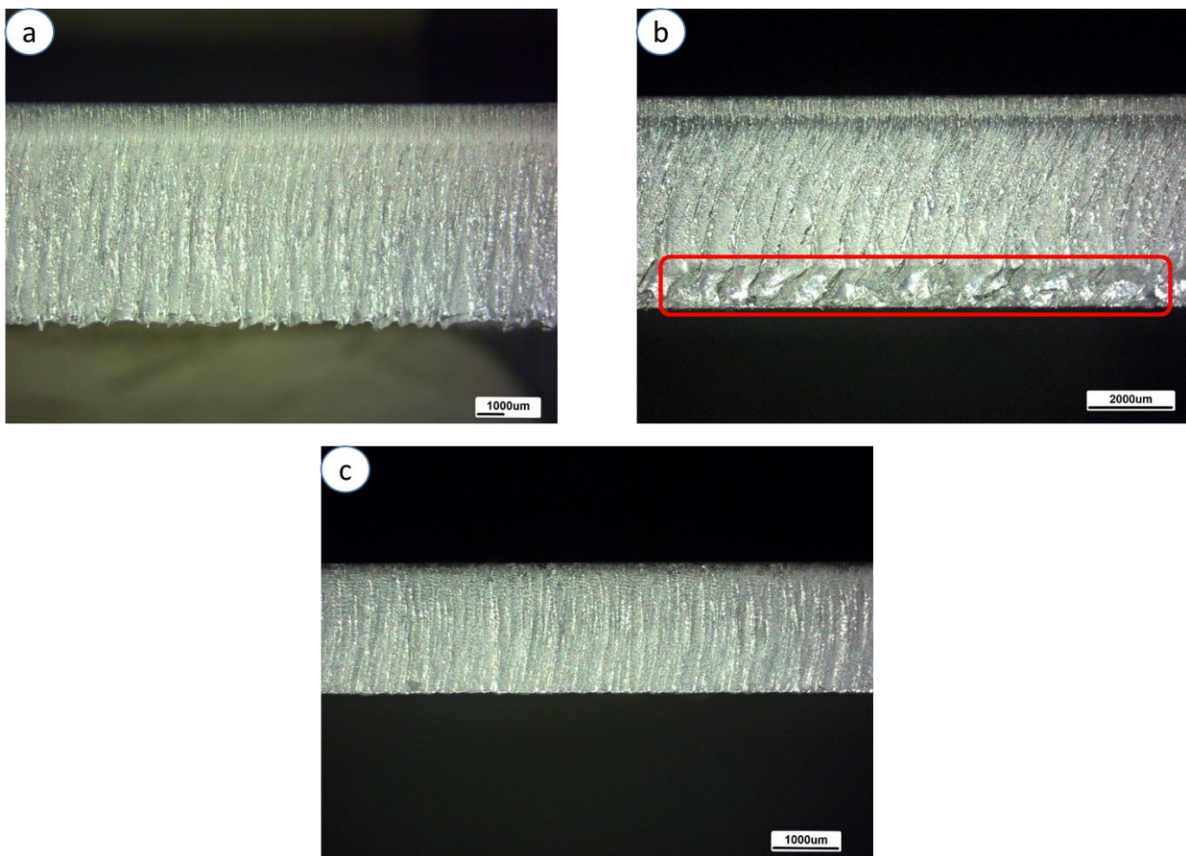
Figure 113: High-definition acquisition images for samples cut at 100 °C – 8 mm (a) – 5 mm (b) – 2 mm (c) - Deterioration highlighted in red for the 5 mm thickness case

From these images a very important peculiarity is evident, namely the formation of a deterioration zone in the 5 mm thick sample, highlighted in red in the picture.

This deterioration, as already analysed in the research work carried out by Cocci and Guerra (52), is almost certainly attributable to an excessively high cutting speed. In fact, if from the point of view of burr formation we have a strong reduction of the latter (in fact, it can be seen that the burr values for this thickness are very reduced and more similar to the case of the 2 mm thickness, and differ markedly from the burr formation values of the 8 mm thick samples), from the point of view of cutting quality the same cannot be said. In fact, in Cocci and Guerra's work, a cutting speed value of about 3100 mm/m is indicated as the threshold value for a 6 mm thick aluminium sample, for not obtaining the deterioration, and as mentioned above in the Table of the cutting parameters (Table 20), our cutting speed used for the 5 mm thick samples were of 6600 mm/min. This resulted in slightly distorted dross and roughness values of the bottom measurement which should be analysed further in the future.

9. Compensating part thermal expansion in the laser cutting process via a predictive model

The final objective of this thesis work was therefore to find a possible solution to the problem caused by the heating of the material during cutting and to find a way to cut correctly even at high temperatures, using for this purpose the model elaborated and analysed in Chapter 4.

At the temperatures analysed during this work, no increase in roughness or burr formation was noted in the aluminium, the cut was always completely performed and without any evident downgrade in quality.

In fact, the only important behaviour noted concerns the dimensional analysis of our samples, which led us to obtain samples of different lengths at the various temperatures under analysis. In fact, the sheet underwent significant thermal expansion when subjected to heating, which led, having imposed a very precise cutting dimension on the laser machine, to obtaining samples of a smaller size than expected. The aim was therefore to adequately compensate for this problem.

The compensation that it was decided to use for this thesis work was through the use of the tool offset corrector, already implemented on the machine, to correct the problem efficiently and repeatably.

The method of operation of this tool offset corrector has been explained in Section 4.2, with a visualisation of its working mode in Figure 25.

The model used to implement this corrector was instead described in Section 4.3, where the equations on which the compensation method was based were shown, and especially the Equation (4.15) in which the value of the tool offset corrector value (Corr1) needs to be imposed for the different correction temperatures.

9.1 Experimental design

A Design of Experiment was therefore set up for all the three thicknesses analysed, with temperature as the only variable factor, looking at the final length in X direction of the samples, applying the designated tool corrector, for each specific thickness (and so different parameters used) and each temperature value.

Starting with the expansion model analysed in Section 4.3, which took into account not only the thermal expansion of the workpiece due to the increase in temperature, but also the width of the cut, to be corrected by means of a tool corrector. Starting from this principle, the tool corrector itself was then used to correct the dimensional problem of the samples.

The value of the tool corrector must therefore be modified, starting from the basic value shown in the Table 29, found using the Equation (4.11), and increased by the value obtained through the regression model in the calculation of the thermal expansion at each specific thickness to compensate for this behaviour, using the Equation (4.15), with the values changed as shown in Table 32.

Table 29: Tool offset correction at Room Temperature (25°C)

Tool offset correction at room temperature (25°C)	
Thickness [mm]	Tool offset correction [mm]
2	0.35
5	0.2
8	0.32

In fact, the correction will have to present the same trend as that obtained in the regression model for the expansion.

This correction then, in addition to showing us that the method used is reliable and correct, gives us further verification that the regression model obtained for the thermal expansion is correct and congruent with our analysis.

Thus, through the regression model used for each thickness analysed, the tool corrector value to be set at the various temperatures was calculated.

As in the previous case, for the calculation of our regression equation, we went to analyse the value of ΔL/Lo, but this time considering the value of the tool corrector and thus its variation ΔCorr for the regression.

We must consider that, as can be seen from Figure 114, the value of the total ΔL will be equal to twice the value of the tool corrector to be set, this happens for geometric and machining reasons, since in the cutting of a rectangular geometry the variation obtained by means of the tool corrector already affects all the sides of the profile, and the simple correction by means of the corrector therefore compensates for the total expansion. The regression analysis carried out will therefore this time be based on the value of $2*\Delta Corr/Lo$, that will compensate for the thermal expansion of the sample, $\alpha\Delta T$.
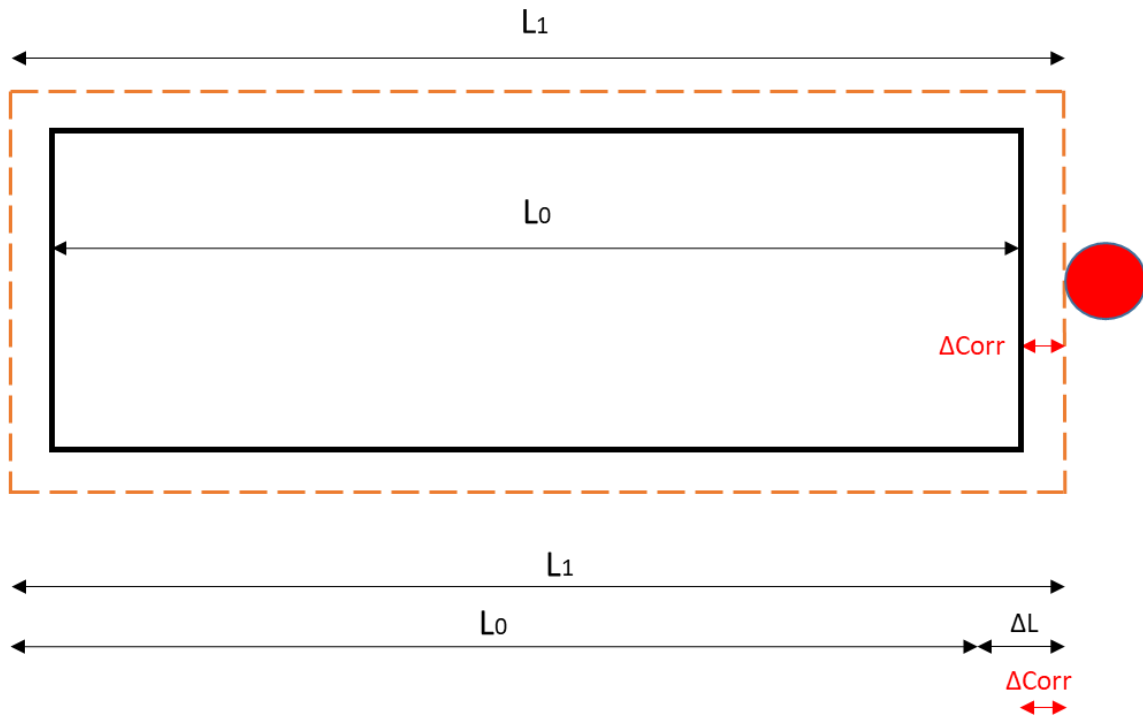
Figure 114: ΔL and ΔCorr comparison to compensate expansion problem

Three different designs of experiment were therefore also carried out for the case of the compensation of the thermal expansion problem, one for each different thickness analysed and to be compensated.

These DOEs were carried out by keeping the cutting process parameters for cutting the samples profiles constant, the ones presents in Table 30, thus varying not only the pre-heating temperature, but also the value of the tool offset corrector, following the regression model found in the previous chapter (Table 31) (Section 8.2.1), and the Equation (4.15) elaborated through the model in Chapter 4.

Table 30: Process parameters for cutting Al 5754

Fixed process parameters for cutting Al 5754							
Thickness [mm]	Power [W]	Cutting speed [mm/m]	Focal position [mm]	Gas type	Gas pressure [bar]	SOD [mm]	Tool offset (25°C) [mm]
8	5580	2000	-7.5	Nitrogen	15	0.7	0.32
5	5080	6600	-4.5	Nitrogen	14	0.7	0.2
2	5580	8000	+3	Nitrogen	8	0.7	0.35

Table 31: Variable process parameter for DOE compensation analysis

Variable parameters	
Temperature	25-100-175-250 °C
Tool offset corrector	Variable for different thicknesses and different temperatures

Therefore, following the equations of the thermal expansion model elaborated in Chapter 4, and with the purpose of correcting this defect, we are going to modify the value of the tool offset corrector in a linear way, following the trend of the results obtained experimentally in Chapter 8 and respecting the regression equations found, considering the angular coefficient of the regression line (thermal expansion coefficient, α).

Therefore, starting from the tool corrector values obtained at room temperature (Corr0), from Equation (4.11), and shown in the Table 30, taking into account the thermal expansion $\alpha\Delta T$ value due to the increase in ΔT, we calculate the new tool corrector values (Corr1), at the different ΔT taken into account through Equation (4.15).

The results for the different thicknesses analysed are shown in Figure 115-Figure 116-Figure 117 and discussed in more detail in Section 9.2.
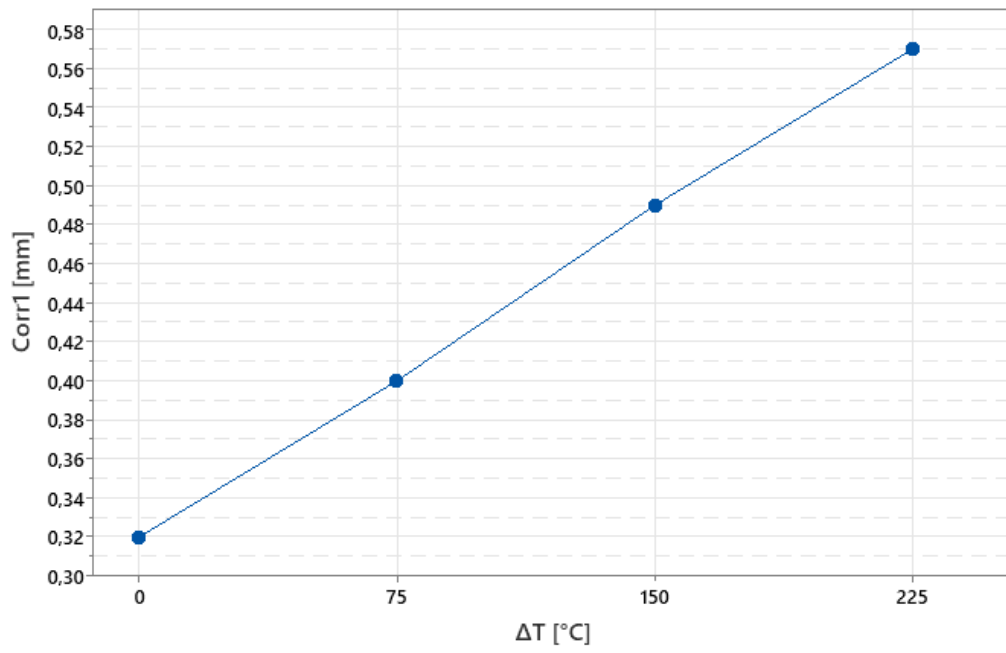
Figure 115: Tool offset correction values calculated at the different temperatures – 8 mm thickness
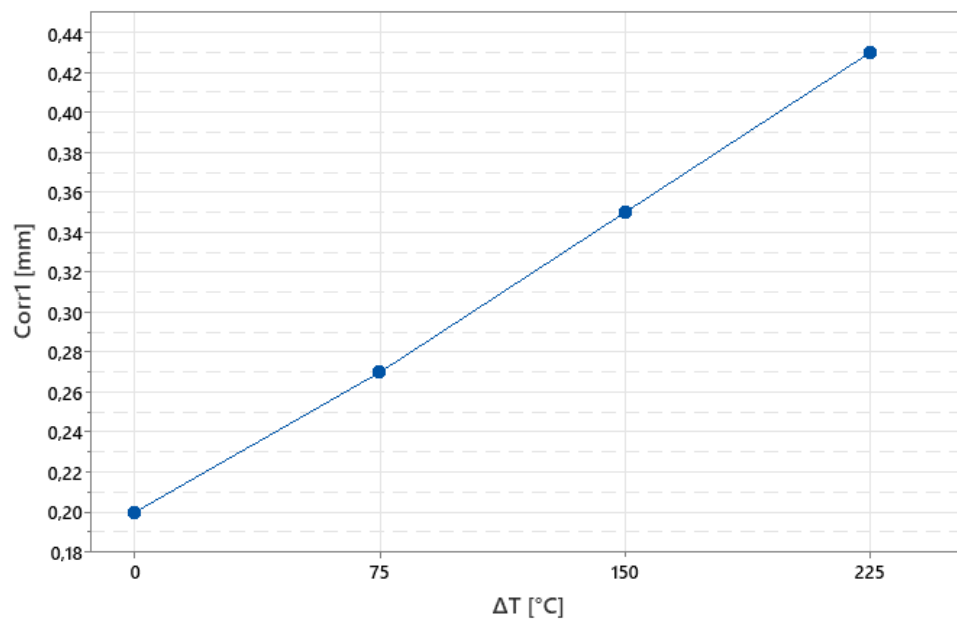
Figure 116: Tool offset correction values calculated at the different temperatures – 5 mm thickness
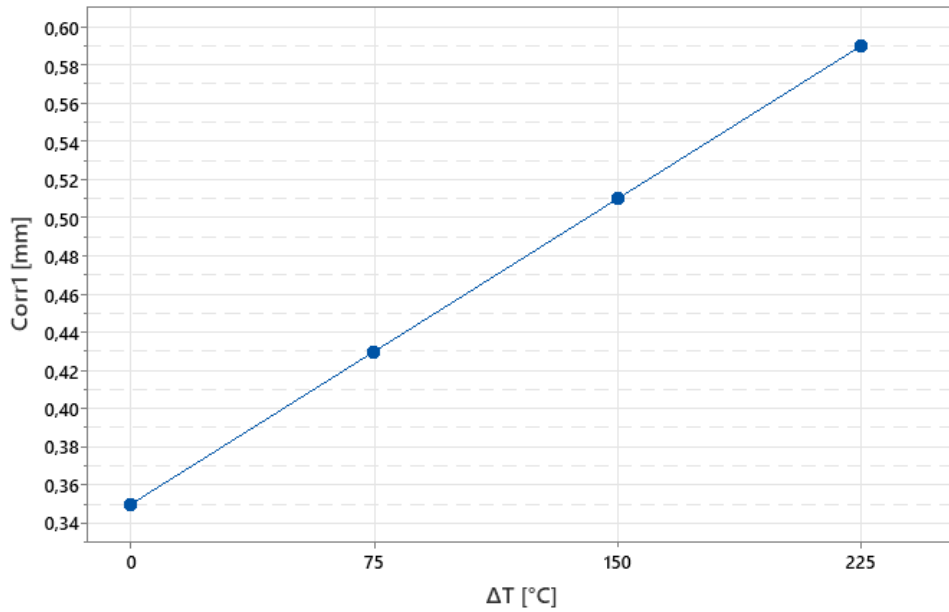
Figure 117: Tool offset correction values calculated at the different temperatures – 2 mm thickness

9.2 Results

The tool corrector values obtained for the various thicknesses analysed and adjusted to compensate for thermal expansion at different temperatures are therefore shown in the Table 32.

Table 32: Tool offset correction calibrated for the different temperature analysed

Tool Offset Correction at different temperatures [mm]				
	ΔT [°C]			
Thickness [mm]	0 °C	75 °C	150 °C	225 °C
2	0.35	0.43	0.51	0.59
5	0.2	0.27	0.35	0.43
8	0.32	0.40	0.49	0.57

After defining the value of the tool corrector at room temperature (Corr0), useful for compensating the dimensional error due to the cutting width, we obtain the values of the tool corrector at the various temperatures, to compensate for the effect of thermal expansion (Corr1), obtained from the regression equation found in the previous chapter, combined with the model equation obtained in chapter 4.

As can be seen from the Figure 115, for the case of the 8 mm thick sheet, we start with a tool corrector set at room temperature (Corr0) of 0,32 mm up to a tool corrector value of 0,57 mm at a temperature of 250 °C, with a linear increase in the corrector value, in fact having an increase of approximately 0,08 mm for each temperature increase of 75 °C (that correspond to a total ΔL of 0,16 mm for each $\Delta T = 75$ °C).

In the case of the 5mm thickness, by using different cutting parameters and a different focus point, we have a different laser spot size and therefore a different cutting thickness. In fact, in Figure 116, we start in this case from a tool corrector value (Corr0) of 0.2 mm at 25 °C to a value of 0.43 mm at the maximum temperature analysed, again with a linear increase of 0.08 mm for every 75 °C increase in temperature.

Finally, for the case of the 2 mm thick sheet, in Figure 117, we start with a tool corrector value of 0.35 mm and arrive at a corrector value of 0.59 mm, again with a constant increase of 0.08 mm every 75°C.

This confirms the linear expansion trend and therefore the need to have a tool corrector value compensation that also varies with a linear law.

The correct execution of the compensation carried out is shown by means of the graphs in the Figure 118, Figure 119 and Figure 120, where we can see the two lines, with and without tool offset compensation, superimposed, for the three different thicknesses analysed.
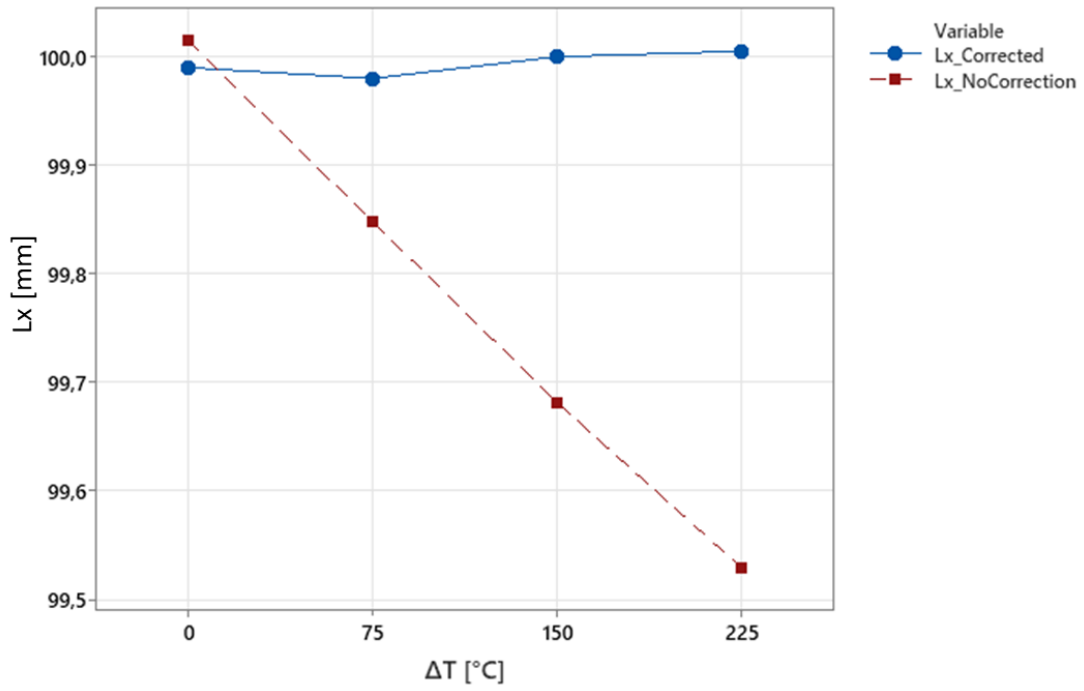
Figure 118: Length of the samples comparison with and without the use of the corrector for the compensation – 8 mm thickness
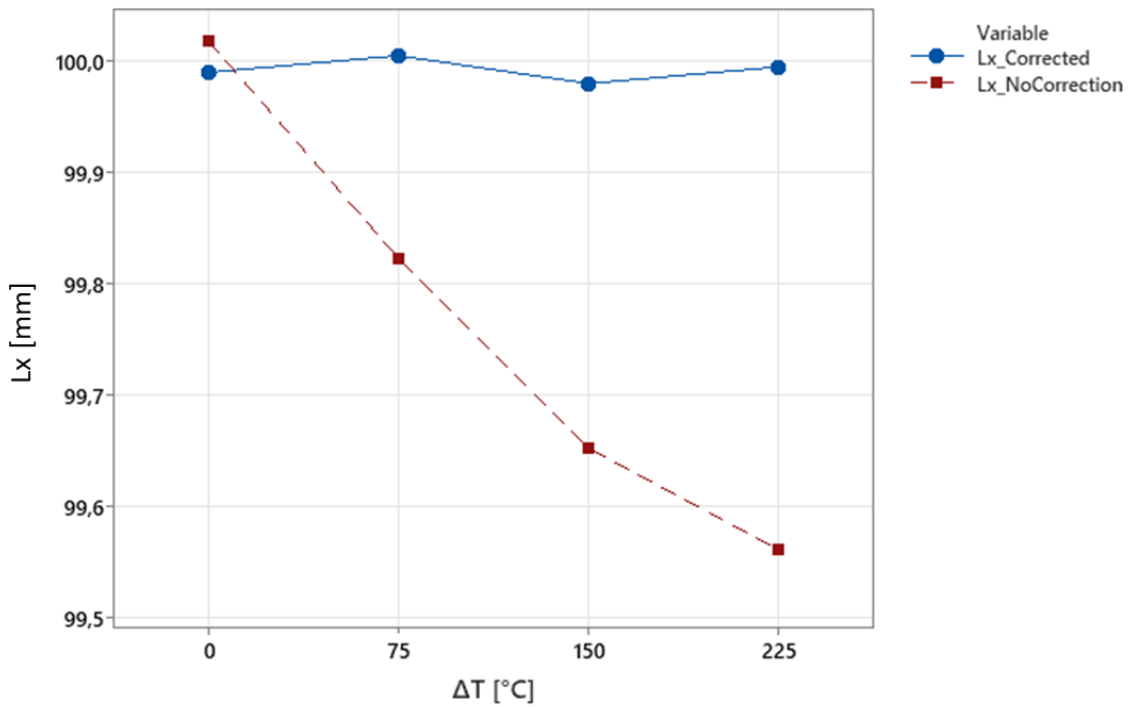
Figure 119: Length of the samples comparison with and without the use of the corrector for the compensation – 5 mm thickness
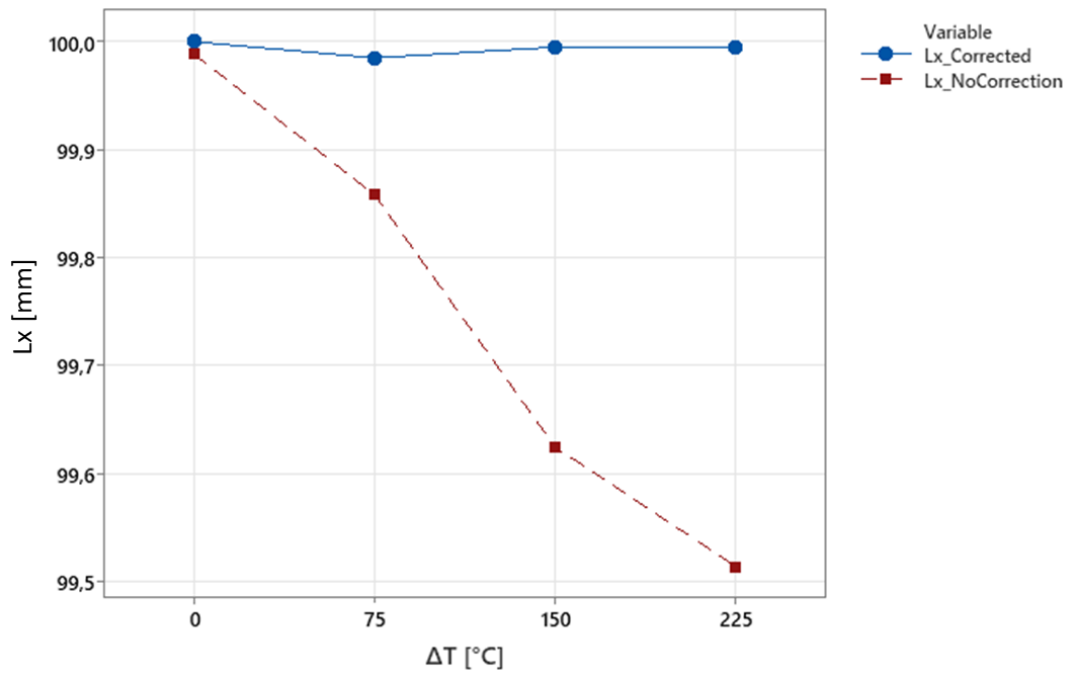
Figure 120: Length of the samples comparison with and without the use of the corrector for the compensation – 2 mm thickness

As can be seen in these figures in fact, the red line represents the dimensions of the sample in the X direction for the thicknesses of 8, 5 and 2 millimetres at the various temperatures, which is reduced by the quantity already known due to pre-heating process analysed in the previous chapter (Lx_NoCorrection), in blue instead we can observe the line of values obtained by varying the value of the tool offset corrector to compensate for this error.

In fact, at all 4 temperatures analysed, we can see how the value of 100 mm in length was re-established as in the reference case at room temperature, making the compensation imposed in response to temperature variations perfectly effective.

10. Conclusions and future development

The objective of this thesis work was therefore to study the behaviour of aluminium Al 5754 as the temperature increases, specifically by analysing the quality of the cutting parameters such as the roughness of the cutting surface, the formation of burrs on the lower surface of the part and also by analysing the final geometric correctness of the part to be cut.

To do this, it was therefore first necessary to create and implement a method for heating the sheet itself before cutting.

Two different methods were therefore presented, one which exploited the laser cut itself by means of particular geometries to obtain the heating of the piece, and one based on the realisation of a specific allocation base which allowed for the housing inside it of cartridge heating elements capable of heating the entire base itself, which in turn would then heat the piece to be cut to the desired temperature.

For both models presented, Design of Experiments were carried out, where constant parameters were maintained, varying the parameters of interest, such as the temperature or the thickness of the sheet metal.

Analysing and comparing the results obtained using the two methodologies, it is therefore possible to make certain deductions.

First of all, as far as the roughness trend is concerned, it seems evident that the increase in temperature does not significantly affect this parameter, the streaks remain constant and the presence of valleys and peaks is not accentuated.

Obviously, roughness measurements present very different values depending on the height of the sample in which it is measured, a behaviour which, however, was already predicted in the literature since we pass from laminar motion to turbulent motion between the inlet of the part and the outlet where we have expulsion of material that is not perfectly cohesive. However, this behaviour remains constant at various temperatures and for the same thicknesses.

While a slight increase in roughness can be noted for some measurements, we remain within an extremely low range that can be considered negligible.

On the other hand, regarding the formation of burrs on the lower surface of the cut piece, while in the case of the method of preheating by means of electrical resistances we do not notice any change in the thickness of the burr formation, in the case of preheating by means of cutting geometries, we notice a slight increase in its presence as the temperature increases.

First of all, we notice an anomalous behaviour in the average value of the burr thickness, where we have an initial decrease followed by an increase in this value, we notice an increase in the standard deviation and when analysing the maximum total variation of burr at the various temperatures, we notice a slight increase. This increase on average, however, remains in the order of about 60 μm, an extremely small value where measurement error must be considered.

Finally, we analysed and compared the dimensional accuracy of the final part, and it is here that we notice the most notable difference between the two methods under consideration.

In fact, in the case of pre-heating by cutting geometries, what emerged was that the final part was found to have had an expansion along one of the two directions analysed and a contraction in the opposite direction. This behaviour was anomalous following the theory of expansion of solids with increasing temperature.

Hypotheses were therefore put forward for this behaviour, namely the possibility of non-homogeneous residual stresses in the part, probably due to the rolling method and direction used in obtaining the aluminium sheet, or again as a possible reason for the non-homogeneous heating of the sheet, due to the methodology used, which required the laser to cut around the area to be heated, not heating all the parts equally and at the same time.

With the second methodology, a pre-heating method was therefore implemented that would guarantee simultaneous, homogenous and controlled heating of the entire size of the part, in order to be able to analyse both hypotheses and refute or confirm them.

In the second design of experiment based on this methodology, we went on to analyse the cut samples by also subdividing them according to their rolling direction.

What emerged this time was a behaviour that was much more in keeping with the prediction of the theoretical model. In fact, not only was the rolling direction found to be completely irrelevant in the dimensional calculation at all the temperatures analysed, demonstrating that this was not responsible for the previous anomalous behaviour, but also that the expansion of the piece on heating in both directions under analysis was obtained, with an expansion that amply respected the theoretical thermal expansion coefficient of the material.

Therefore, the reason for the behaviour reported in the pre-heating by laser cutting geometries was pointed to the heating and consequent non-homogeneous cooling of the part, leading to an unpredictable to anomalous expansion, which was perfectly taken up and resolved by the heating method used subsequently.

Having thus obtained a predictable and well-studied behaviour thanks to the realisation of the pre-heating method using cartridge heating elements, we also had the possibility of studying and realising a compensation solution to this problem.

We therefore devised a system that exploited the use of the tool corrector (a system already presents in the cutting machine to compensate for the cutting thickness), progressively modifying it, respecting the model obtained through experimentation and

thus taking into account the material's thermal expansion coefficient and the temperatures analysed, obtaining excellent results with perfect compensation for the dimensional problem previously encountered.

In conclusion, we have therefore analysed the behaviour of aluminium Al5754 in response to laser cutting carried out after an increase in temperature, analysing its quality and dimensional correctness and finding a solution to the last problem.

Therefore, thanks to the realisation of a reliable, repeatable pre-heating method that guarantees homogeneous heating, it would be interesting to study in the future, if for thicknesses greater than those examined in this work, a predictable behaviour that respects the thermal expansion model can be maintained, as well as the possibility of studying the quality of cutting and expansion not only at higher temperatures but also for extremely different materials.

Lastly, the compensation method used to solve the dimensional problem was intended to lay the foundations for an implementation in the machine, with the possibility of obtaining a modification of this value in the future thanks to an appropriate control and real time monitoring of the temperature of the various zones of the part to be cut, so that, where it is not convenient or not possible to intervene by modifying the cutting path or by using coolants, it is possible to obtain a final part of exact dimensions in any case.

11. Acknowledgement

Bibliography

1. ENGINEERING GEOLOGY Chapter 5-Requirements for Geologic Investigations and Sampling Chapter 6-Preliminary Site Investigation Chapter 7-Detailed Site Investigation Index SOIL CONSERVATION SERVICE UNITED STATES DEPARTMENT OF AGRICULTURE.

2. Alfrey AC. Aluminum. Adv Clin Chem. 1983 Jan 1;23(C):69–91.

3. Aluminum dross recycling - a new technology for recycling aluminium waste products | Signed in. [cited 2022 Sep 15]; Available from: https://www.scopus.com/record/display.uri?eid=2-s2.0-84882795029&origin=inward&txGid=d4703f05bd3d945f0113dee0ef420434

4. David E, Kopac J. Aluminum recovery as a product with high added value using aluminum hazardous waste. J Hazard Mater. 2013 Oct 5;261:316–24.

5. Alluminio: produzione e caratteristiche Available from: https://www.educazionedigitale.it/mitsubishielectric/wp-content/uploads/2018/06/ALLUMINIO-PRODUZIONE-E-CARATTERISTICHE.pdf.

6. Quan Y, Liu P, Kaewunruen S, Rungskunroch P, Shen ZJ. An Improvement on the End-of-Life of High-Speed Rail Rolling Stocks Considering CFRP Composite Material Replacement The End-of-Life of HSR Rolling Stock. Frontiers in Built Environment | www.frontiersin.org [Internet]. 2019;1:89. Available from: www.frontiersin.org

7. Husain Ansari A. REVIEW ON ALUMINIUM AND ITS ALLOYS FOR AUTOMOTIVE APPLICATIONS Experimental Investigation of Aluminium-Reinforced Ceramics Composites Through Stir Casting Process View project FRICTION STIR WELDING View project Tanwir Alam Maulana Mukhtar Ahmad Nadvi Technical Campus Malegaon. 2017 [cited 2022 Sep 17]; Available from: https://www.researchgate.net/publication/317075488

8. Total Internal Reflection [Internet]. [cited 2022 Oct 10]. Available from: https://farside.ph.utexas.edu/teaching/316/lectures/node129.html

9. Aluminium: Specifications, Properties, Classifications and Classes [Internet]. [cited 2022 Sep 17]. Available from: https://www.azom.com/article.aspx?ArticleID=2863

10. History of Laser Cutting: From MASERs to CO2 Laser Cutting [Internet]. [cited 2022 Oct 4]. Available from: https://www.sculpteo.com/blog/2016/10/05/the-history-of-laser-cutting-from-masers-to-co2-laser-cutting/

11. How Fiber Laser Technology Compares to CO2 - Boss Laser [Internet]. [cited 2022 Oct 12]. Available from: https://bosslaser.com/fiber-laser-technology-compares-co2/

12. Fibre Laser Cutters | Fibre Laser Cutting Systems - CTR Lasers [Internet]. [cited 2022 Oct 12]. Available from: https://www.ctrlasers.co.uk/fibre-lasers

13. Scintilla LD. Continuous-wave fiber laser cutting of aluminum thin sheets: effect of process parameters and optimization. Optical Engineering. 2014;53(6):066113.

14. Wendt1 K, Schwenke1 H. Inspection of large CMMs by sequential multi-lateration using a single laser tracker [Internet]. 2003. Available from: www.witpress.com,

15. Pandey AK, Dubey AK. Multiple quality optimization in laser cutting of difficult-to-laser-cut material using grey-fuzzy methodology. International Journal of Advanced Manufacturing Technology. 2013;65(1–4):421–31.

16. Riveiro A, Quintero F, Lusquiños F, Comesaña R, Pou J. Parametric investigation of CO2 laser cutting of 2024-T3 alloy. J Mater Process Technol. 2010 Jun 19;210(9):1138–52.

17. Sharifi M, Akbari M. Experimental investigation of the effect of process parameters on cutting region temperature and cutting edge quality in laser cutting of AL6061T6 alloy. Optik (Stuttg). 2019 May 1;184:457–63.

18. prof Barbara Previtali prof Sergio Savaresi prof Mara Tanelli Tutor prof Roberto Corradi SM. Laser Cutting Monitoring and Control for Real-Time Dross Attachment Regulation.

19. Stournaras A, Stavropoulos P, Salonitis K, Chryssolouris G. An investigation of quality in CO2 laser cutting of aluminum. CIRP J Manuf Sci Technol. 2009 Jan 1;2(1):61–9.

20. Liu Y, Zhang S, Zhao Y, Ren Z. Experiments on the kerf quality characteristic of mild steel while cutting with a high-power fiber laser. Opt Laser Technol. 2022 Oct 1;154.

21. Sharifi M, Akbari M. Experimental investigation of the effect of process parameters on cutting region temperature and cutting edge quality in laser cutting of AL6061T6 alloy. Optik (Stuttg). 2019 May 1;184:457–63.

22. Rao B SD, Sethi A, Das AK. Fiber laser processing of GFRP composites and multi-objective optimization of the process using response surface methodology. J Compos Mater. 2019 May 1;53(11):1459–73.

23. Mayr J;, Jedrzejewski J;, Uhlmann E;, Donmez M, Alkan ;, Knapp W;, et al. Thermal issues in machine tools. Available from: https://doi.org/10.3929/ethz-a-007593138

24. Thermal Expansion [Internet]. [cited 2022 Oct 12]. Available from: https://www.aplusphysics.com/courses/honors/thermo/expansion.html

25. James JD, Spittle JA, Brown SGR, Evans RW. Measurement Science and Technology A review of measurement techniques for the thermal expansion coefficient of metals and alloys at elevated temperatures A review of measurement techniques for the thermal expansion coefficient of metals and alloys at elevated temperatures. Meas

Sci Technol [Internet]. 2001 [cited 2022 Oct 14];12:1. Available from: www.iop.org/Journals/mt

26. Thermophysical Properties of Matter, Volume 12—Thermal Expansion, Metallic Elements and Alloys - Touloukian Y S, Kirby R K, Taylor R E and Desai P D 1975 [Internet]. [cited 2022 Oct 14]. Available from: https://apps.dtic.mil/sti/pdfs/ADA129115.pdf

27. Eltherington J. Standard Test Method for Linear Thermal Expansion of Solid Materials with a Vitreous Silica Dilatometer. • Welding, Brazing, and Soldering [Internet]. 1998 [cited 2022 Oct 14];831:289–99. Available from: http://www.eltherington.co.uk/,2002http://irc.swansea.ac.uk/www.asminternational.org

28. Dilatazione termica volumica - Scienza FISICA [Internet]. [cited 2022 Oct 12]. Available from: https://www.scienzafisica.it/dilatazione-termica-volumica/

29. Mayr J;, Jedrzejewski J;, Uhlmann E;, Donmez M, Alkan ;, Knapp W;, et al. Thermal issues in machine tools. [cited 2023 Jan 31]; Available from: https://doi.org/10.3929/ethz-a-007593138

30. Mayr J;, Jedrzejewski J;, Uhlmann E;, Donmez M, Alkan ;, Knapp W;, et al. Thermal issues in machine tools. [cited 2023 Jan 31]; Available from: https://doi.org/10.3929/ethz-a-007593138

31. Schwenke H, Franke M, Hannaford J, Kunzmann H. Error mapping of CMMs and machine tools by a single tracking interferometer. CIRP Annals. 2005 Jan 1;54(1):475–8.

32. Wendt1 K, Schwenke1 H. Inspection of large CMMs by sequential multi-lateration using a single laser tracker. 2003 [cited 2023 Jan 31]; Available from: www.witpress.com,

33. Donmez MA, Blomquist DS, Hocken RJ, Liu CR, Barash MM. A general methodology for machine tool accuracy enhancement by error compensation. Precis Eng. 1986 Oct 1;8(4):187–96.

34. mult Dipl-Wirt Ing Eversheim Dr-Ing F Klocke Dr-Ing T Pfeifer Dr-Ing Dr-Ing E M Weck Berichte aus der Produktionstechnik DIW. Analyse und Kompensation thermoelastischer Verlagerungen. 2002 [cited 2023 Jan 31]; Available from: www.shaker.de

35. Chou C, DeBra DB. Liquid Temperature Control for Precision Tools. CIRP Annals. 1990 Jan 1;39(1):535–43.

36. Wang H, Dong H, Zhang L, Niu Y, Liu T, Li X, et al. Prediction of dynamic temperature rise of thermocouple sensors based on genetic algorithm- back propagation neural network. IEEE Sens J. 2022 Nov 4;1–1.

37. (PDF) THE DETERMINATION OF THE EMISSIVITY OF ALUMINUM ALLOY AW 6082 USING INFRARED THERMOGRAPHY [Internet]. [cited 2022 Oct 14]. Available from: https://www.researchgate.net/publication/291802248_THE_DETERMINATION_OF_THE_EMISSIVITY_OF_ALUMINUM_ALLOY_AW_6082_USING_INFRARED_THERMOGRAPHY

38. Weng KH, Wen C da. Effect of oxidation on aluminum alloys temperature prediction using multispectral radiation thermometry. Int J Heat Mass Transf. 2011 Nov;54(23–24):4834–43.

39. Incropera, F., Dewitt, D.: Fundamentals of Heath and Mass Transfer, John Wiley and Sons, New York, 2002. [Internet]. [cited 2022 Oct 14]. Available from: https://ostad.nit.ac.ir/payaidea/ospic/file8487.pdf

40. Wen C da, Mudawar I. Emissivity characteristics of polished aluminum alloy surfaces and assessment of multispectral radiation thermometry (MRT) emissivity models. Int J Heat Mass Transf [Internet]. 2005 Mar [cited 2022 Oct 14];48(7):1316–29. Available from: https://www.researchgate.net/publication/223753492_Emissivity_characteristics_of_polished_aluminum_alloy_surfaces_and_assessment_of_multispectral_radiation_thermometry_MRT_emissivity_models

41. Wen C da, Mudawar I. Emissivity characteristics of roughened aluminum alloy surfaces and assessment of multispectral radiation thermometry (MRT) emissivity models. Int J Heat Mass Transf [Internet]. 2004 Aug [cited 2022 Oct 14];47(17–18):3591–605. Available from: https://www.researchgate.net/publication/222655928_Emissivity_characteristics_of_roughened_aluminum_alloy_surfaces_and_assessment_of_multispectral_radiation_thermometry_MRT_emissivity_models

42. Wen C da, Mudawar I. Modeling the effects of surface roughness on the emissivity of aluminum alloys. Int J Heat Mass Transf [Internet]. 2006 Nov [cited 2022 Oct 14];49(23–24):4279–89. Available from: https://www.researchgate.net/publication/222685457_Modeling_the_Effects_of_Surface_Roughness_on_the_Emissivity_of_Aluminum_Alloys

43. Wilson AJC, Bragg WL. THE THERMAL EXPANSION OF ALUMINIUM FROM oo TO 6 5 0 0 ~.

44. LS5 and LC5: sheet laser cutting and more [Internet]. [cited 2023 Jan 29]. Available from: https://en.industryarena.com/blmgroup/news/ls5-and-lc5-sheet-laser-cutting-and-more--9338.html

45. Thyssenkrupp_Material Data Sheet_Aluminium5754.

46. Airoldi Metalli. Product sheet ALLOY5754 sheet and coil cold rolled. Available from: https://www.airoldimetalli.com/wp-content/uploads/2018/05/5754LAM_ENG.pdf

146

47. 5754-H24 Aluminum [Internet]. [cited 2023 Mar 29]. Available from: https://www.matweb.com/search/DataSheet.aspx?MatGUID=e40b7c1abf33410a8ddd59c441faa5a8

48. EN ISO 9013:2017 - Thermal cutting - Classification of thermal cuts - Geometrical product [Internet]. [cited 2023 Jan 29]. Available from: https://standards.iteh.ai/catalog/standards/cen/ce98a203-83d3-45cb-912e-59839727cccd/en-iso-9013-2017

49. ISO 21920-2:2021(en), Geometrical product specifications (GPS) — Surface texture: Profile — Part 2: Terms, definitions and surface texture parameters.

50. ISO 13715:2000 - Technical drawings — Edges of undefined shape — Vocabulary and indications [Internet]. [cited 2023 Feb 1]. Available from: https://standards.iteh.ai/catalog/standards/iso/b9604b11-557c-474f-b6e6-2e8a1a571a8e/iso-13715-2000

51. Ottaviani Macchine. Scheda-Tecnica-Trapano-Fresa-BIMAK-45ACM.

52. Author A, Cocci D, Guerra S. Combined Defect Estimation and Closed-Loop Control for Quality Op-timization in Oxidation and Fusion Laser Cutting TESI DI LAUREA MAGISTRALE IN AUTOMATION AND CONTROL ENGINEERING-INGEGNERIA.

List of Figures

150

152

List of Tables

List of equations

12. Appendix

12.1 Hypothesis verification of Chapter 7
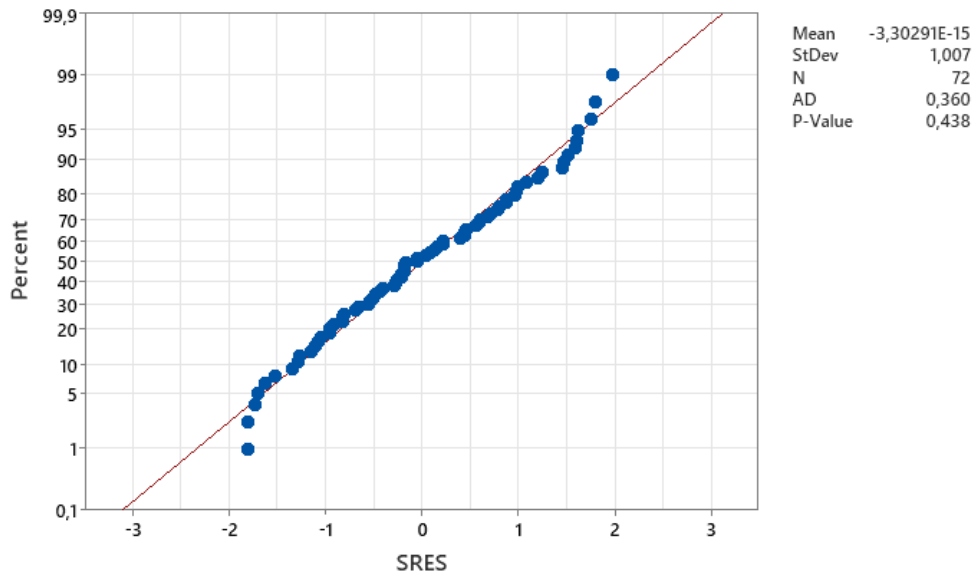
Figure 121: Profile roughness - Probability Plot of Standardized residuals to test for normality - Cutting of high density nested geometries
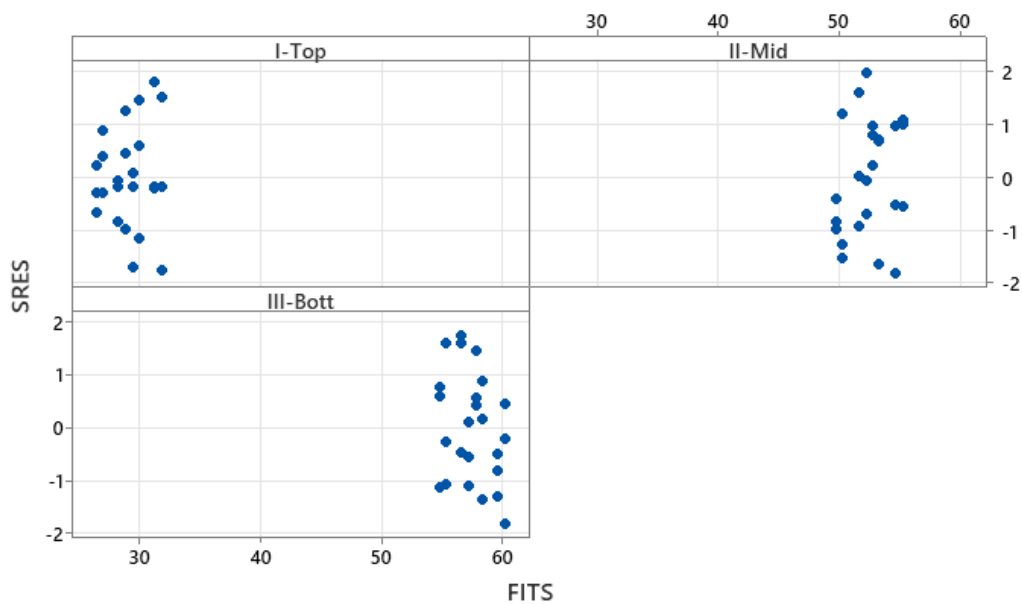
Figure 122: Profile roughness - Scatterplot of Standardized residuals versus Fits - Cutting of high density nested geometries

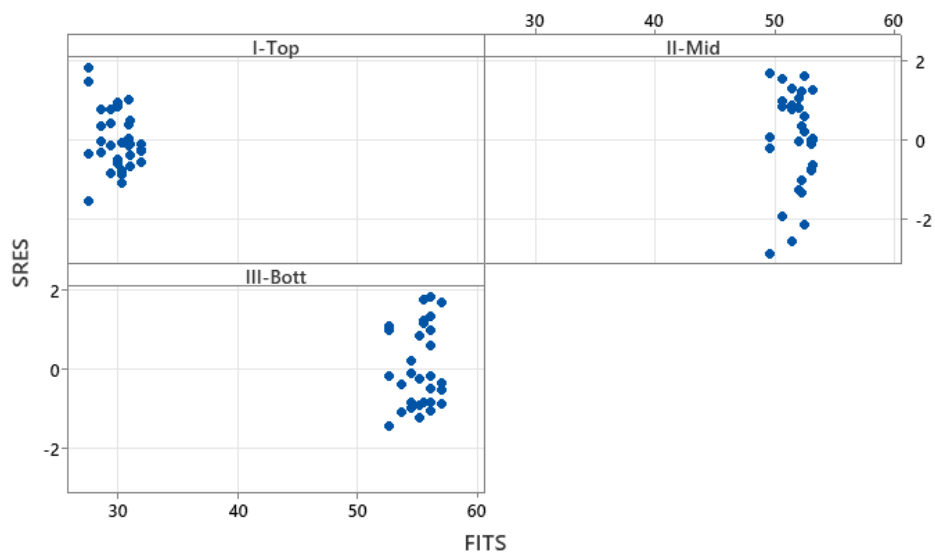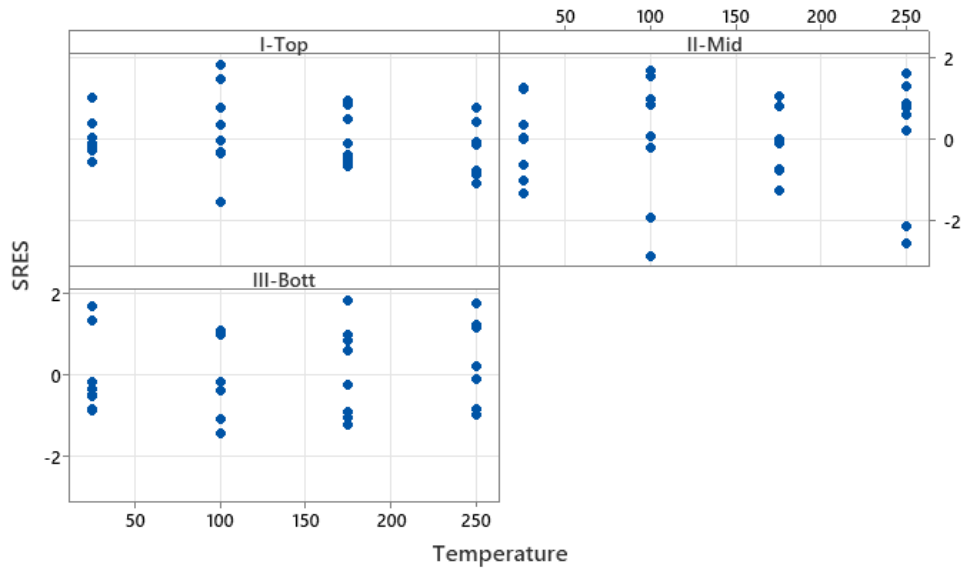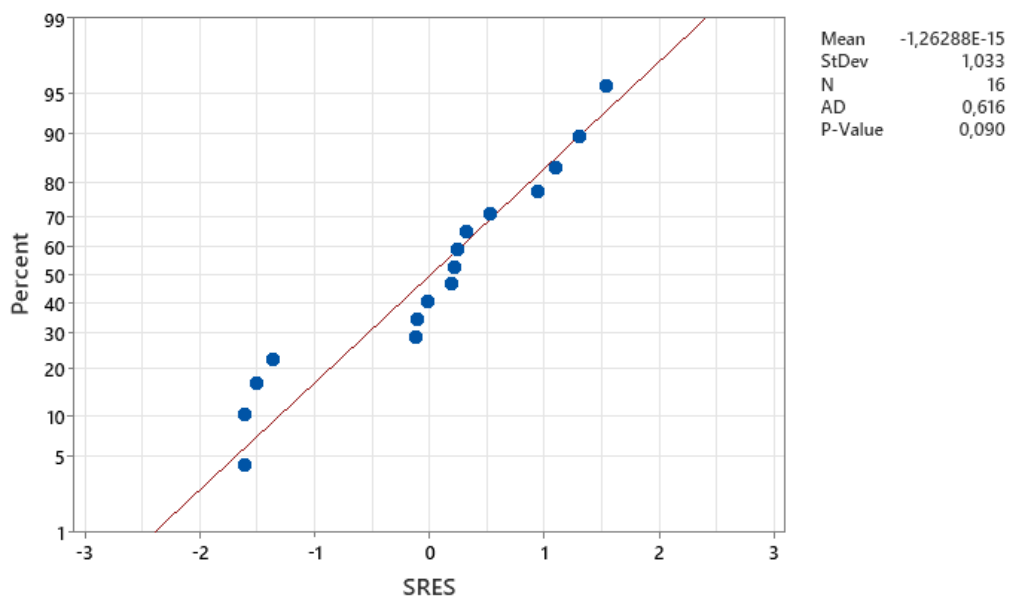## 12.2 Hypothesis verification of Chapter 8

12.2.1 Profile roughness
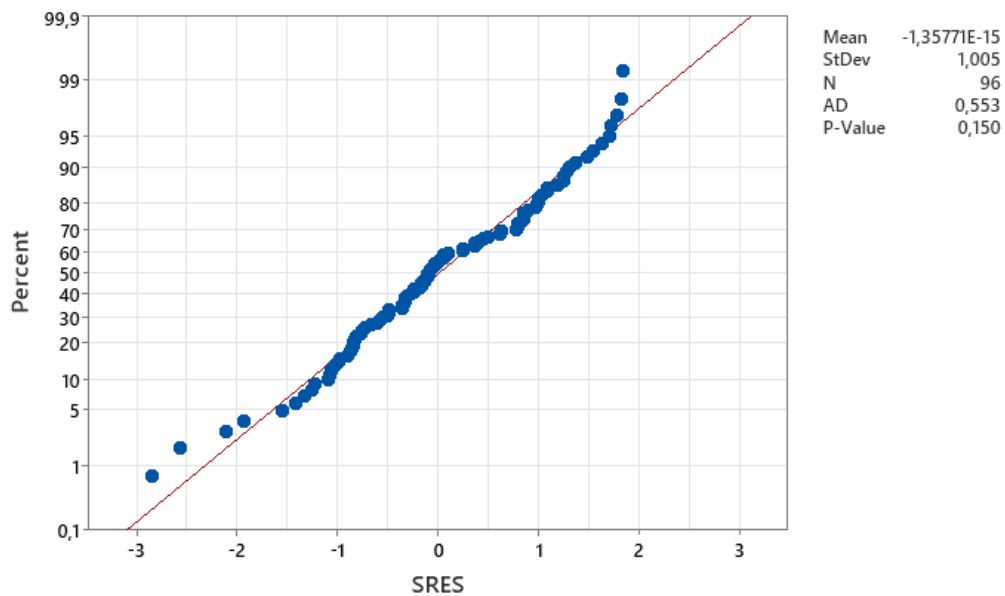
Figure 123: Profile roughness - Probability Plot of Standardized residuals to test for normality - Cutting under controlled preheating conditions

Figure 124: Profile roughness - Scatterplot of Standardized residuals versus Fits - Cutting under controlled preheating conditions

Figure 125: Profile roughness - Scatterplot of Standardized residuals versus Temperature [°C] - Cutting under controlled preheating conditions

12.2.2 Burr attachment
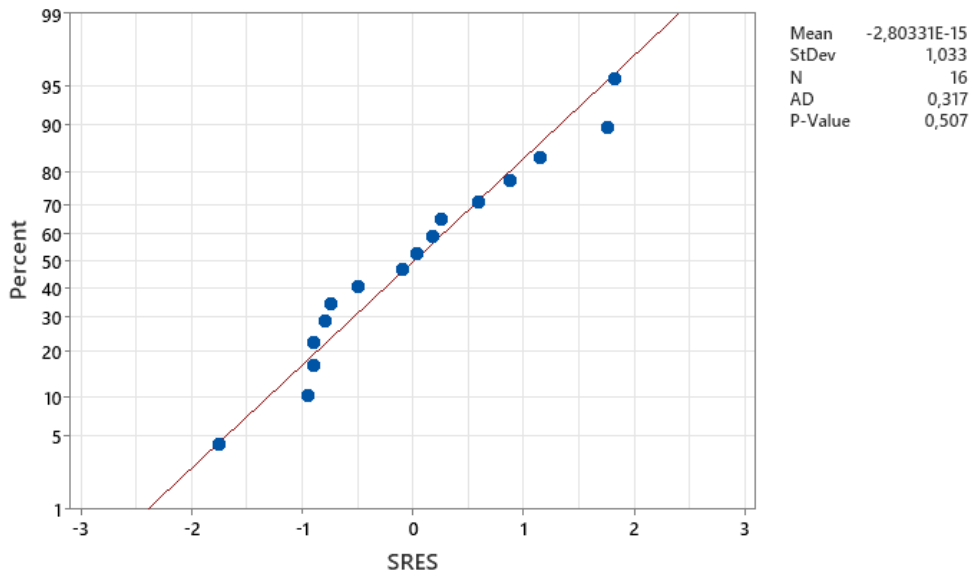
Figure 126: Burr attachment - Probability Plot of Standardized residuals to test for normality - Cutting under controlled preheating conditions – 8 mm thickness
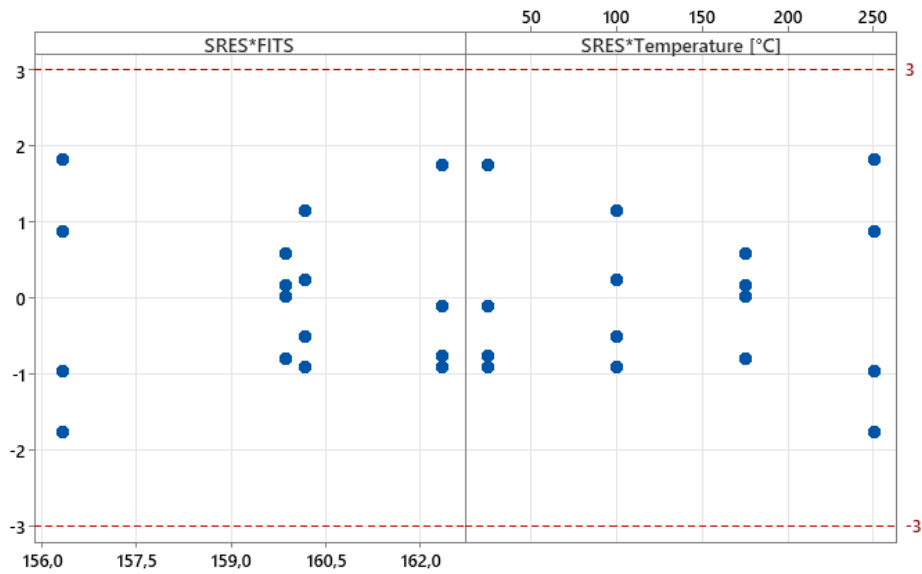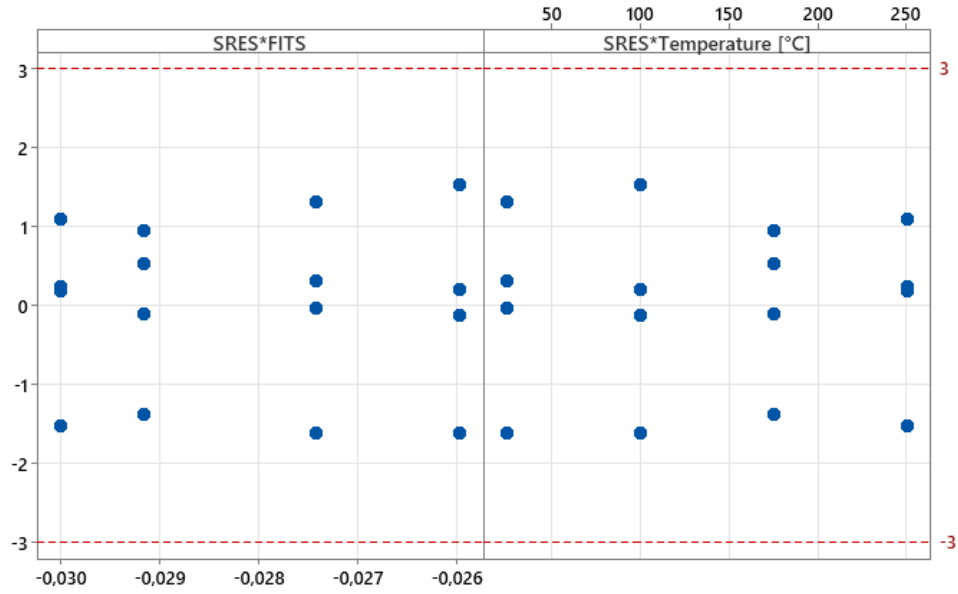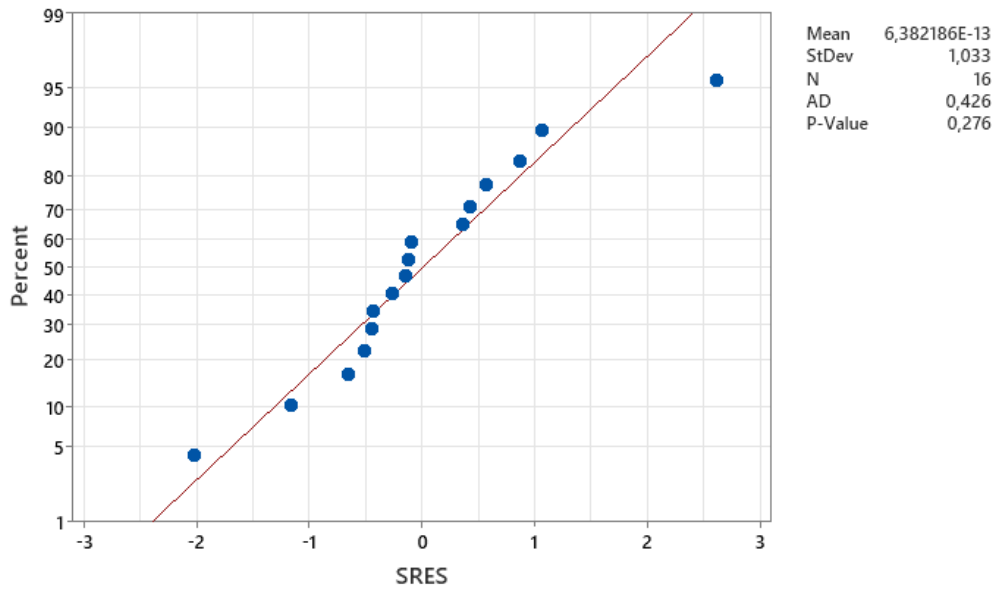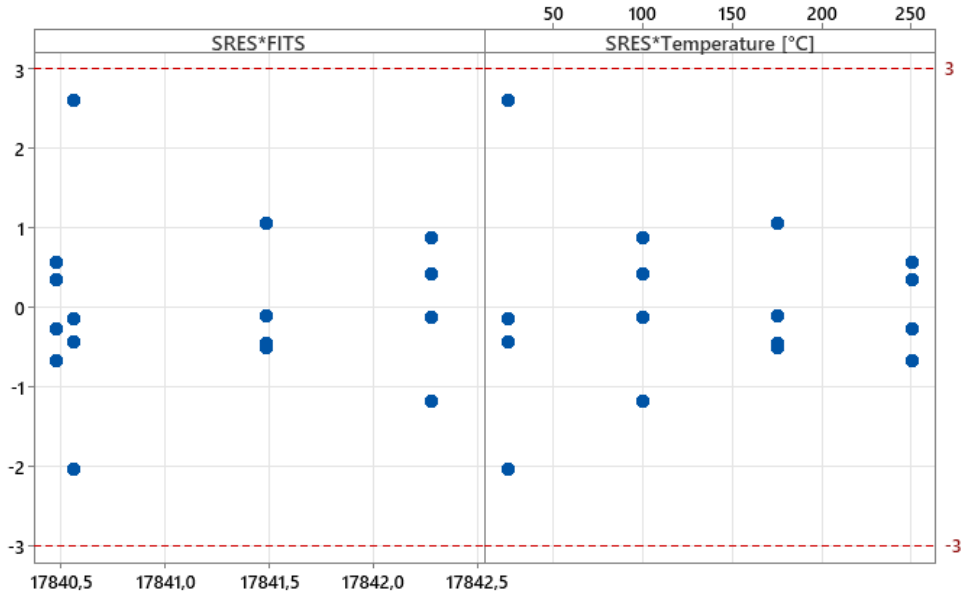
Figure 127: Burr attachment - Scatterplot of Standardized residuals versus Fits and versus Temperature [°C] - Cutting under controlled preheating conditions – 8 mm thickness
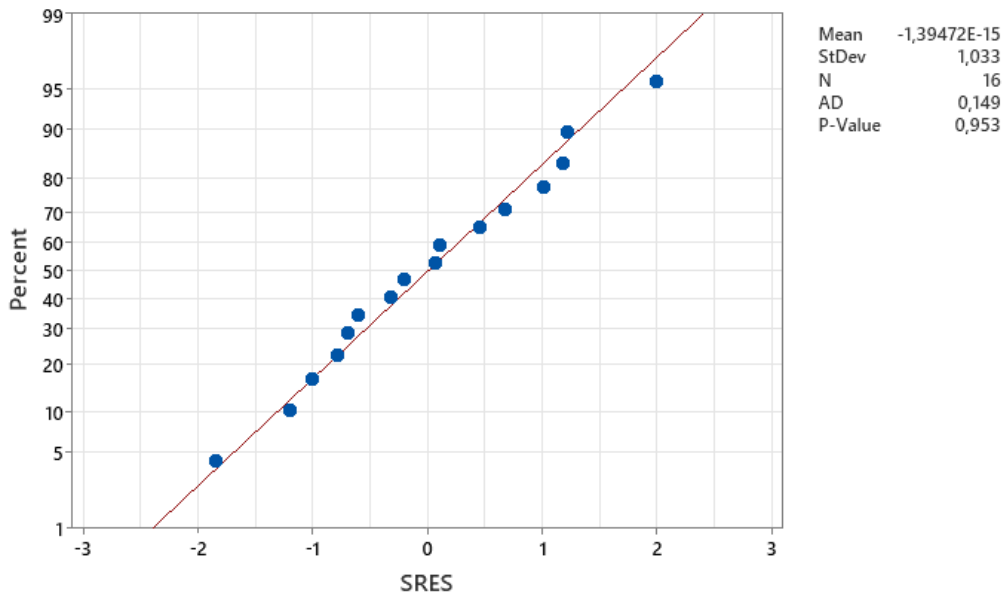

Figure 128: Burr attachment - Probability Plot of Standardized residuals to test for normality - Cutting under controlled preheating conditions – 5 mm thickness

Figure 129: Burr attachment - Scatterplot of Standardized residuals versus Fits and versus Temperature [°C] - Cutting under controlled preheating conditions – 5 mm thickness

Figure 130: Burr attachment - Probability Plot of Standardized residuals to test for normality - Cutting under controlled preheating conditions – 2 mm thickness

Figure 131: Burr attachment - Scatterplot of Standardized residuals versus Fits and versus Temperature [°C] - Cutting under controlled preheating conditions – 2 mm thickness

12.2.3 Geometrical analysis

Figure 132: Geometrical analysis - Probability Plot of Standardized residuals to test for normality - Cutting under controlled preheating conditions – 8 mm thickness
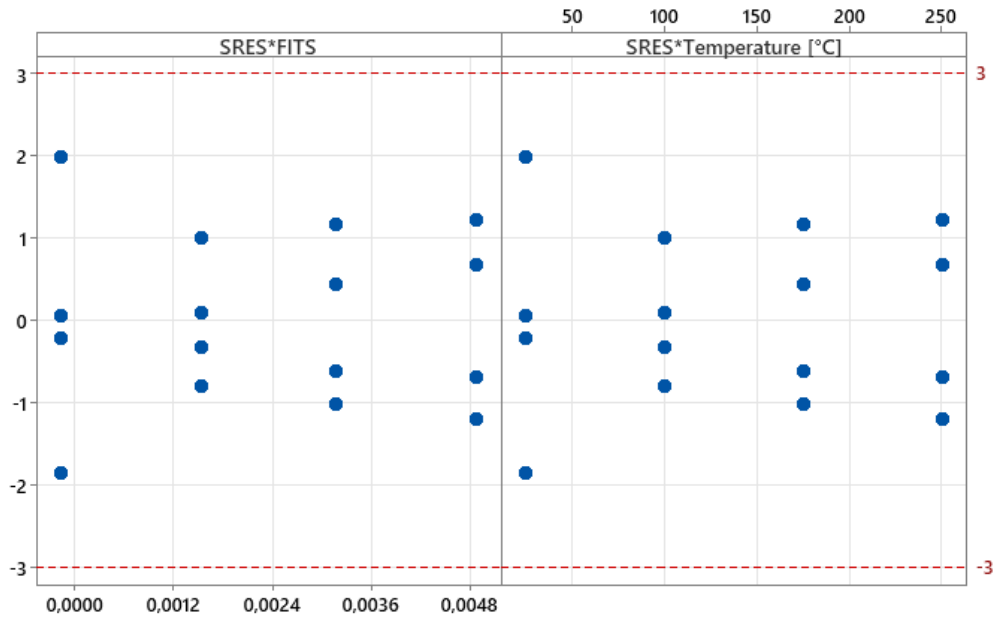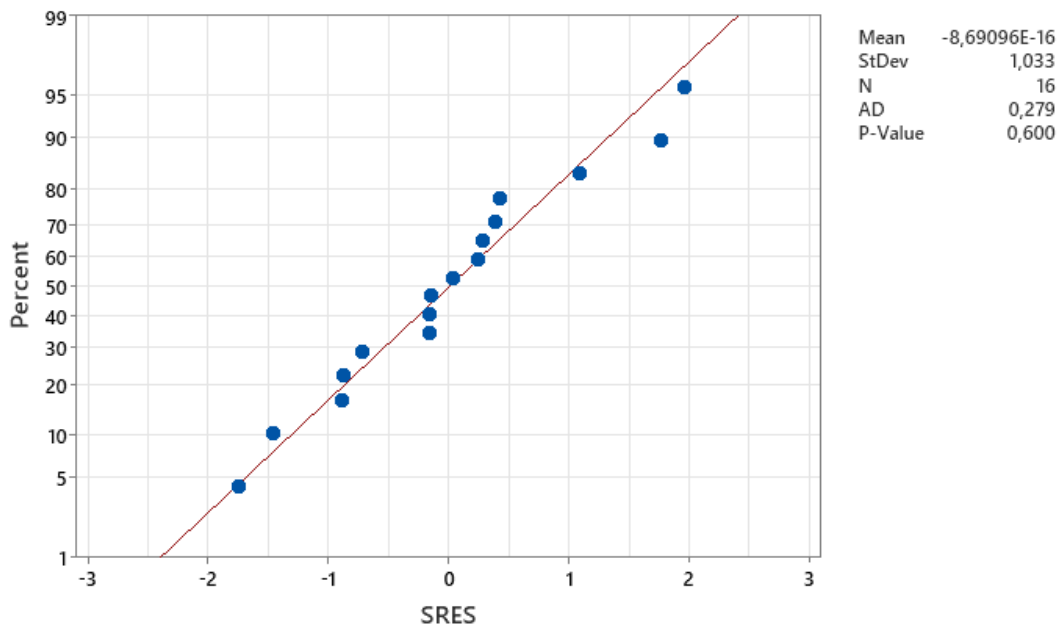
Figure 133: Geometrical analysis - Scatterplot of Standardized residuals versus Fits and versus Temperature [°C] - Cutting under controlled preheating conditions – 8 mm thickness

Figure 134: Geometrical analysis - Probability Plot of Standardized residuals to test for normality - Cutting under controlled preheating conditions – 5 mm thickness
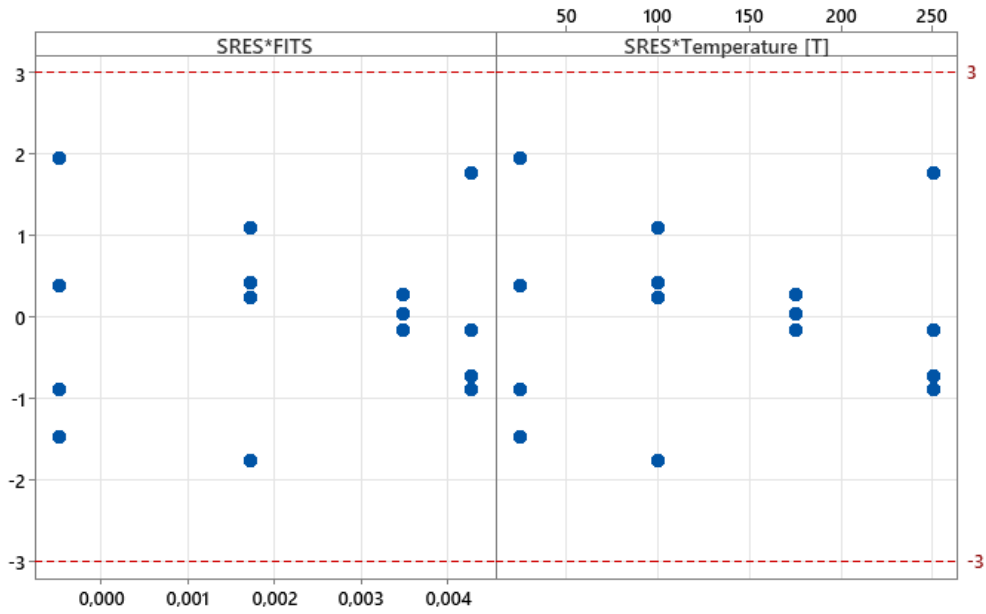
Figure 135: Geometrical analysis - Scatterplot of Standardized residuals versus Fits and versus Temperature [°C] - Cutting under controlled preheating conditions – 5 mm thickness
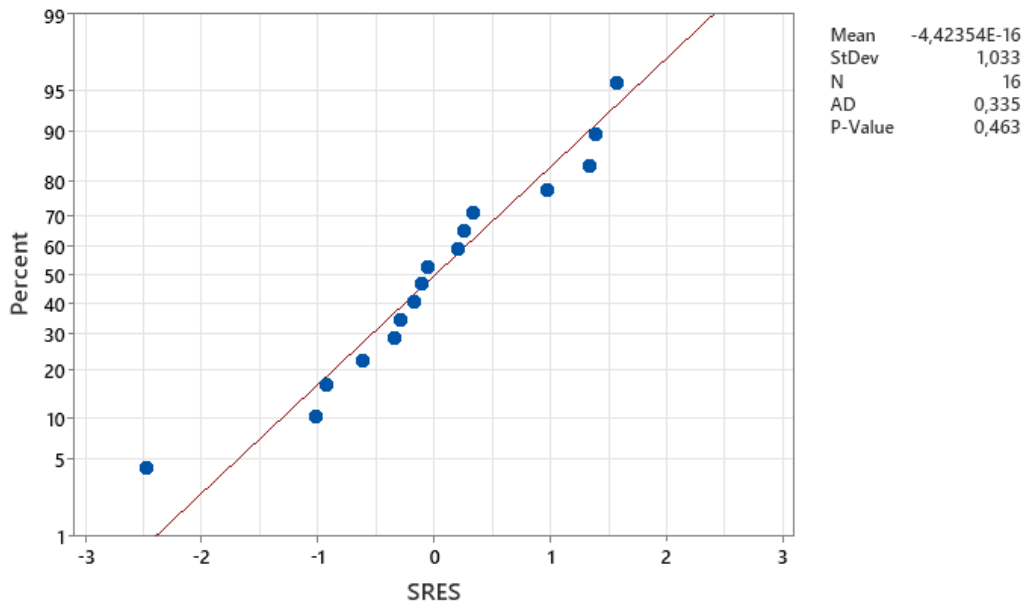

Figure 136: Geometrical analysis - Probability Plot of Standardized residuals to test for normality - Cutting under controlled preheating conditions – 2 mm thickness
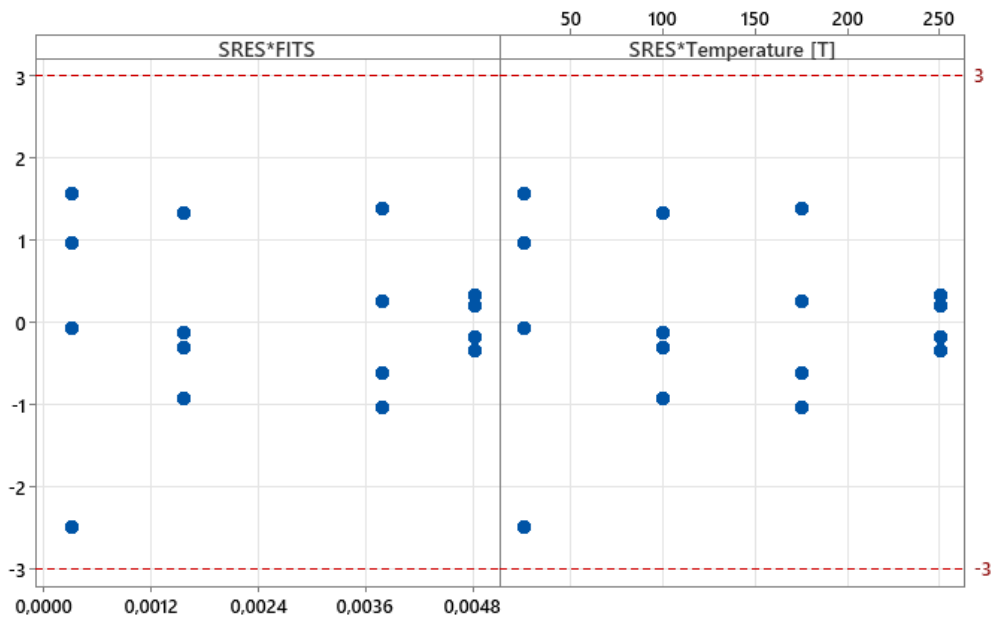
Figure 137: Geometrical analysis - Scatterplot of Standardized residuals versus Fits and versus Temperature [°C] - Cutting under controlled preheating conditions – 2 mm thickness